REPUBLIC OF IRAQ
MINISTRY OF HIGHER EDUCATION AND
SCIENTIFIC RESEARCH
AL-FURAT AL-AWSAT TECHNICAL UNIVERSITY
ENGINEERING TECHNICAL COLLEGE - NAJAF

DESIGN AND IMPLEMENTATION OF NONRECIPROCAL REFLECTION-LESS RADIO FREQUENCY SYSTEM

BAHAA HAMZAH JASIM

(M. Sc. In Communications Techniques Eng.)

2022

DESIGN AND IMPLEMENTATION OF NONRECIPROCAL

REFLECTION-LESS RADIO FREQUENCY SYSTEM

THESIS
SUBMITTED TO COMMUNICATION TECHNIQUES ENGINEERING
DEPARTMENT IN PARTIAL FULFILLMENT OF THE REQUIREMENTS
FOR THE TECHNICAL MASTER DEGREE
IN

COMMUNICATION ENGINEERING

By

BAHAA HAMZAH JASIM

Supervised by

Dr. NASR NOMAS Al-KHAFAJI

October/2022

COMMITTEE REPORT

We certify that we have read this thesis titled **"Design and Implementation of Nonreciprocal Reflection-Less Radio Frequency System "** which is being submitted by **Bahaa Hamzah Jasim** and as examining Committee, examined the student in its contents. In our opinion, the thesis is adequate for award of degree of Master.

Signature: Signature:

Name: Name:

Dr. Nasr Nomas Al-Khafaji   **Asst. Prof. Dr. Wasan Kadhim Saad**

(Supervisor)   (Member)

Date: /   / 2022   Date: /   / 2022

Signature: Signature:

Name: Name:

Prof. Dr. Bashar J. Hamza   **Prof. Dr. Saad Saffah Hassoon**

(Member)   (Chairman)

Date: /   / 2022   Date: /   / 2022

Approval of the Technical Engineering Collage

Signature:

Name: **Asst. Prof. Dr. Hassanain Ghani**

Dean of Technical Engineering Collage

Date: /   / 2022

LINGUISTIC CERTIFICATION

This is to certify that this thesis entitled **"Design and Implementation of Nonreciprocal Reflection-Less Radio Frequency System "** was reviewed linguistically. Its language was amended to meet the style of the English language.

Signature:

Name:

Date: /   / 2022

ABSTRACT

The power reflection and reciprocity are the main challenges facing the radio-frequency RF circuit designers for many reasons. When the power is totally reflected from any RF circuit especially from out of the band of interest, the preceding RF circuit can be damaged or get failed. Also, the isolation between the transmit and receive signals is important. These two problems will be investigated and diminished into good extent only in one design which is proposed for the first time in the literature.

In this thesis, a programmable quasi-reflectionless nonreciprocal filter is proposed. The proposed filter can change its status relying on the control-voltage applied to its control terminals. It can be changed from reflectionless into reflective filter or from transmitting filter into receiving filter or vice versa. It may be automatically done if the artificial intelligence techniques with FPGA or Arduino devices are utilized. The thesis first discusses and proposes a solution for the power reflection. As known in most RF circuit designs, they are only impedance matched at the desired frequency. It means all power will be reflected back from where it comes. The proposed filter alters the route of reflected power into absorptive loads. Several orders of U-shaped quasi-reflectionless filters are simulated, but the third order one is chosen for fabrication to validate the proof-of concept.

The second part in the thesis deals with solving the problem of reciprocity. Conventionally, the reciprocity is broken through using the magnetic materials as in circulators. Many disadvantages accompanied with this type of technology are like bulky, non-compatible with printed circuits, and expensive. However, the spatial-temporal modulation technique STM is adopted in this research. Because the main resonators are static and its properties cannot be changed, varactor diodes are integrated to the main

resonators. The varactor diodes can alter its capacitance values if the applied voltage changes. Thus, the DC, frequency and phase of the modulation signals are governed carefully to control the direction of signals propagation. The main factor determining the propagation direction is the progressive direction of phase shift. Sometime, the S21 is supported and S12 is not, and vice versa. Again here, the dual-band and tunable nonreciprocal BPF are presented.

Finally, the designs solved the two main problems are combined in one design called the programmable quasi-reflectionless nonreciprocal band pass filter with tuning-capabilities

ACKNOWLEDGMENTS

"Alhamdu lillahi rabbil 'alamin"

First and foremost, I would like to express my sincere gratitude and acknowledgment for Dr. Nasr Nomas Al-Khafaji for his valuable guidance, advice, and timely care extended to me during my research period. I am able to successfully complete this research work and deliver this thesis because of his immense patience and constructive feedback.

I would like to acknowledge the help of both Mr. Amjad Adnan and Mr. Mustafa Khafaji for their continuous support throughout this work.

I would like to thank my uncle Habib and his family for always being there through the good and the bad times and for their everlasting love and support.

I would like to thank my family. My brothers and sisters for always being there through good times and bad and for their constant love and support.

I would like to thank my wife who suffered so much for me, form the deep of my heart thank you.

Special thanks are to my many friends who have given me their support and help throughout my MSC.

"To my father and mother mercy and forgiveness"

DECLARATION

I hereby declare that the thesis is my original work except for quotations and citations which have been duly acknowledged.

Date: /   / 2022   Bahaa Hamzah Jasim

TABLE OF CONTENTS

LIST OF TABLES

LIST OF FIGURES

LIST OF ABBREVIATIONS

Abbreviation	Description
AC	Alternating Current
ABS	Absorptive Stub
BPF	Bandpass Filter
BSF	Bandstop Filter
$DBPF$	Dual Bandpass Filter
FBW	Fractional Bandwidth
HBF	Highpass Filter
LPF	Lowpass Filter
mag	Magnitude
RF	Radio frequency
TEM	Transverse EM
f_m	Modulation frequency
TZ	Transmission zero
IM	Intermodulation
MW	Microwave
ADS	Advanced Design System
VDC	Voltage Direct Current
BW	Bandwidth
$S - Parameter$	Scattering Parameter
STM	Spatial Temporal Modulation
DC	Direct Current
dB	Decibel
K_m	Modulation index
Z_{0e}	Even Characteristic impedance
Z_{0o}	Odd Characteristic impedance

LIST OF SYMBOLS

Symbol	Definition
V_s	Source voltage
I_1	Current at port 1
I_2	Current at port 2
V_1	Voltage at port 1
V_2	Voltage at port 2
Z_s	Source impedance
Y_o	Characteristic admittance
Z_0	Characteristic impedance
Z_{02}	Terminal impedance at port2
$a1$	Incident wave at port 1
ω_0	Center angular frequency
$b2$	Reflected wave at port 2
C	Capacitance
C_0	Static capacitance
f_0	Center or resonance frequency
FBW	Fractional bandwidth
G	conductance
h	Height of substrate
L	Inductance
L	Length of transmission line
L_{Ar}	Passband ripple
Q_e	External quality factor
R	Resistance
t_{in}	Location of tapped-line
$T_n(\Omega)$	Chebyshev function

LIST OF SYMBOLS

Symbol	Definition
W	Width of transmission line
Z_f	Characteristic impedance of the transmission
Z_{01}	Terminal impedance at port 1
γ	Complex propagation constant
$a2$	Incident wave at port 2
$b1$	Reflected wave at port 1
$b2$	Reflected wave at port 2
Z_{in}	Input impedance
Z_{in1}	Input impedance at port 1
Z_{in2}	Input Impedance at port 2
l	Length of the transmission line
n	Order or degree of the filter
S	Scattering parameters
ω_1	First edge angular frequency
f_1	First edge frequency
L_{As}	Minimum stopband attenuation
S_{12}	Isolation coefficient
S_{21}	Transmission coefficient
ω_2	Second edge angular frequency
f_2	Second edge frequency
S_{11}	Reflection coefficient at port 1
S_{22}	Reflection coefficient at port 2
ΔC	Modulation depth
ε	Ripple constant
ε_e	Effective dielectric constant
ε_r	Relative dielectric constant
C_n	Variable capacitors
$M_{i,i+1}$	Coupling coefficients between the two adjacent resonators

CHAPTER 1

GENERAL INTRODUCTION

1.1   Introduction

Nowadays, wireless communication systems have become an essential part of our modern life, as they are utilized in various aspects of daily used products. Thus, providing fast and reliable communication, at any time, is necessary. Also, several applications use the wireless communication such as the Internet emerge recently. All those applications increase the number of the subscribers. However, the used frequency spectrum is limited, and it becomes very crowed.

To solve this crowed spectrum , the research is divided into two paths. The first path is to use higher frequencies, while the second path is to exploit and reuse the frequency bands as much as possible. With higher frequencies, the losses increase and the wireless devices should be carefully designed [1]. Also, the manufacturing techniques become very expensive. On the other side, reusing the frequencies requires that the wireless systems have high performance and good quality (i.e., higher spectral efficiency). There are various methods for increasing the spectral efficiency. The In-Band Full-Duplex (IBFD) is one of these methods which recently attracts a lot of researchers and vendors [2]. The main idea is that most communication systems contain terminal stations such as mobile phones and base stations that work to send and receive wireless signals (transceiver or full duplex devices). The full duplex use different bands for receiving and transmitting channels. This method wastes the frequency channels [3]. The

half-duplex devices either transmit or receive at once, and the same frequency channel uses for both transmit and receive. However, it is not practical to employ half-duplex devises. Advantages of half and full-duplex devices are combined in one technique called in-band full duplex IBFD. Therefore, the IBFD enables the wireless systems to transmit and receive simultaneously across the same frequency spectrum [3]. This doubles the spectrum efficiency as shown in Figure1.1. Therefore, these systems are of great importance for the next-generation networks.
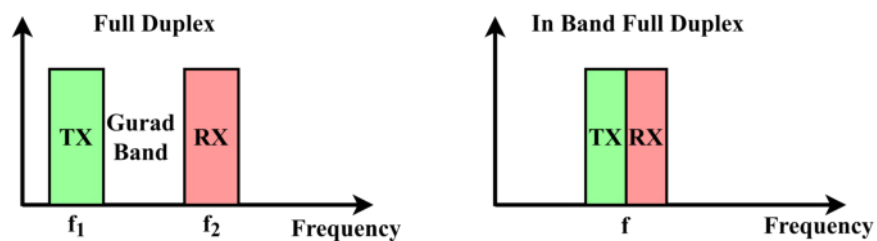
Figure 1.1: In band full duplex

Where, RF front-end circuits consist of two signals paths [4]. One is for transmitting, while the other is for receiving as shown in Figure 1.2. In IBFD, both paths share the same frequency channel, so the interference is very high. To avoid the interference between the receiving and transmitting channels, devices should allow RF signals to propagate only in one direction. Most RF devices, especially the passive type, allow signals to propagate in both directions. This inherent property is called the reciprocity.
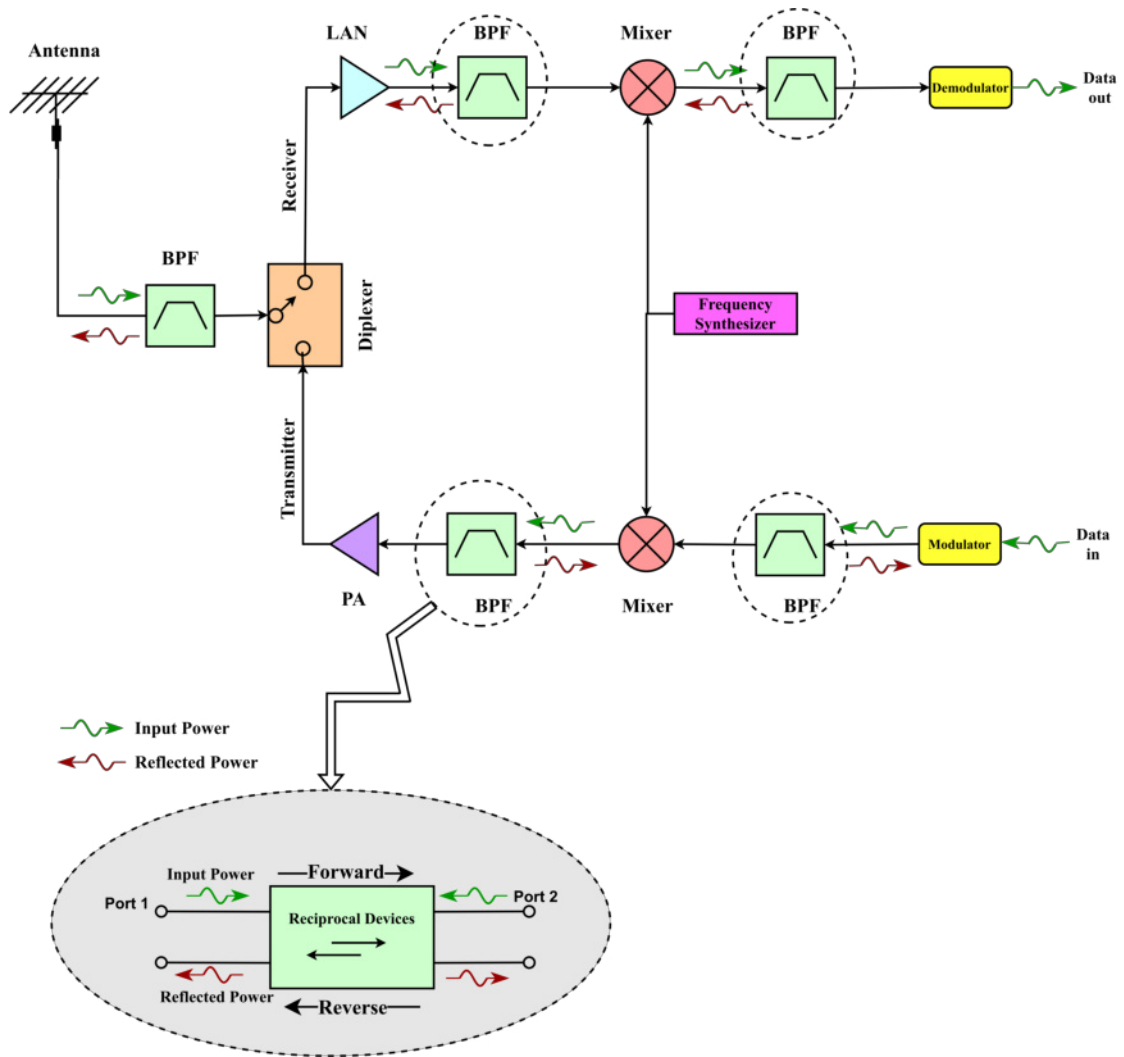
Figure 1.2: Front end diagram

The main idea behind this problem is the transmission of signals in both directions causes internal interference in these devices that leads to an attenuation of the desired signals as shown in Figure 1.3. Moreover, all RF devices are matched at a specific band of frequencies, whereas at other bands are mismatched. Thus, the signals will totally be reflected into the former circuits causing serious problems that will be discussed in detail in the next chapters. The power reflection and the reciprocity are the main target of this thesis.

The common structure of RF front-end wireless communication systems has several blocks and each block performs a specific function. The filter considers as a channel selector, because it passes only a certain frequency band. Filters are among the most im-
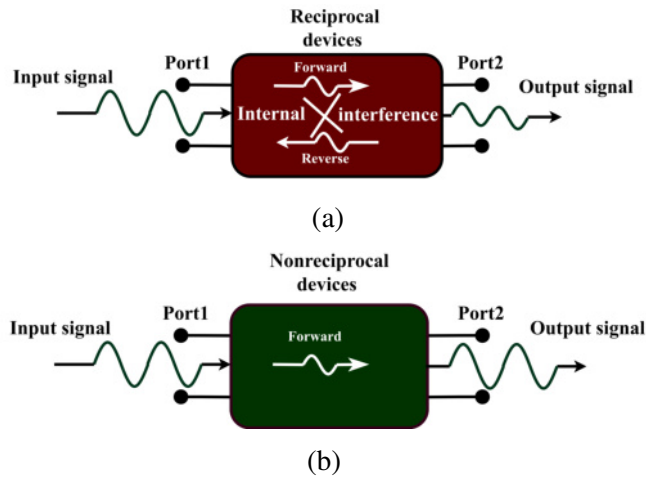
Figure 1.3: Reciprocity problem a) reciprocal devices b) nonreciprocal devices

portant of these devices in the architecture of wireless systems, where they are the basic building blocks of these systems. Filters are two-port devices that passes a certain range of frequencies (i.e. channel bandwidth), while other frequencies will be rejected. In the conventional filters (reflective filters), the rejected signals will be reflected back from where they come due to the high mismatching. This reflection will cause deterioration in the performance of the nonlinear devices such as mixers, amplifiers, oscillators, etc. For example, the conventional filter that is placed after the mixer in Figure 1.2 reflects power back into the mixer, causing in the generation of additional spurious signals. As a result of re-mixing it with the desired signals in an iterative process, some frequency products may fall within the operational frequency range, resulting in the performance deterioration as shown in Figure 1.4. Due to the presence of a large number of these devices in the front-end chain, effects of the reflected power may lead to a complete failure of the system.
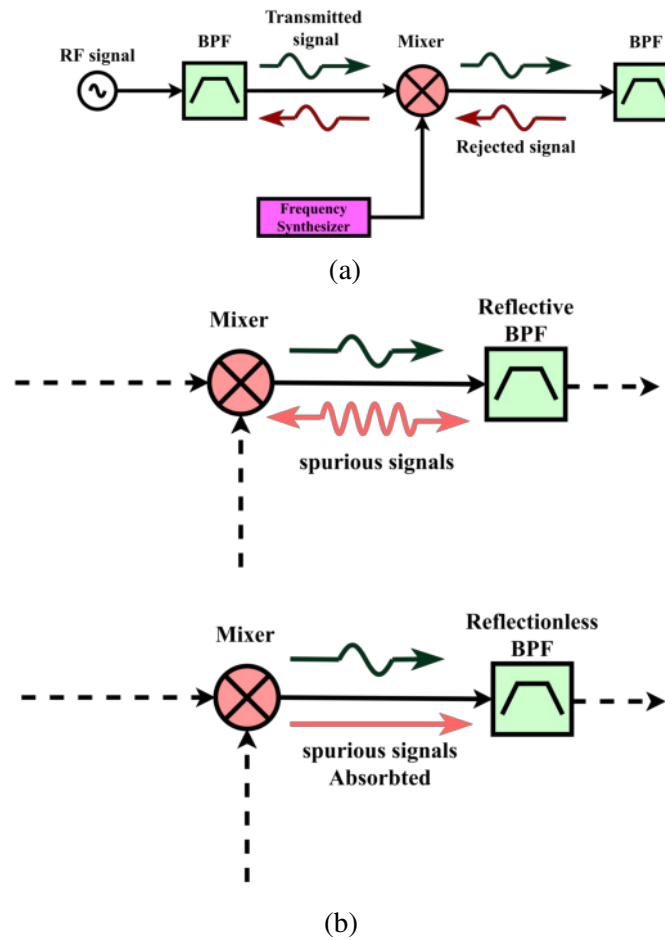
Figure 1.4: Reflection power problem a) reflection power from reflected BPF to the mixer b) spurious signals with two types BPF

1.2 Problem Statement

There are several issues facing the RF components designers that have been focused in this research, and they are summarized as follow:

1. The passive RF components have two issues ; Power reflected from out of the frequency band of the interest which leads to damage the adjacent components (main problem) ; Inherent reciprocity that causes interference between the receive and transmit paths.

2. In devices with static frequency responses, this means that each single RF device can only operate with single frequency band. To make the device operating with

several bands simultaneously, there should be replicas for each single RF component to cover all required bands. The structure will be complicated, large, and expensive (secondary problem).

1.3   Objectives

The main objective of this thesis is design and implantation of nonreciprocity and reflectionless response at the same structure of the filter in RF system .To achieve this objective , several sub-objectives must be accomplished:

1. To solve two issues, which includes; reflection power by proposing quasi-reflectionless filter and the reciprocity for the signal by proposing a nonreciprocal filter.

2. To proposed a new reflectionless nonreciprocal structure filter which depended on combine two filters to enhance performance of the system.

1.4   Contributions

There are many Contributions that has been in this thesis such as :

1. A mathematical models is derived.

2. A static reflectionless microwave filter have been designed.

3. Spatial-temporal modulation technique is used to make the RF signals direction propagating only in one way.

4. Multi-function filter have been designed, that can change its responses into:

   i   conventional non tunable single and dual-bandpass filter.

   ii   tunable single and dual-band pass filter.

   iii   magneticless nonreciprocal single and dual-band pass filter.

iv tunable magneticless nonreciprocal single and dual-band pass filter.

1.5 Organization of Thesis

The thesis consists of five chapters organized as follows:

Chapter 2 introduces the theory of two port network including network variables, theories and concepts of the microstrip transmission lines. Also, it provides other important aspects as reflectionless filters based on the complementary duplexer technique and the nonreciprocity based on spatial-temporal modulation STM technique.

Chapter 3 introduces the third order U-shaped quasi-reflectionless bandpass filter.

Chapter 4 presents the entire proposed design of programmable quasi-reflectionless nonreciprocal bandpass filter.

Chapter 5 concludes and future of the thesis.

CHAPTER 2

THEORETICAL BACKGROUND AND LITERATURE SURVEY

2.1   Introduction

RF/microwave components include filters, antennas, circulators, diplexers, power dividers, and collectors. These components may differ in terms of physical perception, but the structure of their components is common to all. Because these components operate at high frequencies, it is difficult to use voltmeters and ammeters to measure voltages and currents directly. This chapter aims to describe the concepts of different networks and to present the important equations in the analysis of two port networks.

2.1.1   Network Variables

Most components RF/microwave systems are two-port devices such as a filter where their components can be represented as shown in Figure 2.1, where I_1 and V_1 are the current and voltage variables at ports 1, while I_2 and V_2 are the current and voltage variables at ports 2. Also, each port has terminal impedances are Z_{01} and Z_{02}, and the source voltage is V_s.
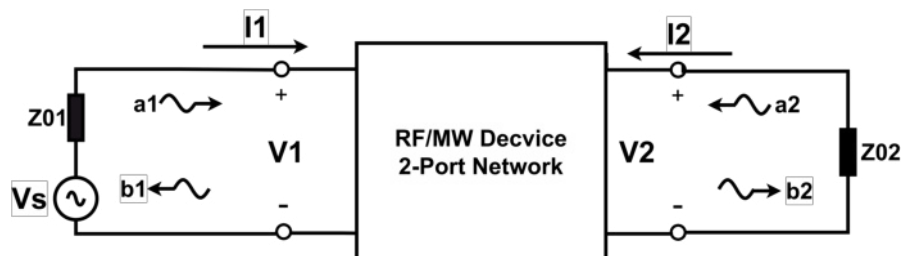
Figure 2.1: RF/MW 2-port network

In frequencies of RF/microwave, it is difficult to measure current and voltage, so

the wave variables are entered, a_1, a_2, b_1, b_2, where a_1 and a_2 refer to the incident waves and b_1 and b_2 refer to the reflected waves

2.1.2   Transmission-Line Networks

The input impedance at port one in the RF/MW 2-port network as shown in Figure 2.1 is given by [5]

$$Z_{in1} = Z_0 \frac{Z_{02} + Z_0 \tanh \gamma l}{Z_0 + Z_{02} \tanh \gamma l} \tag{2.1}$$

where Z_0 is the characteristic impedance, while l and γ are the length of the transmission line and complex propagation constant, respectively. When the transmission line is a lossless line that means $\gamma = j\beta$ and Eq.2.1 becomes

$$Z_{in1} = Z_0 \frac{Z_{02} + jZ_0 \tan \beta l}{Z_0 + jZ_{02} \tan \beta l} \tag{2.2}$$

One of the important types of two-port transmission networks are single-port transmission networks with open or short terminated, where their impedances are found from Eq.2.1 or 2.2

$$Z_{in1}\big|_{Z_{02}=\infty} = \frac{Z_c}{\tanh \gamma l}$$
$$Z_{in1}\big|_{Z_{02}=0} = Z_c \tanh \gamma l \tag{2.3}$$

When transmission line is lossless and with load impedance in form of short or open circuits as shown in Figure 2.2.

The expressions of Z_{in1} become

$$Z_{in1}\big|_{Z_{02}=\infty} = \frac{Z_c}{\tanh \gamma l}$$
$$Z_{in1}\big|_{Z_{02}=0} = Z_c \tanh \gamma l \tag{2.4}$$

9

(a)

(b)
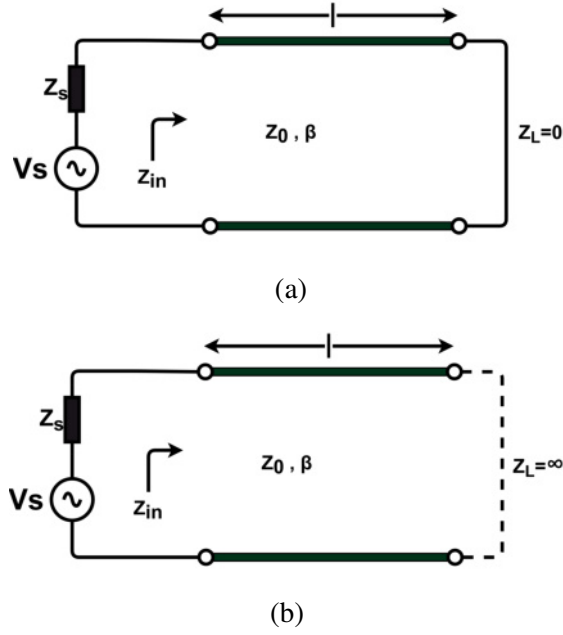
Figure 2.2: Short and open terminal of 2-port transmission (a) load impedance as short form (b) load impedance as open form.

$$Z_{in1}\big|_{Z_{02}=\infty} = \frac{Z_c}{j\tan\beta l}$$

$$Z_{in1}\big|_{Z_{02}=0} = jZ_c\tan\beta l$$

(2.5)

2.1.3 S-Parameters

The scattering matrix is one of the important criteria that provides a complete description of the behavior of multi-port networks, and as mentioned earlier, it is difficult to measure current or voltage at high frequencies and enter wave variables. So, the scattering matrix describes the relationship between the wave reflected to the incident wave at any port, as defined as

$$S_{11} = \frac{b_1}{a_1}\bigg|_{a_2=0} \quad S_{12} = \frac{b_1}{a_2}\bigg|_{a_1=0}$$

$$S_{21} = \frac{b_2}{a_1}\bigg|_{a_2=0} \quad S_{22} = \frac{b_2}{a_2}\bigg|_{a_1=0}$$

(2.6)

where $a_n = 0$ means full impedance matching between the ports ,in another word no reflection of terminal impedance at port n, so the scattering matrix or S matrix can be

10

written

$$\begin{bmatrix} b_1 \\ b_2 \end{bmatrix} = \begin{bmatrix} S_{11} & S_{12} \\ S_{21} & S_{22} \end{bmatrix} \cdot \begin{bmatrix} a_1 \\ a_2 \end{bmatrix} \tag{2.7}$$

where S11 and S22 are the reflection coefficients, while the transmission coefficients are S12 and S21. These parameters are called the S- parameters of the scattering matrix [S].

At microwave frequencies, these coefficients can be measured directly as well. They are complex coefficients, and the appropriate expression for them is amplitudes and phases, that is, $S_{mn} = |S_{mn}|e^{j\phi_{mn}}$ for $m, n = 1, 2$. For filter characterization, we may define two parameters [5]

$$L_A = -20 \log |S_{mn}| \quad \text{dB} \quad m, n = 1, 2(m \neq n)$$
$$\tag{2.8}$$
$$L_R = 20 \log |S_{nn}| \quad \text{dB} \quad n = 1, 2$$

where L_A is insertion loss that implies to loss in the power between ports n and m, and the return loss L_R represents the power that loss due to reflected at the same port n, also, there are other parameters may be used instead L_R is the voltage standing wave ratio VSWR, That definitions as

$$VSWR = \frac{1 + |S_{nn}|}{1 - |S_{nn}|} \tag{2.9}$$

In a filter or any frequency selective network, the signal suffers from some delay when it is transmitted through it. To describe the performance of the filter related to the delay, two other parameters play an important role. The first is the phase delay in [1], which is defined by

$$\tau_p = \frac{\phi_{21}}{\omega} \tag{2.10}$$

11

This delay is considered the real delay of the baseband signal and is referred to the envelope delay.

In network analysis and synthesis, the reflection coefficients S11 and S22 may be desirable in terms of the terminal impedance, as the following

$$S_{11} = \frac{Z_{in1} - Z_{01}}{Z_{in1} + Z_{01}} \tag{2.11}$$

Similarly, we can have

$$S_{22} = \frac{Z_{in2} - Z_{02}}{Z_{in2} + Z_{02}} \tag{2.12}$$

where Z_{in1} and Z_{in2} are the input impedances looking into port 1 and port2 of the network , respectively.

One of the useful properties of the S parameter in network analysis is the symmetrical network (reciprocal network), which means that $S12 = S21$. For a lossless passive 2-port network, the transmitted and reflected power must equal the total incident power. In below Eq.2.13 explain these conditions

$$
\begin{aligned}
S_{21}S_{21}^* + S_{11}S_{11}^* = 1 \quad &\text{or} \quad |S_{21}|^2 + |S_{11}|^2 = 1 \\
S_{12}S_{12}^* + S_{22}S_{22}^* = 1 \quad &\text{or} \quad |S_{12}|^2 + |S_{22}|^2 = 1
\end{aligned}
\tag{2.13}
$$

2.1.4 Y - Parameters

Y- parameters or short-circuit terminal of a RF/MW 2-port network are defined as

$$
\begin{aligned}
Y_{11} &= \left.\frac{I_1}{V_1}\right|_{V_2=0} \quad & Y_{12} &= \left.\frac{I_1}{V_2}\right|_{V_1=0} \\
Y_{21} &= \left.\frac{I_2}{V_1}\right|_{V_2=0} \quad & Y_{22} &= \left.\frac{I_2}{V_2}\right|_{V_1=0}
\end{aligned}
\tag{2.14}
$$

When the terminal of circuit at port n is perfect short that means $V_n = 0$. The definitions of the [Y] matrix that contain the Y parameters can be written as

$$
\begin{bmatrix} I_1 \\ I_2 \end{bmatrix} = \begin{bmatrix} Y_{11} & Y_{12} \\ Y_{21} & Y_{22} \end{bmatrix} \cdot \begin{bmatrix} V_1 \\ V_2 \end{bmatrix} \tag{2.15}
$$

Previously, subsection 2.7.2 presents the previous solutions to the problem of reciprocity in filters. As it is known that the filter is a two-port device; so the Y-parameters analysis can describe the reciprocity of filters by the condition $Y12 = Y21$. Also, when this filter is lossless, the Y parameters are all purely imaginary.

2.1.5 Z- Parameters

Z- parameters or open-circuit terminal of a RF/MW 2-port network are defined as

$$
\begin{aligned}
Z_{11} &= \left.\frac{V_1}{I_1}\right|_{I_2=0} & Z_{12} &= \left.\frac{V_1}{I_2}\right|_{I_1=0} \\
Z_{21} &= \left.\frac{V_2}{I_1}\right|_{l_2=0} & Z_{22} &= \left.\frac{V_2}{I_2}\right|_{I_1=0}
\end{aligned} \tag{2.16}
$$

when the terminal of circuit at port n is perfect open that mean $In = 0$. The definitions of the [Z] matrix that contain the Z parameters can be written as

$$
\begin{bmatrix} V_1 \\ V_2 \end{bmatrix} = \begin{bmatrix} Z_{11} & Z_{12} \\ Z_{21} & Z_{22} \end{bmatrix} \cdot \begin{bmatrix} I_1 \\ I_2 \end{bmatrix} \tag{2.17}
$$

Also, Z-parameters may describe the reciprocity networks by condition Z12 = Z21, while the lossless condition implies all Z parameters are purely imaginary.

Inspecting Eqs. 2.17 and 2.17, we obtain an important relation

$$
[Z] = [Y]^{-1} \tag{2.18}
$$

2.1.6 ABCD Parameters

The Z- , Y- , and S- matrices can be used to characterize the RF/MW network , when these network is represent in series or parallel combinations of 2-port network .

In practice, two or more than of 2-port network such as filters are actually represented by a series of cascaded form. So, ABCD matrix is used to characterized these networks.

2-port RF/MW Network in Figure 2.3 illustrates the relationship between the voltage and current on each port that can be defined through the ABCD matrix as

$$
\begin{bmatrix} V_1 \\ I_1 \end{bmatrix} = \begin{bmatrix} A & B \\ C & D \end{bmatrix} \cdot \begin{bmatrix} V_2 \\ I_2 \end{bmatrix}
\tag{2.19}
$$
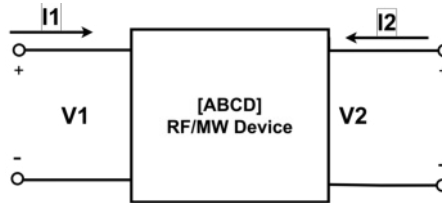
Figure 2.3: ABCD -Parameter

For cascaded 2-port network in series of n –network as shown in Figure 2.18 , the voltage and current at port 1 can be define as

$$
\begin{bmatrix} V_1 \\ I_1 \end{bmatrix} = \begin{bmatrix} A_1 & B_1 \\ C_1 & D_1 \end{bmatrix} \begin{bmatrix} A_2 & B_2 \\ C_2 & D_2 \end{bmatrix} \dots \begin{bmatrix} A_n & B_n \\ C_n & D_n \end{bmatrix} \begin{bmatrix} V_{n+1} \\ I_{n+1} \end{bmatrix}
\tag{2.20}
$$
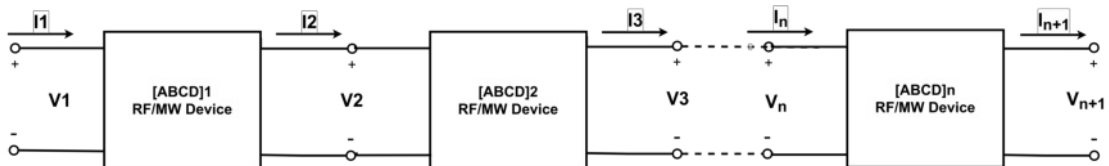
Figure 2.4: Cascaded of series 2-port network

There are two special characteristics of the ABCD matrix

1) $AD = BC$ when network is reciprocal and $A = D$ For symmetrical network

2) A and D are purely real when the network is lossless , while B and C are both purely imaginary.

2.2 K/J Inverters

There are two types of inverters, the first is impedance inverter or K-inverter and the other is admittance inverter or (J-inverter). Ideally, these inverters work as a quarter–wavelength impedance transformer with a specific real characteristic impedance of K or J at all frequencies. Figure 2.5 shows the two-port K/J inverter with one port terminated by a load ZL.

(a)

(b)
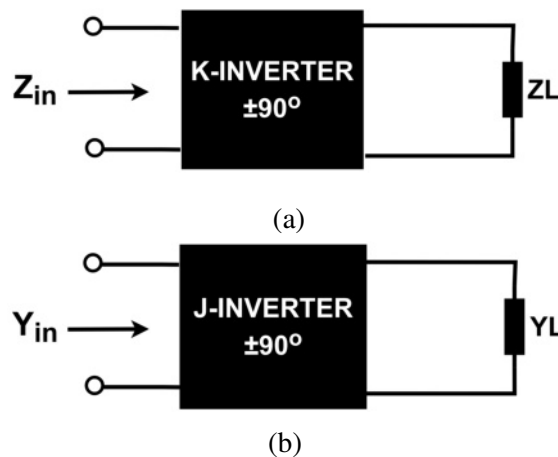
Figure 2.5: K/J inverters (a) K-inverter (b) J- inverter

The input impedance of the other port is

$$Z_{in} = \frac{K^2}{Zl} \tag{2.21}$$

When ZL is conductive / inductive, Zin will become inductive / conductive, that mean, the inverter has a phase shift of $\pm 90^0$. The matrix of ABCD in previously presented ,may be used to decelerates k- inverters matrix in [1].as define as

15

$$\begin{bmatrix} A & B \\ C & D \end{bmatrix} = \begin{bmatrix} 0 & \pm jK \\ \mp \frac{1}{jK} & 0 \end{bmatrix} \tag{2.22}$$

Also J-inverter operates in a similar way of K-inverter, and the input admittance of the other port is

$$Yin = \frac{J^2}{Yl} \tag{2.23}$$

where YL is conductive / inductive, Yin will become inductive / conductive. That means the inverter has a phase shift of $\pm 90^0$. Also, J- inverters matrix can be obtained by ABCD matrix as following

$$\begin{bmatrix} A & B \\ C & D \end{bmatrix} = \begin{bmatrix} 0 & \pm jJ \\ \mp \frac{1}{jJ} & 0 \end{bmatrix} \tag{2.24}$$

2.3   Filters Theories and Concepts

The filter is one of the basic components of wireless communication systems. It has an important role in controlling the frequency response by allowing or rejecting the specified band frequencies. there are four types of response low-pass, high-pass, Bandpass, and band-reject [5].

In general, the lowpass prototype is the basis of the filter design transformed into other types of filters. Figure2.6 shows the response of each type of filter [1].

2.3.1   Prototype Lowpass Filter

In general, a prototype lowpass filter means that the element of the filter in the normalized form such as the resistance/ conductance of the source has a normalized value equal to one (i.e $g0 = 1$), and normalized cutoff frequency to be unity; that means $\Omega c = 1$ (rad/s).

16
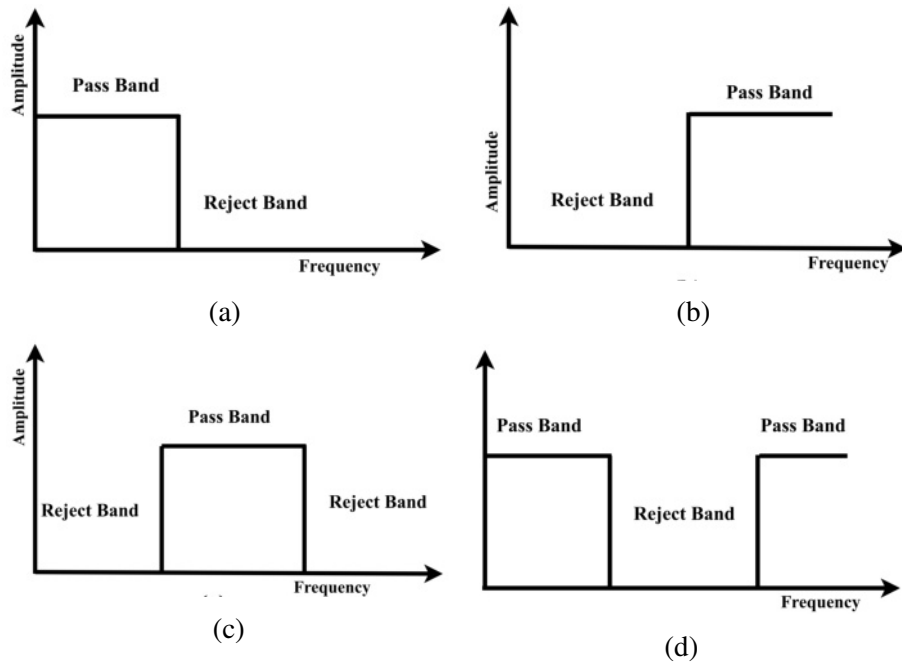
Figure 2.6: Four basic type of filter (a)response of the lowpass filter(LPF) (b) response of the highpass filter(HPF) (c)response of the bandpass filter(BPF) (d) response of the bandstop filter(BSF)

Figure 2.7 illustrates that all types of filter are designed from a prototype low pass filter by using frequency and element transformations.
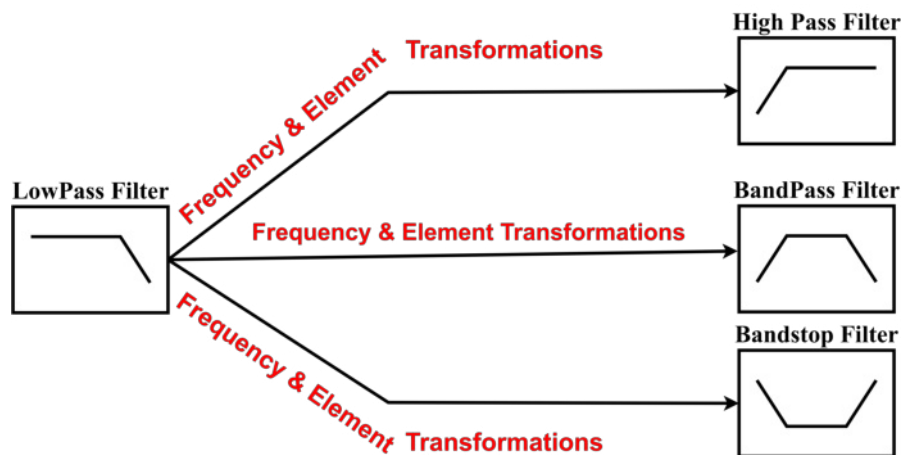
Figure 2.7: Lowpass prototype with frequency and element transformation

Lowpass prototype has different shapes depending on the filter structure and properties as shown in Figure 2.8, as there are two main types of responses from filters are Butterworth and Chebyshev that will be covered in the next section

In Figure 2.8 , it will be noted that the resistance / conductance of the source is

17
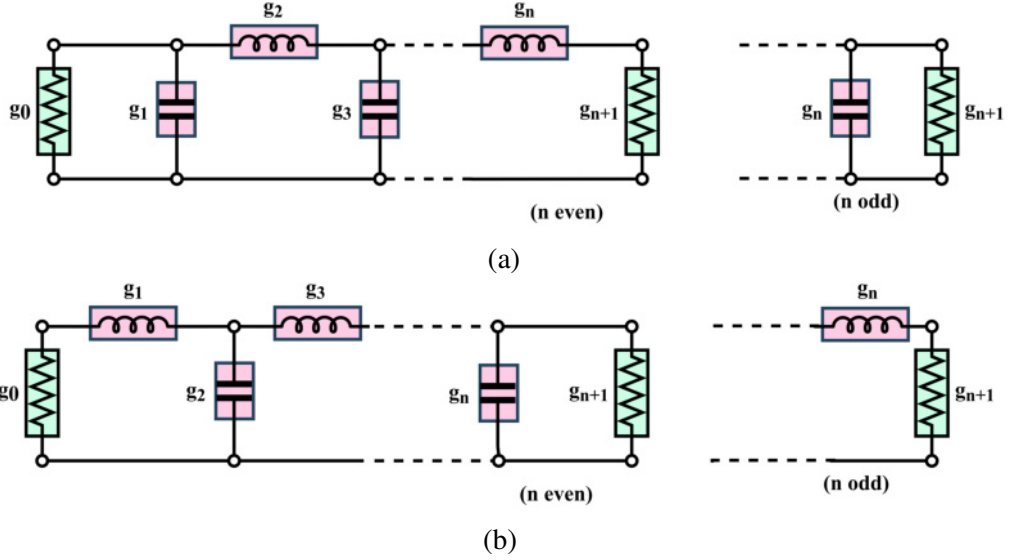
Figure 2.8: Lowpass filters prototype structure (a) shunt series-resonant branches (b) series shunt resonant branches

g_0 in normalized form, for $= 1$ to n, g_i represents the other element in form of series inductance or capacitance of the shunt capacitor. So, n is also the number of reactive elements; therefore, and g_{n+1} is defined as load resistance/ conductivity of the load resistance or the load conductance.

2.3.1.1   Butterworth Response of Prototype Lowpass Filters

Butterworth filters have a transfer function in squared form in the passband and the insertion loss LAr at the cutoff frequency Ωc is given [5]

$$L_{Ar}(\Omega) = 10 \log_{10} \left[1 + \varepsilon^2 \left(\frac{\Omega}{\Omega_c} \right)^{2n} \right]. \tag{2.25}$$

where n is the order or degree of filter, that determined the number of normalized elements g in the low-pass filter prototype and ε is the ripple constant related to a given passband ripple LAr in dB.

$$\varepsilon = \sqrt{10^{\frac{L_{Ar}}{10}} - 1}, \tag{2.26}$$

18

The maximally flat response of this type comes from the squared amplitude transfer function in Eq.2.27, this transfer function has a maximum (2n - 1) number with zero derivatives at = 0 , but it deteriorates when approaching the cutoff frequency as shown in Figure 2.9.

$$|S_{21}(j\Omega)|^2 = \frac{1}{1 + \Omega^{2n}} \tag{2.27}$$
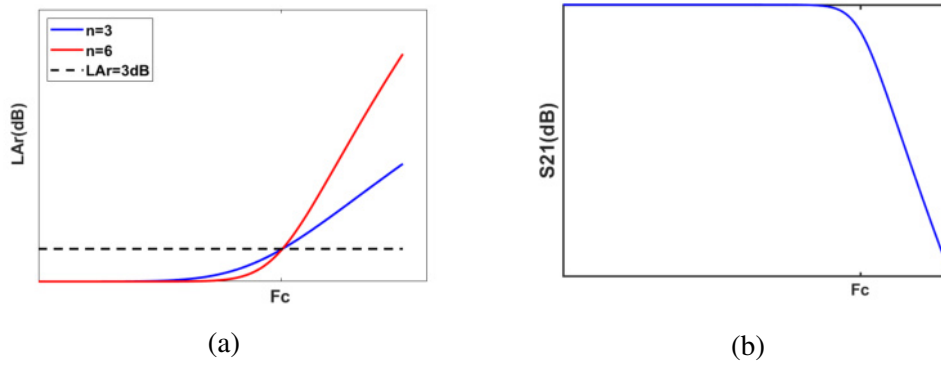
Figure 2.9: Butterworth (maximally flat) lowpass responses (a) insertion loss LAr (b)transmission confection S21

The normalized values of the Butterworth element in Figure 2.8 can be computed in relation to insertion loss LAr = 3.01 and the normalized cutoff frequency $\Omega c = 1$ as follows [5],

$$g_0 = 1.0$$

$$g_i = 2\sin\left(\frac{(2i-1)\pi}{2n}\right) \quad \text{for } i = 1 \text{ to } n \tag{2.28}$$

$$g_{n+1} = 1.0$$

and n is the order of filter that determines the specification of a Butterworth lowpass prototype response, can be computed when minimum stopband attenuation LAs dB at the normalized frequency equal to stop frequency ($\Omega = \Omega s$ for $\Omega s > 1$)is given by

$$n \geq \frac{\log\left(10^{0.1L_A} - 1\right)}{2\log\Omega_s} \tag{2.29}$$

2.3.1.2 Chebyshev Response of Prototype Lowpass Filter

In chebyshev response, the filter has an equal ripple in the passband and is maximally flat at the stopband as shown in Figure 2.10. The transfer function that describes this type of response is amplitude-squared while it has a transfer function below with a cutoff frequency $\Omega c = 1$ and passband ripple LAr dB. The chebyshev insertion loss in [1] as defined as:

$$L_A(\Omega) = 10\log_{10}\left\{1 + \varepsilon^2\cosh^2\left[n\cosh^{-1}\left(\frac{\Omega}{\Omega_c}\right)\right]\right\}, \text{ for } |\Omega| \geq \Omega_c.$$
$$L_A(\Omega) = 10\log_{10}\left\{1 + \varepsilon^2\cos^2\left[n\cos^{-1}\left(\frac{\omega}{\Omega_c}\right)\right]\right\}, \quad \text{ for } |\Omega| \leq \Omega_c, \tag{2.30}$$

where ε is ripple constant can be given by

$$\varepsilon = \sqrt{10^{\frac{L_{Ar}}{10}} - 1}, \tag{2.31}$$

(a)   (b)
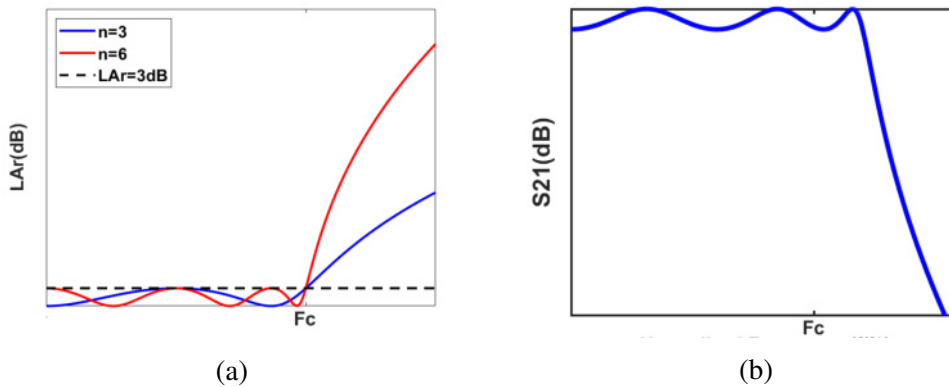
Figure 2.10: Chebyshev lowpass responses (a) insertion loss LAr (b)transmission confection S21

The transmission confection S21 is given by

$$|S_{21}(j\Omega)|^2 = \frac{1}{1 + \varepsilon^2 F_n^2(\Omega)} \tag{2.32}$$

$F_n(\Omega)$ is the function of Chebyshev of the first kind of order n as defined as

$$F_n(\Omega) = \begin{cases} \cos\left(n\cos^{-1}\Omega\right) & |\Omega| \leq 1 \\ \cosh\left(n\cosh^{-1}\Omega\right) & |\Omega| \geq 1 \end{cases} \tag{2.33}$$

For the element in the two-port prototype filter networks as shown in Figure 2.8 may be calculated by using the following formulas:

$$g_0 = 1.0$$

$$g_1 = \frac{2}{\gamma}\sin\left(\frac{\pi}{2n}\right)$$

$$g_i = \frac{1}{g_{i-1}}\frac{4\sin\left[\frac{(2i-1)\pi}{2n}\right]\cdot\sin\left[\frac{(2i-3)\pi}{2n}\right]}{\gamma^2 + \sin^2\left[\frac{(i-1)\pi}{n}\right]} \quad \text{for } i = 2, 3, \ldots n \tag{2.34}$$

$$g_{n+1} = \begin{cases} 1.0 & \text{for } n \text{ odd} \\ \coth^2\left(\frac{\beta}{4}\right) & \text{for } n \text{ even} \end{cases}$$

where n is the filter order that can be found at the stopband frequency $\Omega = \Omega s$:

$$n \geq \frac{\cosh^{-1}\sqrt{\frac{10^{0.1L_{As}}-1}{10^{0.1L_{Ar}}-1}}}{\cosh^{-1}\Omega_s} \tag{2.35}$$

2.3.2 Frequency and Impedance Transformation

The Practical filter's characteristics are frequency and element values that can be obtained from lowpass filter prototype that has a normalized value of elements in Figure 2.8 after applying frequency and element transformations.

The transformation or mapping of the frequency refers transform the normalized

frequency of lowpass prototype ω to practical frequency of filter such as lowpass filter (LPF), highpass filter (HPF), bandpass filter (BPF), and bandstop (BSF).

In addition, the scaling of impedance is the other important transformation that is required to accomplish the element transformation, in which normalized value $g_0 = 1$ will be removed and converted to the source impedance after multiplied by scaling factor γ_0 as defined as

$$\gamma_0 = \begin{cases} Z_0/g_0 & \text{for } g_0 \text{ being the resistance} \\ g_0/Y_0 & \text{for } g_0 \text{ being the conductance} \end{cases} \tag{2.36}$$

where $Z_0 = 1/Y_0$ is the source impedance . In principle, applying the admittance or impedance scaling on a filter network is not effect of the response shape.

$$L \rightarrow \gamma_0 L$$
$$C \rightarrow C/\gamma_0$$
$$R \rightarrow \gamma_0 R \tag{2.37}$$
$$G \rightarrow G/\gamma_0$$

2.3.2.1 Transformation of Bandpass filter

Bandpass Transformation refers to transforming a lowpass prototype has normalized frequency ωc and element g, to bandpass having a bandwidth $\omega 2 - \omega 1$, where $\omega 2$ and $\omega 1$ are high and low frequencies respectively. The transformation of required Bandpass in [5]. The frequency is

$$\Omega = \frac{\Omega_c}{FBW}\left(\frac{\omega}{\omega_0} - \frac{\omega_0}{\omega}\right)$$

$$FBW = \frac{\omega_2 - \omega_1}{\omega_0} \tag{2.38}$$

$$\omega_0 = \sqrt{\omega_1 \omega_2}$$

where ω_0 is the center angular frequency and FBW is the fractional bandwidth. By applying this frequency mapping the element g in form inductive in the lowpass prototype will transform into a resonant circuit in a form of a series LC in the bandpass filter. The capacitive element is transformed into resonant circuit in a form of a parallel LC as shown in Figure 2.11. The transformation element of bandpass filter are

$$L_s = \left(\frac{\Omega_c}{FBW\omega_0}\right)\gamma_0 g$$

$$C_s = \left(\frac{FBW}{\omega_0\Omega_c}\right)\frac{1}{\gamma_0 g} \qquad \text{for } g \text{ representing the inductance}$$

$$\tag{2.39}$$

$$C_p = \left(\frac{\Omega_c}{FBW\omega_0}\right)\frac{g}{\gamma_0}$$

$$L_p = \left(\frac{FBW}{\omega_0\Omega_c}\right)\frac{\gamma_0}{g} \qquad \text{for } g \text{ representing the capacetance}$$
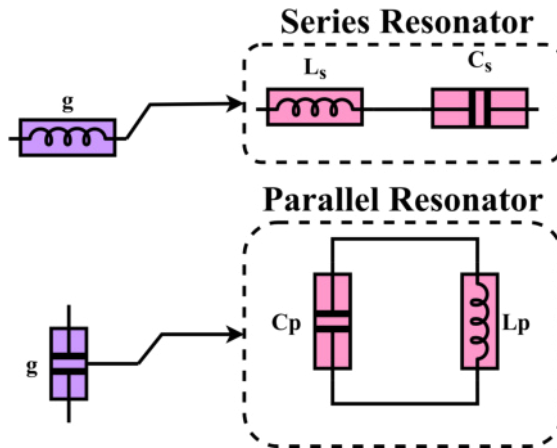
Figure 2.11: Bandpass Transformation

2.3.2.2 Transformation of Bandstop filters

The lowpass prototype can be converted to bandstop filter by the frequency transformation as below [5],

$$\Omega = \frac{\Omega_c FBW}{(\omega_0/\omega - \omega/\omega_0)} \tag{2.40}$$

The transformation of the bandstop filter is opposite to that in the bandpass, where the element g, as inductive in the lowpass prototype, will transform into resonant circuit in a form of a parallel LC in the bandstop filter. The capacitive element is transformed into resonant circuit in a form of a series LC as shown in Figure 2.12.

$$\Omega = \frac{\Omega_c FBW}{(\omega_0/\omega - \omega/\omega_0)}$$

$$C_p = \left(\frac{1}{FBW\omega_0\Omega_c}\right)\frac{1}{\gamma_0 g}$$

$$L_p = \left(\frac{\Omega_c FBW}{\omega_0}\right)\gamma_0 g \qquad \text{for } g \text{ representing the inductance} \tag{2.41}$$

$$L_s = \left(\frac{1}{FBW\omega_0\Omega_c}\right)\frac{\gamma_0}{g}$$

$$C_s = \left(\frac{\Omega_c FBW}{\omega_0}\right)\frac{g}{\gamma_0} \qquad \text{for } g \text{ representing the capacitance}$$

At higher frequencies, the lumped elements become small in size so it is difficult to use them in filter design. Alternatively, transmission lines can perform the same functions as lumped elements. In addition, it is easy to manufacture or print as integrated circuit. One of the most important transmission lines is the microstrip, which we will discuss in the next
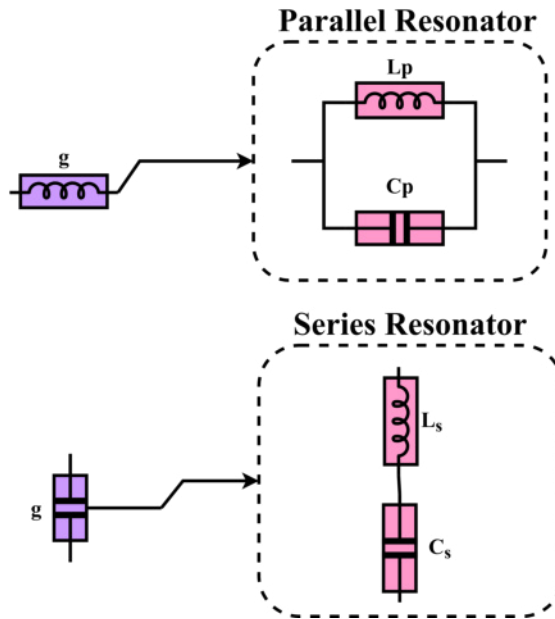
Figure 2.12: Bandstop Transformation

2.4 Microstrip

Most electronic systems can be implemented in the form of planar printed boards (PCBs). It is a common practice in the manufacture of components for RF/MW systems [6]. Microstrip lines can be manufactured by lithographic printing and easily integrated by other active and passive microwave circuits, the structure of which is shown in the figure below.
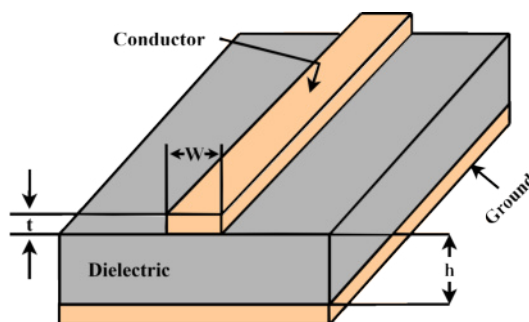
Figure 2.13: Microstrip line

where W is the width of microstrip and h is the thickness of dielectric substrate that placed on ground (conducting)

2.4.1 Effective Dielectric Constant, Characteristics Impedance

Approximately, the expression for effective dielectric constant εe of a microstrip line is given by [5],

$$\varepsilon_e = \frac{\varepsilon_r + 1}{2} + \frac{\varepsilon_r - 1}{2} \frac{1}{\sqrt{1 + 12h/W}} \tag{2.42}$$

where W is the width of microstrip line and εr , h are relative dielectric constant and height of the substrate. The characteristics impedance Z_0 of the microstrip line can be calculated by

$$Z_0 = \begin{cases} \frac{60}{\sqrt{\varepsilon_e}} \ln\left(\frac{8h}{W} + \frac{W}{4h}\right) & \text{for } \frac{W}{h} \leq 1 \\ \frac{120\pi}{\sqrt{\varepsilon_e}[\frac{W}{h} + 1.393 + 0.667\ln(\frac{W}{h} + 1.444)]} & \text{for } \frac{W}{h} \geq 1 \end{cases} \tag{2.43}$$

where

$$\frac{W}{h}$$

$$= \begin{cases} \frac{8e^A}{e^{2A} - 2} & \text{for } W/h < 2 \\ \frac{2}{\pi}\left[B - 1 - \ln(2B - 1) + \frac{\varepsilon_r - 1}{2\varepsilon_r}\left\{\ln(B - 1) + 0.39 - \frac{0.61}{\varepsilon_r}\right\}\right] & \text{for } W/h > 2 \end{cases}$$

$$A = \frac{Z_0}{60}\sqrt{\frac{\varepsilon_r + 1}{2}} + \frac{\varepsilon_r - 1}{\varepsilon_r + 1}\left(0.23 + \frac{0.11}{2}\right)$$

$$B = \frac{366\pi}{2Z_0\sqrt{\varepsilon_r}}$$

$$\tag{2.44}$$

After identifying the necessary equations for the microstrip line, it is necessary to know that the microstrip enters into the constructer of the most important components of microwave frequencies, which are the filters. There are many filters such as coupled resonator filter, stepped impedance filter, hairpin filter and others[1]. We will discuss the details of two types of them in the next section: parallel coupled resonator filter and hairpin filter.

2.4.2 Parallel Coupled lines

It is one of the important types of microstrip, consisting of two lines close to each other, which allows the electromagnetic field to be coupled between them, so it is called the coupling lines. Coupling lines are used in the construction of many components of microwaves systems, such as filters and antennas. So, many filters can be easily constructed using dual parallel transmission lines such as bandpass filters (BPFs) or bandstop filters (BSFs) with filter fraction bandwidth less than 20%. Wider filters are more difficult to manufacture because dual lines are more compact [5].

There are two types of coupling lines: open-ended and short-end coupled lines. Figure 2.14 shows the open-end coupling line and Equivalent circuit of it that enters into the structure of filters for ease of manufacture.
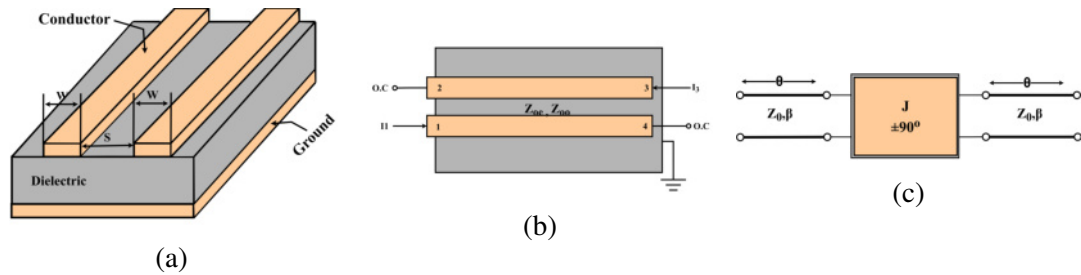
Figure 2.14: Microstrip coupled line (a) microstrip coupled line (b) Coupled lines BPF (c) open end coupled line Equivalent circuit

For designing narrowband, BPF can be used cascating sectioning Figure 2.14c, where the resonant frequency of the filter occurs at angle ($\theta = \pi/2$). The molding of coupled line section can be calculated by adding an even mode impedance. The derived impedance of three sections in Figure 2.14c results from multiplying ABCD parameter of each section with other as follows [1],

$$Z_{Oe} = Z_0 \left[\mathbf{1} + JZ_0 + (JZ_0)^2 \right]$$
$$\boldsymbol{Z_{Oo}} = Z_0 \left[\mathbf{1} - JZ_0 + (JZ_0)^2 \right]$$

(2.45)

27

For the design of Bandpass, filters consist of N-section in Figure 2.14 , the important results defined

$$Z_0 J_1 = \sqrt{\frac{\pi FBW}{2g_1}}$$

$$Z_0 J_n = \frac{\pi FBW}{2\sqrt{g_{n-1}g_n}} \text{ For n} = 2, 3 \dots \text{N} \tag{2.46}$$

$$Z_0 J_{N+1} = \sqrt{\frac{\pi FBW}{2g_1}}$$

where

$$FBW = \frac{f_2 - f_1}{f_0} \tag{2.47}$$

2.4.3   U-Shaped Bandpass Filter

The conventional U-shaped coupled resonators are first examined since they consider the core of our proposed work. The straight $\lambda/2$ resonators are large compared to the U-shaped resonators, so the latter type is adopted in our structure. Moreover, the input and output ports can be placed close to each other to enhance the filter selectivity by adding zeros into the filter response. The U-shaped figure comes from folding the arms of the straight $\lambda/2$ resonators into U shape to reduce the size as shown in Figure 2.15.Several of the U-shaped resonators are adjacently placed, and the amount of power transferred among them relies on the space separating them, like the parallel coupled resonators. Hence, the same design equations for parallel coupled $\lambda/2$ resonators can be used. However, to fold the resonators, it is necessary to take into account the reduction in the coupling length, which in turn, reduces the coupling between the resonators. The coupled length is slightly less than a quarter wavelength because each resonator has two bends and there should be a distance to separate between them [7].

To design the U-shaped bandpass filter, the classical filter methodology can be utilized [1]
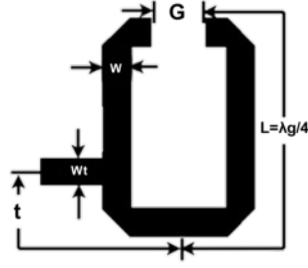
Figure 2.15: The U-shaped bandpass resonator

$$Q_{e1} = \frac{g_0 g_1}{FBW}, Q_{en} = \frac{g_n g_{n+1}}{FBW} \tag{2.48}$$

$$M_{i,i+1} = \frac{FBW}{\sqrt{g_i g_{i+1}}} \tag{2.49}$$

where Q_{e1} and Q_{en} are the external quality factors of the resonators at the input and output, respectively, and $M_{i,i+1}$ are the coupling coefficients between the two adjacent resonators. The g_i is the i-th normalized filter element. The FBW is the fractional band-width. The feeding method used is the tapped-line which is the 50Ω microstrip input (output) feeding transmission line. The location of tapped-line feed is approximately given by:

$$t = \frac{2L}{\pi} \sin^{-1}\left(\sqrt{\frac{\pi Z_0}{2Q_\theta Z_f}}\right) \tag{2.50}$$

where Z_f is the characteristic impedance of the transmission line forming the U-shaped resonator, Z_0 is the characteristic impedance of feeding input (output) transmission line, and L is half the length of the single resonator which is about a quarter wavelength at the design frequency. The advanced system design (ADS) is used to extract the external quality factor and coupling coefficients. Figure 2.16 shows these two parameters. As can be seen in Figure 2.16a, the feeding location (t) plays a vital role in how to control the external quality factor. The external quality factor decreases as t increases. Less input power can be injected into the resonator when t increases. In other words, when

the feeding transmission line approaches to the open-end of the resonator, the power coupling between the feeding transmission line and resonator decreases. Moreover, the space separating between the adjacent resonators controls the amount of power transferred between them, see Figure 2.16b. Thus, these two parameters (i.e., Q_e, and M) are investigated and optimized carefully.

<div align="center">(a)</div>

<div align="center">(b)</div>
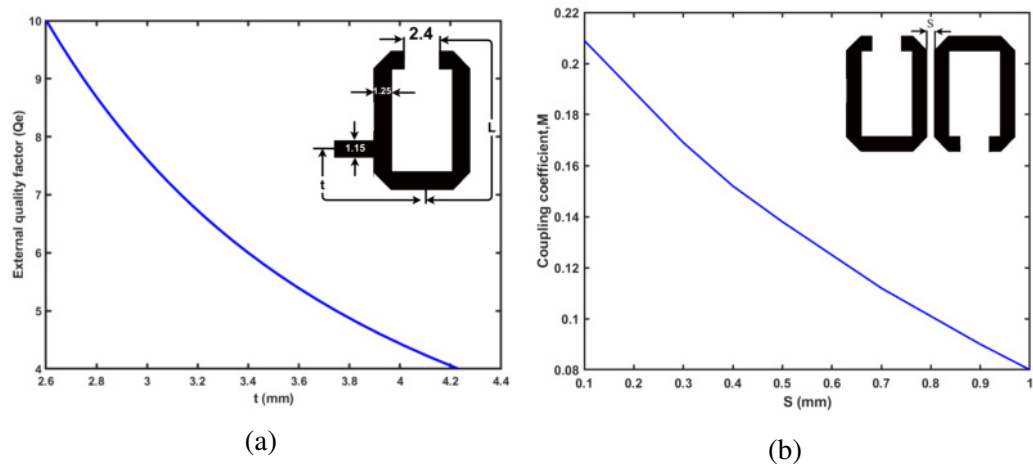
Figure 2.16: Design curves obtained by ADS simulations for designing the microstrip U-shaped BPF (a)external quality factor (b)coupling coefficient

These microstrip bandpass filters operate to pass a certain range of frequencies (i.e., the channel bandwidth), while other frequencies will be rejected as shown in Figure 2.17. In the conventional filters, the rejected signals will be reflected back from where they come due to the high mismatching. This reflection will cause deterioration in the performance of the nonlinear devices such as mixers, amplifiers, oscillators, etc. [8], [9]. To circumvent this problem, the solution is to use the nonreciprocal circulator or isolators to redirect the reflected power into absorptive loads. However, this solution will complicate the design and increase the cost [5].

To avoid using the bulky conventional nonreciprocal devices, the reflectionless filters have attracted a lot of attention recently. These filters have the ability to mitigate the reflected signals for all frequencies for passbands and stopbands, so they are called the reflectionless. Also, there are quasi-reflectionless filters, being able to decrease the
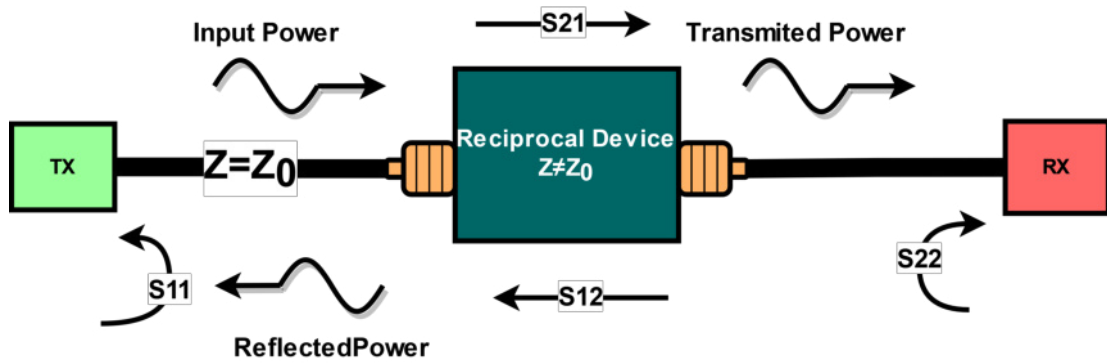
Figure 2.17: Problem of the reciprocity

reflected signals for a wide range of stopband frequencies. The reflected signals are dissipated inside the filter itself by the absorptive parts. Thus, the filter is well matched not only for the passband but also for the stopband [10]. To do so, designers have reported several schemes such as the complementary duplexer, lossy resonators, directional filter, etc. in [10],[11]. The previously mentioned methods, the Complementary diplexer method was used, are explained in detail in the next section

2.5 Quasi-Reflectionless Filters Base on Complementary Duplexer

An obvious way to construct an absorption filter is a diplexer and terminates the branch associated with the unwanted portion of the spectrum with a resistor. Despite the simplicity of its principle, there are many details that must be taken into account. For one, a conventional diplexer will only have low reflections from one side [12],[13]. In[14] it has low reflections from both sides, a bidirectional diplexer is needed.

For reflectionless bandpass filter by using Complementary diplexer as shown in Figure 2.18, the architectures of these filter includes two-channel; the first main of bandpass channel while the other bandstop channel with opposite or complementary transfer functions of the first channel [11], [15]. Therefore, it is the main bandpass channel that defines the characteristics within the band, where it is connected between the input and output terminals and through which the desired signals can travel, while the auxiliary

31

band channel is connected at the input and output ports and terminals with absorptive impedance.
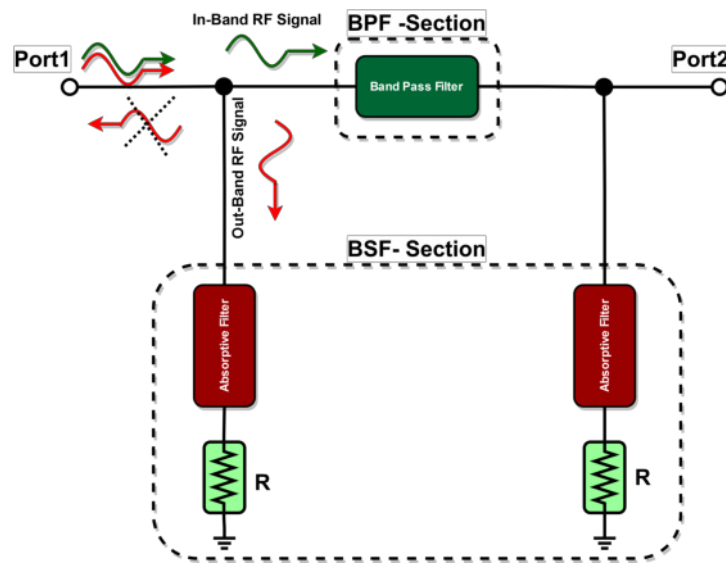
Figure 2.18: Reflectionless BPFs in microstrip technology based on two-port complementary duplexer

After identifying the methods used to solve the problem of reflection power, there is an inherent problem in microwave circuits, which is the problem of reciprocity. There are many concepts of the principle of reciprocity in different physical fields, including electromagnetism, electrodynamics and acoustics in [16–22].

In the field of electromagnetism, the principle of reciprocity means that waves move in the same direction forward and backward in most scenarios. In more formal terms, reciprocity means that the wave propagation remains unchanged if the source and observation points are not change. In microwave engineering, the effects of reciprocity are spread everywhere, such as the antenna that sends in the same way as the receiver, or the energy divider that divides the signal into two signals in one direction and as an energy collector in the opposite direction

Also, according to Lorenz's theory, any medium is linear time-invariant with symmetric permeability and permittivity tensors that must be reciprocal. Since any linear network has a finite number of ports, its scattering matrix S must satisfy the symmetry

or reciprocity condition $S^T = S$ as shown in Figure 2.19a.

The reciprocity in microwave filter means that the signals can travel in both ways on a transmission line without any change. This represents a big problem when an RF device is a full duplex because backward-propagating reflections can inject noise into circuits and even damage devices.
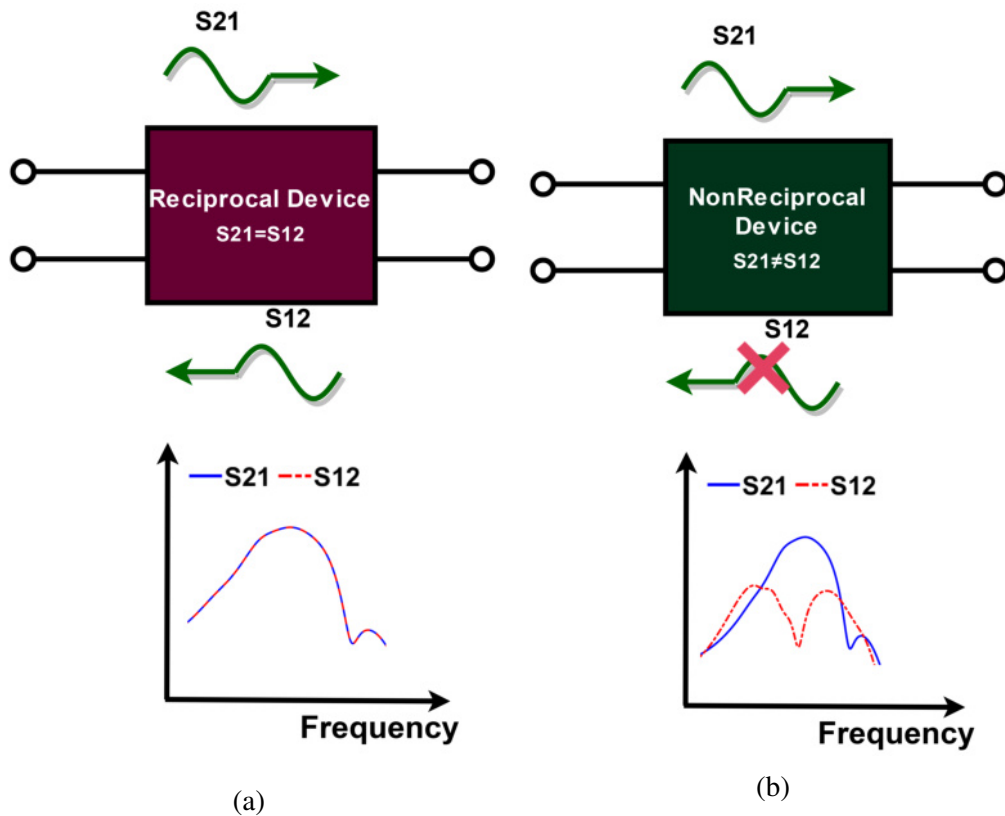
Figure 2.19: Microwave devices (a) reciprocal devices (b) nonreciprocal devices

To break the reciprocity as shown in Fig.2.19(b), the magnetic materials are primarily used to break the reciprocity in which the magnetic field forces signals to pass only in one directions such as in circulators and isolators. These components are bulky and difficult to integrate with printed circuits [23], [24].

In [25], another way, using magneticless components to break the reciprocity, can be integrated with printed circuits. There are three techniques: (i) using the active component such as transistors, (ii) using the non-linearity in impregnation of media

materials (iii) using modulation technique. we will focus on time modulation magnetic less non reciprocal method.

2.6 Nonreciprocity based on Spatial-Temporal Modulation(STM) Technique

Lump-element circuit model of a Bandpass filter topology, as shown in Figure 2.20, consists of three resonant circuits in a form of parallel LC connected to each other by coupling inverter (J12 and J23) in one direction, their terminals connected to ports TX and RX. A parallel static inductance (L0) and capacitance (C0) that determined the center frequency f_0 of the filter
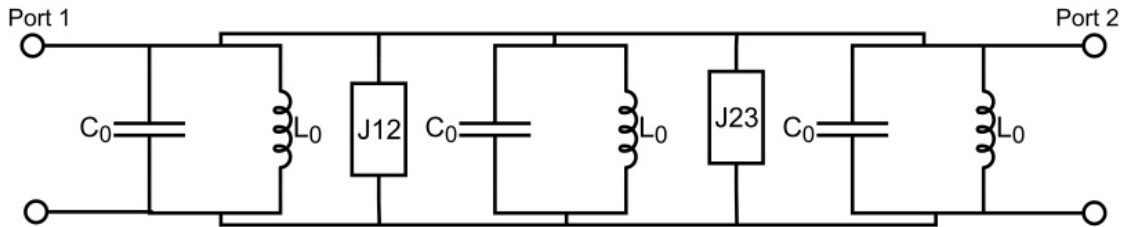
Figure 2.20: 3-pole lumped element reciprocal BPF

The three resonators are modulated with variable capacitors (varcaps) to break the reciprocity of the resonators [26],

$$C_n(t) = C_0 + \Delta C \cos(2\pi f m t + (n-1)\phi) \qquad (2.51)$$

and the capacitance modulation index (Km) is defined as

$$Km = \frac{\Delta C}{C_0} \qquad (2.52)$$

where ΔC is the modulation depth and the modulation frequency (fm). Notice that the modulated signals of all resonators have the same modulation frequency (fm) but they have difference progressive phases ϕ . The forward direction of the phase of each resonators is increased by ϕ deg. Therefore, the amplitudes of the signals remain

34

identical but their phases are different. So, this modulation technique is known as spatiotemporal modulation (STM), because it involves phase variation in time (t) and space (ϕ direction).

When the modulation signals are applied to resonators, they produce various harmonics at f0 $\pm$ fm rather than f0. Between these two frequencies, different phases are produced that interfere with each other constructively in the forward direction and destructive in the opposite direction, hence, allowing to achieve transmission in one port and isolation in another

Figure 2.21 shows the effect of the STM modulation technique on the circuit in Figure 2.20. Each oscillation frequency of resonators $f_n = \frac{1}{2\pi\sqrt{LC_n}}$) is moduatted by signals with amplitude Vm, frequency fm and phase (n-1)ϕ injected through common cathode node of varactor diodes Cn. Moreover, resistors R1 is large to combine the modulation signals with the DC bias Vdc and to ground node of varactor as well [26].

Also, it is worth noting that electronic varactor diodes are based on nonlinear P-N diode, i.e., so the variable capacitance of varactors can be defined as

$$C_n = C_0 + \sum_{k=1}^{\infty} a_k v_n^k \tag{2.53}$$

where a_k are the polynomial coefficients of the nonlinear characteristics CV models around the excitation point, while C0 is the effective static capacitance of each common-cathode varactor diodes pair that set by the DC bias of Vdc, So AC voltage that across the n-th resonator is defined as

$$v_n = v_n^{rf} + v_n^{\text{mod}} \tag{2.54}$$

where v_n is a series of combined signals of modulated incident signal to resonator and modulated signal, because the amplitude of the modulated signal is larger than incident

35
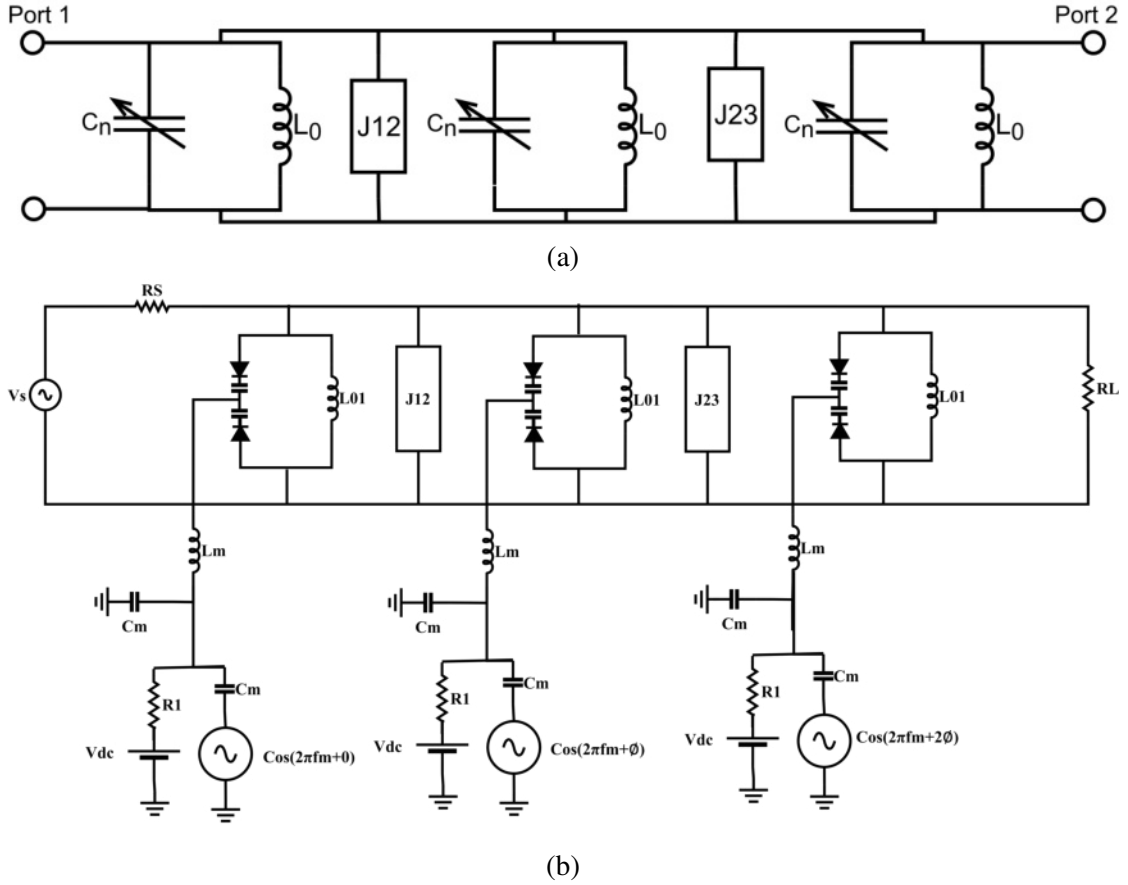
Figure 2.21: 3-pole lumped element nonreciprocal BPF (a) resonator circuite as a parallel static insuctance and varable capacitance (b)resonator circuite as a parallel static insuctance and varactor diode

signal under the assumption $v_n^{rf} \ll v_n^{mod}$, then Eq.2.53can be simplified to

$$C_n = C_0 + a_1 v_n^{\mathrm{mod}} + a_2 \left(v_n^{\mathrm{mod}}\right)^2 + \dots \tag{2.55}$$

To simplify further, we can keep the conditions of the first degree to become the equation

$$C_n = C_0 + a_1 V_m \cos\left(\omega_m t + \varphi_n\right) \tag{2.56}$$

which is exactly the same as Eq.2.51 after substituting φ_n=(n-1)ϕ , $a_1 v_m = \Delta C$ and $\omega_m = 2\pi fm$

2.7 Literature Survey

Filters are the basic building blocks in wireless communication systems, So, they are considered the hot topics that researchers prefer these systems. Therefore, researchers always offer their contributions to develop it or reduce one of the defective issues in it. power reflected at out-of-the-band and the TX/RX isolation (nonreciprocity) are defective issues that have received a lot of attention lately. Some of the previous researchers presented possible solutions to reduce the power reflected issue, which we will present in the first section. The second section will deal with previous studies presented possible solutions to achieve nonreciprocity. [5],[10].

2.7.1 Power Reflection Issue

Reflected signals occur in all RF components due to very high mismatches in the out-of-band frequencies. reflectionless filters can mitigate the reflected signals for all frequencies for passbands and stopbands, so they are called reflectionless. The reflected signals are dissipated inside the filter itself by the absorptive parts. These filters have attracted a lot of attention recently.

To do so, designers have reported several schemes such as the complementary duplexer, lossy resonators, directional filter, etc. The filters can be designed using either the lumped elements or the transmission lines. When using the lumped elements, the even-odd mode analysis will be the appropriate way to design reflectionless filters. Morgan and Boyd [27] in 2011 presented and design a new class of reflectionless filter. The circuits are symmetrical, so the even and odd modes of the S11 have the same magnitudes but with opposite phases,resulting in the cancellation of S11. Also, the authors introduced the procedure to convert from lowpass filters into highpass filters, bandpass filters, and bandstop filters with all mathematical background. Morgan et . al.

In [28] in 2018 introduced an extended work of thier previous concepts work [27]. The n-order distributed counterpart reflectionless filters relied on lowpass prototypes are reported in 2019 by J.Hong [29]. The main channel contains only one resonator, while the absorptive part can be any order to enhance the filter response. To obtain a certain transmission response, symmetrical lumped reflectionless filter is proposed in 2019 by J.Lee et.al [30]. The design requires a large number of lumped elements with operation frequency limitations associated with the lumped elements, so this problem are solved in 2014 by C.Jackson [31] using the distributed (transmission lines). Richards and Kuroda identities transformations are utilized.

One of other important schemes of reflectionless filters is complementary duplexer which consists of two channels; the main one is to pass the interesting signals from the input to the output, while the other is to absorb the unwanted signals. M.Khalaj-Amirhosseini et.al [12] in 2017, authors used only one absorptive stub located at the input port to reduce the reflections exploiting the complementary duplexer technique. The same previous idea is also used by R.Gomez-Garcia et.al [13] in 2018, but the filter is multiband where even the absorptive stub is multiband stop filter. C.Luo et.al [32] in 2019,introduced the theoretical design of a particular kind of input-reflectiveless RF/microwave bandpass filters (BPFs) and bandstop filters (BSFs) is provided using a coupling-matrix technique. They are based on diplexer topologies with complementary transfer functions of variable order. The energy that is not transmitted by this branch of these reflectionless filters is totally dissipated by the loading resistor of the other channel.However, R.Gomez-Garcia et.al [14] in 2019 , a symmetric quasi-reflectionless is reported by adding the absorptive stubs at both two ports. The two absorptive stubs are the same order.

Reflectionless filters, based on lossy stubs, consist of a transmission line (stub) in series with an absorptive resistor to mitigate the reflection. Absorptive bandstop filters

based on lossy resonator are presented by J.-Y.Shao and Y.-S.Lin [33] in 2015. Jeong et. al [34] in 2019 ,presented only one port 3-pole distributed absorptive bandpass filter in which the first resonator is loaded with a resistor in series with short stub. Wu, Xiaohu et.al [35] in 2019, presented the input and output of the coupled-line sections are loaded with an absorptive stub made comprised of a series resistor and a shorted quarter-wavelength stub. These stubs appear as an open circuit at the center frequency. To improve absorption performance across the entire bandwidth, a single absorptive stub can be divided into two identical stubs that load both ends of the coupled lines.While in 2020 Wu, Xiaohu et.al [36], presented a coupled-line bandpass filter loaded with a 2-pole bandstop that converts to absorptive stubs to achieve passband flatness and good impedance matching on both in-band and out-of-band. The out-of-band rejection was improved due to the cross-coupling between the absorptive stubs. Another topology to implement reflectionless BPFs is the use of directional filters by Kim and Jeong Phill [37]in 2011, but this type has disadvantages such as high insertion loss, limited bandwidth, and large size.

2.7.2 Reciprocity Issue

As mentioned previously, the filters are passive elements that work according to the principle of reciprocity. The reciprocity is defined as the transmission of signals in both directions without any change. It has been shown to be a real problem, especially in full duplex systems. So this subsection contains some research effort to break the reciprocity, making the device work in only one direction. These efforts are still in its early stage. Thus, there are of research possibilities that can increase the non-reciprocity.

The magnetic materials are primarily used to break the reciprocity in which the magnetic field forces signals to pass only in one directions such as in circulators and isolators. These components are bulky and difficult to integrate with printed circuits by

Seewald et.al [38] in 2010. So no practical printed nonreciprocal components are found until the emergence of the spatio-temporal technology. However, some techniques are used to obtain nonreciprocal components, and they suffer from several drawbacks like limited bandwidth, low efficiency, high noise, etc. Active devices are utilized in different topologies to obtain gyrators by Morse et.al [39] in 1964, and circulators and isolators by Tanaka et.al [40]in 1965. However, this approach is not preferred because the active bias adds noise and non-linear distortions by Carchon et.al[41]in 2000. The saptio-temporal modulation technique is the best alternative to circumvent all the previous problems. Biedka et.al [42]in 2017 ,presented ultrawideband nonreciprocity is achieved by using of six transmission lines of equal length and five switches that are turned on and off sequentially to obtain separate transmission and reception. Magneticless non-reciprocity can also be achieved by magneticless angular momentum bias depending on the spatiotemporal azimuthal modulation (STM) of the relative permittivity of the ring resonator by Sounas et.al[43] in 2013. Magnetic less circulators are constructed from three LC resonators in form Δ- and Y with spatiotemporally modulating in[44, 45].Nafe et.al [44] in 2019,presented three 2-pole bandpass (series LC resonators) filters connected in a Y topology to form the circulator . Each resonator coupling with the other by a shunt capacitor C12. The nonreciprocity is achieved based on angular momentum biasing that is implemented by modulating the capacitance of each resonator at the same frequency, but with a 120 phase shift across the three filter branches. The circulator introduced by Kord, Ahmed [45] in 2018 has two structures, the first consists of three one-pole LC bandpass filters coupled in a Y topology, and the second consists of three one-pole LC bandstop filters connected in a Δ-topology. the nonreciprocity is achieved at the same in [44].

Non-reciprocal BPF has been reported by Wu, Xiaohu et.al [46] in 2019 to achieve BPF and isolator functions in a single device by Spatio-temporal modulation of a lumped-

element coupled resonator filter.

This technique was expanded using planar microstrip resonators by Wu, Xiaohu et.al [47] in 2020 .The structure of a frequency reconfigurable microstrip non-reciprocal bandpass filter based on spatial-temporal modulation. It consists of three open-ended resonators in a U-shaped form coupled with each other by coupling J-invertor and three-time varying capacitance (varactor diodes) are loaded directly into the open ends of the resonators .The frequency nonreciprocity is achieved by modulating these varactors with a progressive phase shift and the same frequency modulation through a single inductor in the center of the resonator to improve the biassing isolation.

Having discussed and reviewed the two techniques (i.e., the reflectionless and the nonreciprocal) in separate parts as demonstrated above because no one presents a structure combining them in the same design.

In this thesis, we will fill the gap in the literature by combining these two techniques in a single design to obtain nonreciprocal reflectionles bandpass filter that can be Programmable to Several functions including (only reflectionless but reciprocal ,only nonreciprocal but reflection , reflection and nonreciprocal in the same time and conventional filter). Table 2.1 shows comparison with the state of the previous literature.

Table 2.1: Comparison with the state of the previous literature

References	Type of response	Method	S11 in dB	S21 in dB	S12 in dB	Center frequency	Band in MHz	Tunable Range
[14]	Quasi-Reflectionless	Complementary duplexer	-7 dB in (f/f0 = 0.68 − 0.9)	- 0.9 dB	- 0.9 dB	2.5	455	----
[35]	Quasi-Reflectionless	Lossy stubs	-5.5 dB in (f/f0 = 0.68 − 0.9)	- 0.63 dB	- 0.63 dB	2.45	550	----
[46]	Nonreciprocal	STM	> -15 dB	-1.5 dB	> -20 dB at in band	200 MHz	30	----
[47]	Nonreciprocal	STM	> -16.1 dB	-3.9 dB	> -20 dB at in band	1 GHz	42	885-1031 MHz
this work	Nonreciprocal	STM	> -23 dB	-3.17 dB	-21.2dB at f=3.7 GHz >-10 dB (3.1-3.97GHz)	3.5 GHZ	670	----
this work	Quasi-Reflectionless	Complementary duplexer	- 43 at 3.5GHz > -10 at(2.5 − 3)GHz > -15 at (3.8 − 5)GHz	-1.77 dB	-1.77 dB	3.5 GHZ	670	----
this work	Tunable Nonreciprocal	STM	>-25 dB at (3.37-3.6GHz)	-2.9 at (3.37-3.6)GHz	>-25 at 3.4-3.5GHz > -10dB at (3.- 4GHz)	3.5 GHZ	670	3.37-3.6 GHz
this work	Nonreciprocal Quasi-Reflectionless	Complementary duplexer and STM	> -10 dB in (f/f0=0.68 − 0.9) > -15 dB in (f/f0 = 1.5 - 1.53)	-3.36 dB	> -22 dB at in band	3.5 GHZ	670	----

CHAPTER 3

DESIGN AND IMPLEMENTATION OF NONRECIPROCAL

REFLECTIONLESS RADIO FREQUENCY SYSTEM

3.1 Introduction

This chapter, firstly, discusses and proposes a solution to the power reflection problem. The proposed filter alters the route of reflected power into absorptive loads. Several orders of U-shaped filters that almost don't reflect light are simulated, but the third order is chosen to be made in order to prove the proof-of-concept.Because it is less complicated, expensive, and an acceptable response compared to the higher order. Secondly, this chapter deals with solving the problem of reciprocity by making the device operate in only one direction (nonreciprocal devices). Reciprocity is broken based on spatial-temporal modulation (STM). The proposed filter is mathematically analysed and numerically simulated to demonstrate its performance. Several parameters that have an influence on the overall performance are investigated. Again, here, the dual-band and tunable nonreciprocal BPF are presented. Finally, the designs that solve the two main problems are combined into one design called the quasi-reflectionless nonreciprocal band pass filter with tuning capabilities.

3.2 Methodology of Nonreciprocal Reflectionless Filter

Figure 3.1 shows the flowchart of the methodology of proposed filter filter.
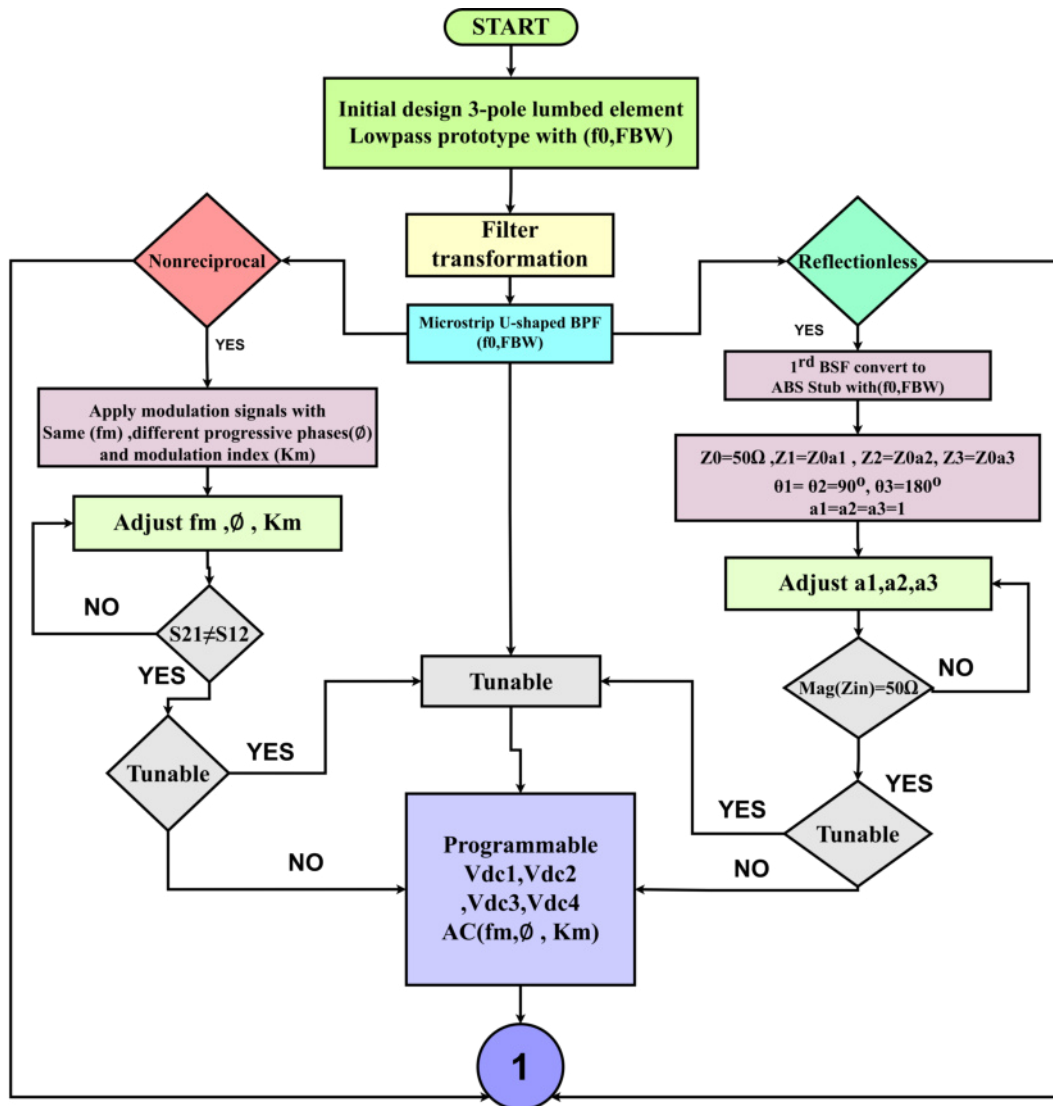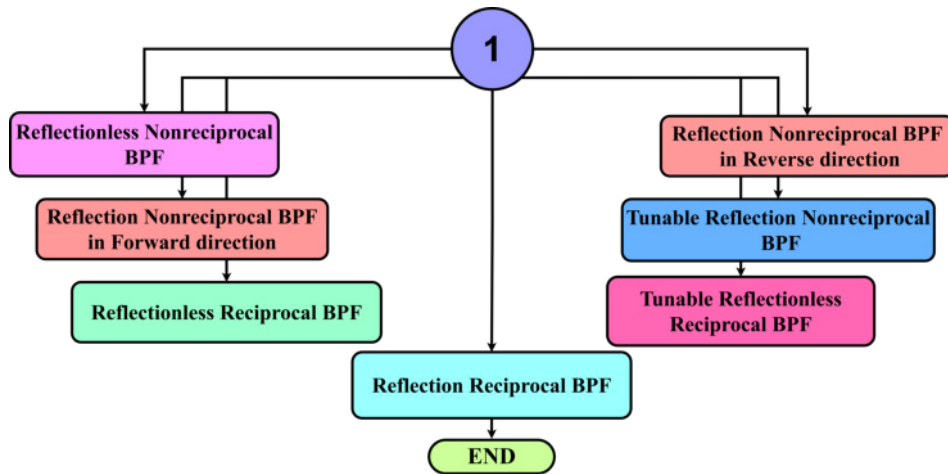
Figure 3.1: Methodology flowchart of nonreciprocal reflectionless filter a) part 1 b) part 2

3.3 Third Order U-Shaped Quasi-Reflectionless Bandpass Filter

In this section, a comprehensive study on how to analyze, design, fabricate and test of the 3-pole U-shaped quasi-reflectionless BPF is introduced. Several parameters will be investigated to optimize the overall performance.

3.3.1 Mathematical Background of The proposed Filter

In this subsection, the main points discussing the mathematical background and main filter parts are introduced.First, explains the operation of the absorptive stubs ABSs. Second, determines the input impedance of one-port U-shaped quasi-reflectionless BPF design

3.3.1.1 Absorptive Stub (ABS)

In this part, a detailed analysis of converting one pole bandstop filter to absorptive stub (ABS)is provided. Instead of using the output port, it is replaced by a resistor as shown in Figure3.2. The resistor acts to absorbs the power.Figure 3.2 illustrates the conversion procedure of the ABS stub.

In Figure3.2a, an open-end quarter wavelength shunt stub is proposed as first order bandstop filter. Z_{st} and θst are its characteristic impedance and its electrical length. ZA and ZB denote the input and output port impedances, respectively. The electrical length of $\theta st = 90^0$ at the stopband center frequency f_0.

$$\text{Zin} 1 = -jZst \cot(\theta st) \tag{3.1}$$

where $Zin1$ is the input impedance of shunt stub. If Zst increases, it may lead to obtain narrower FBW. This causes a serious difficulty in implementation. To circumvent
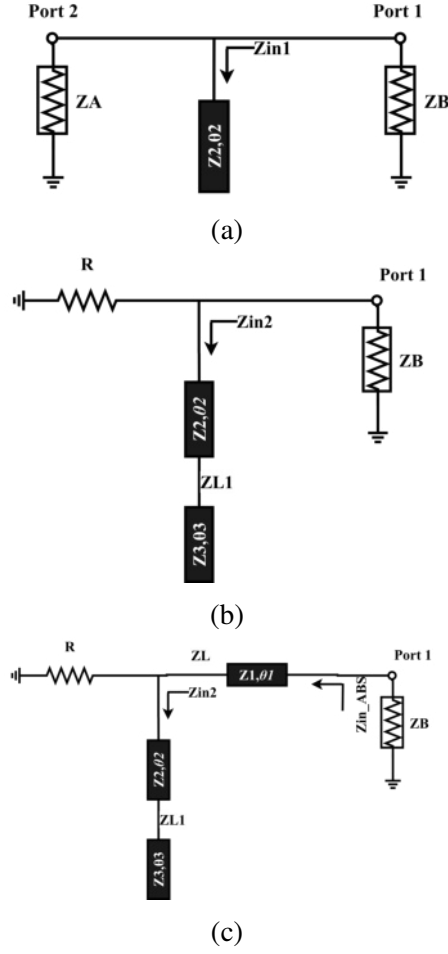
Figure 3.2: The procedure of converting the conventional one-pole band stop filter into its ABS counterpart (a) the conventional one-pole bandstop filter (transmission line model) (b) the conventional one-pole bandstop filter (simplified circuit with the same responses) (c) the proposed absorptive filter

this problem, another transmission line with an electrical length of $\theta 3 = 180^0$ and a characteristic impedance of Z3 is added in series into the shunt stub as shown in Figure 3.2b. The input impedance seen at the beginning of the shunt stub can be calculated as in

$$Z\in 2 = Z2 \frac{-jZ3\cot(\theta 3) + jZ2\tan(\theta 2)}{Z2 + Z3\cot(\theta 3)\tan(\theta 2)} \tag{3.2}$$

$Zin2$ can be matched to the input port by inserting a quarter-wavelength transformer, with an impedance of $Z1$ and electrical length of $\theta 1$, between the input port and the shunt stub. Then, the input impedance of entire absorptive part Z_{inABS}, depicted in Figure 3.2c is:

$$Z_{in-ABS} = Z1 \frac{ZL + jZ_1 \tan(\theta1)}{Z_1 + jZL \tan(\theta1)}$$

(3.3)

$$ZL = \frac{-jRZ2Z3 \cot(\theta3) + jRZ2^2 \tan(\theta2)}{-jZ2Z3 \cot(\theta3) + jZ2^2 \tan(\theta2) + jRZ3 \cot(\theta3) + jRZ2 \tan(\theta2)}$$

For any lossless two-port network, such as the one in Fig.3a, the conservation of power requires [5]

$$|S_{11}|^2 + |S_{21}|^2 = 1$$

(3.4)

while for the absorptive single-port circuit depicted in Figure 3.2c, the power is either reflected back to port 1 or absorbed by the resistor R. Here, we define the S_{11_ABS} and S_{a-ABS} as the reflection and absorption coefficients of the absorptive filter, respectively. Therefore, we have:

$$\left|S_{11\_ABS}\right|^2 + \left|S_{a\_ABS}\right|^2 = 1$$

(3.5)

Figure 3.3 compares the responses resulting from the designs depicted in Figure 3.2. The reflection coefficient ($S11$), transmission or absorption coefficients ($S21$), and the magnitudes of input impedances are provided. Here, a bandstop filter operating at 3.5 GHz with 0.1 dB passband ripple and 83% stopband fractional bandwidth is used as an example. The circuits in Figure 3.2 were, analyzed, designed, and simulated to at $3.5GHz$, where the x-axes show the normalized frequencies. The lowpass prototype element values are found to be $g0 = 1, g1 = 0.3052, g2 = 1$. The circuit parameters of BSF are $ZA = 50\Omega, ZB = 50\Omega, Zst = 211.5\Omega$ and the parameters of ABS are $R = 50\Omega, Z1 = 56.5\Omega, Z2 = 71.5\Omega, Z3 = 71.5\Omega, \theta1 = \theta2 = 90^0$, and $\theta3 = 180^0$.

The blue traces represent responses of the BSF(a), and the responses confirm the BSF behavior. Although the BSF(b) has one port, its responses (red traces) are the same
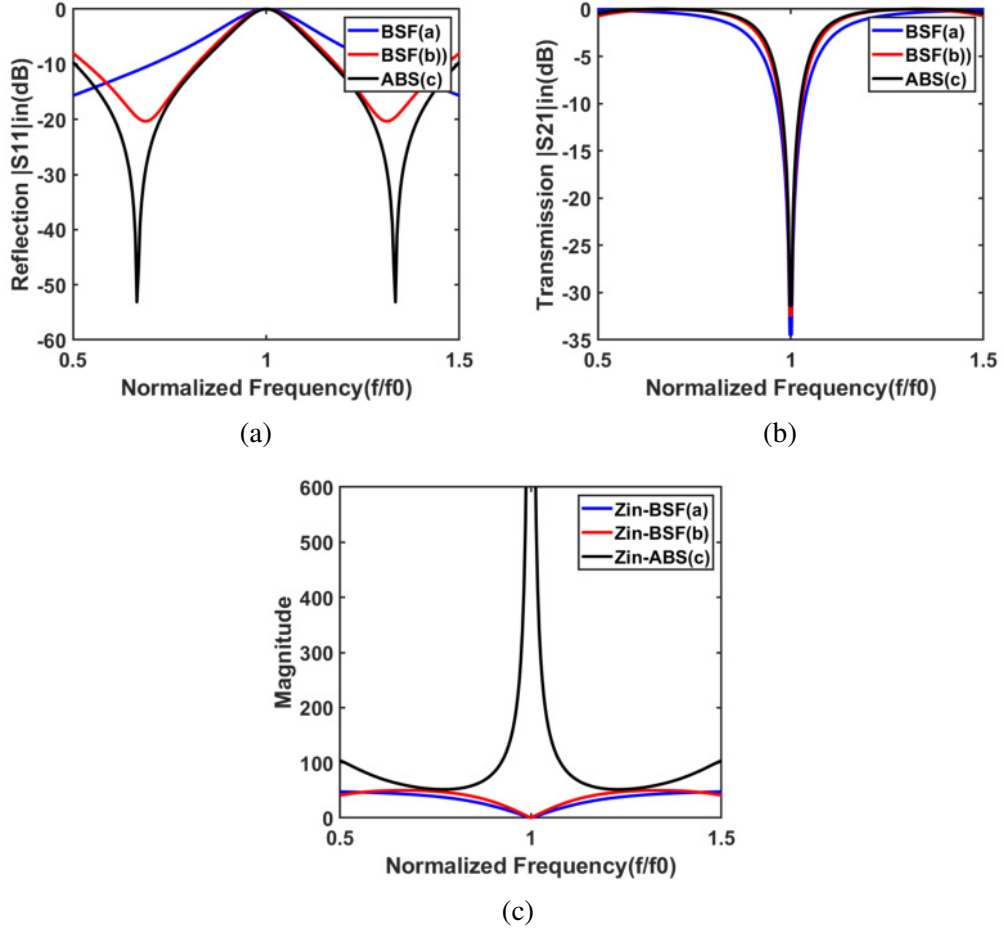
Figure 3.3: Reflection and transmission (absorption) coefficients, and magnitudes of the input impedances for the designs evolved in Figure 3.2 (a)Reflection$S11$ (b)transmission $S21$ (c)magnitudes of the input impedances $mag(Z)$

as the former one. Away from the resonance, the power will be absorbed by the resistor (Figure 3.2b) instead of transferred into the output port (Figure 3.2a). At the resonance, both the first two designs have short circuit input impedances. Thus, the reflected signals will be out-of-phase with the main RF signals, and the destructive interference will occur. In our proposed design, the input impedance should be very high (i.e., close to the open circuit behavior) to ensure the RF signals can pass directly to the main bandpass filter. The last design in Figure 3.2 uses an impedance inverter which is a quarter-wavelength transmission line. As demonstrated in Figure 3.2c, the input impedance is very high, more than 500Ω, guaranteed to make the instructive interference. Also, there are two symmetrical transmission poles located before and after the resonance

frequency. They aid to enhance the overall performance.

There are a few observations obtained from Figures 3.2 and 3.3

1. Circuit in Figure3.2b is an equivalent to circuit Fig.3.2a in term of a magnitude of the input impedance .

2. Figure 3.3c shows the $mag(Z_{in-BSF})$ and $mag(Z_{in-ABS})$. The value of $mag(Z_{in-BSF)}$ at the resonant frequency is zero (i.e. short circuit), whereas, the value of $mag(Z_{in-ABS})$ is optimized to be as high as possible.

3. Figure 3.3b demonstrates that all the three circuits introduced in Figure 3.2 have the same transmission (absorption) in both the stopband and passband.

3.3.1.2 Input Impedance of One–Port U-Shaped Quasi-Reflectionless BPF

The U-shaped quasi-reflectionless bandpass filter based on the complimentary duplexer method will be designed and analyzed here. It has two channels. The first (main) channel is to pass the desired signals into the output (i.e., the BPF), while the second (auxiliary) channel is to absorb the undesired signals (i.e., the ABS). Figure 3.4 shows the proposed filter but with only the input port and one ABS for the sake of simplicity. Z_{in} is the input impedance at the port one which represents the parallel combination of the input impedance of the U-shaped $BPF(Z_{in-BPF})$ and the input impedance of the absorptive stub (Z_{in-ABS}). $Z_i n$ can be written as:

$$Z_{in} = \frac{Z_{in-BPF} * Z_{in-ABS}}{Z_{in-BPF} + Z_{in-ABS}} \qquad (3.6)$$

The reflection coefficient $(S11)$ of the quasi-reflectionless bandpass filter is :

$$S_{11} = \frac{Z_{in} - Z_0}{Z_{in} + Z_0} \qquad (3.7)$$
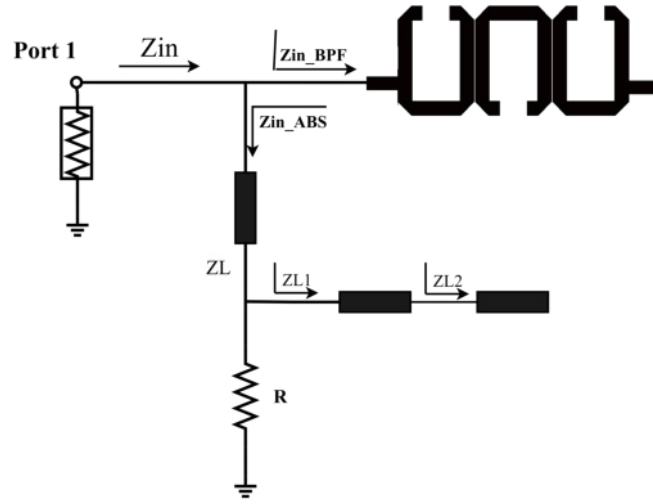
Figure 3.4: U-shaped quasi-reflectionless BPF.

To further explore the mechanism of reflectionless behavior, the magnitude of Zin must be matched to Z_0 at all frequencies. However, the magnitude of Z_{in-BPF} should be matched to Z_0 at in-band frequencies and mismatched at out-of-band frequencies, whereas the magnitude of Z_{in-ABS} should be mismatched to Z_0 at in-band frequencies and matched to Z_0 at out-of-band frequencies. This theoretical explanation results in $S11$ equal to zero at all frequencies. Practically, this is impossible because the input impedances of the two channels forming the quasi-reflectionless BPF are functions with frequency and not equal to 50Ω throughout a frequency range. However, the proposed design offers the input impedance close to 50Ω at a wide frequency range. Fig.6 displays the magnitudes of Z_{in-BPF} and Z_{in-ABS}. It is evident from the results that when the BPF is matched, the ABS is mismatched, and vice versa.
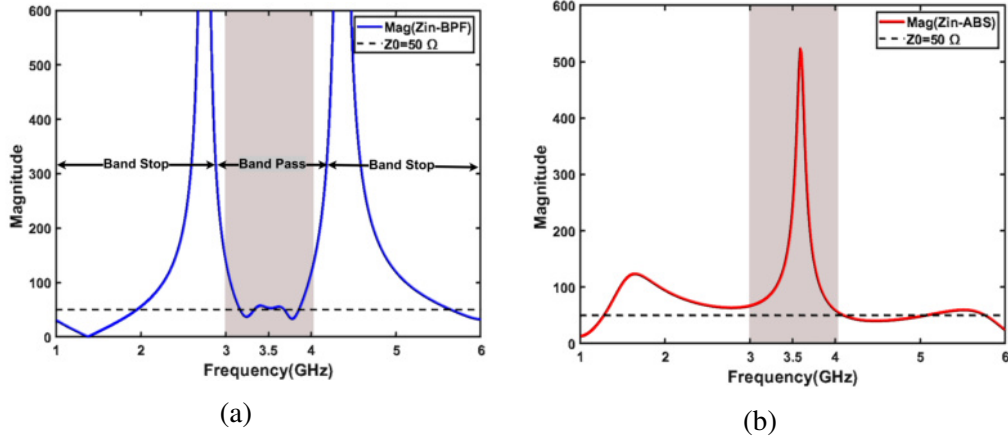
Figure 3.5: Input impedance of one-port U-shaped quasi-reflectionless (a)magnitude Z_{in-BPF} (b)magnitude Z_{in-ABS}

3.3.2 U-Shaped Quasi-Relfectionless Bandpass Filter Design

This section is divided into four parts. The first part deals with the design of conventional and quasi-reflectionless 3-pole U-shaped BPF. Then, in the second part, discussing effects of the ABS stub on the overall bandwidth of the proposed design is introduced. Next,U-shaped quasi-reflectionless filters with various orders are investigated. Ultimately, improving the out-of-band rejection based on the cross-coupling technique is presented.

3.3.2.1 3-Pole U-Shaped Quasi-Reflectionless BPF

In this subsection, the 3-pole U-shaped quasi-Rflectionless BPF is designed and analyzed. For this design, the fractional bandwidth $FBW = 20\%$ or $FBW = 0.2$ at a resonant frequency $f_0 = 3.5GHz, n = 3$ (Butterworth lowpass type). The lowpass prototype parameters, with respect to a normalized lowpass cutoff frequency $\omega_c = 1$, are $g_0 = 1, g_1 = 1, g_2 = 2$ and $g_3 = 1$. Table3.1 shows the physical dimensions of 3-pole U-shaped BPF relying on Eqs.2.48-2.50 and curves provided in in Figure 2.16. In Fig.3.6c, two ABS stubs are connected into the output and input ports, converting the conventional bandpass filter into the quasi-rflectionless bandpass filter.

51
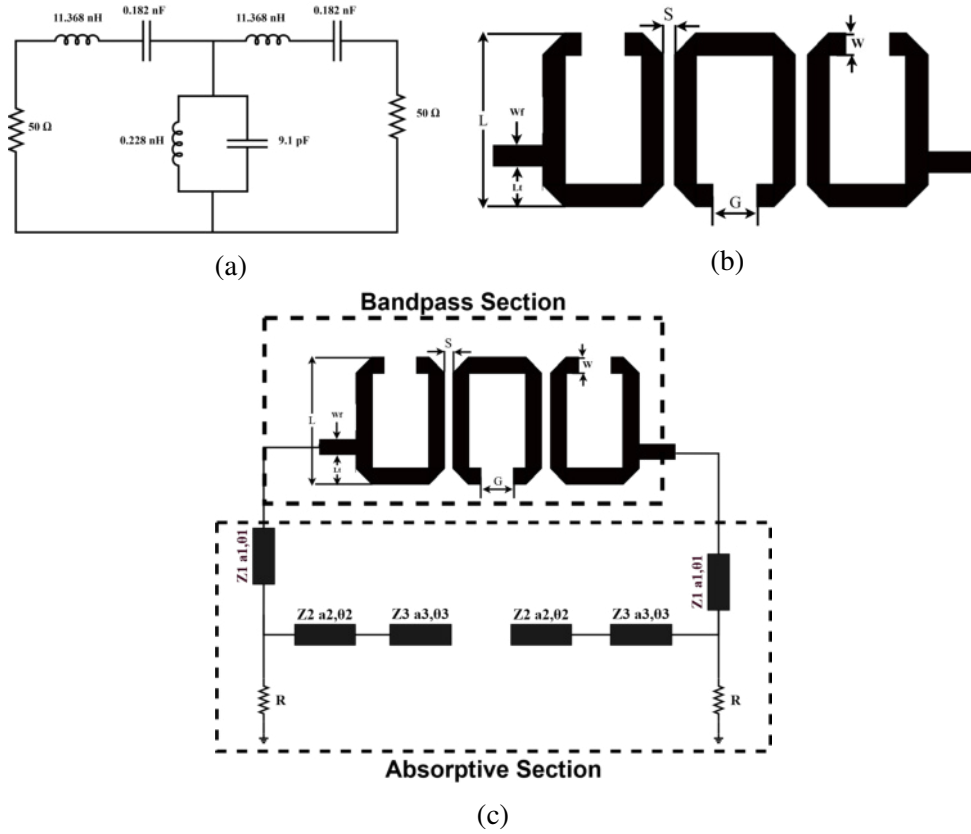
Figure 3.6: (a) Lumped element 3-pole BPF (b) the layout of 3-pole U-shaped BPF (c) the layout of 3-pole U-shaped BPF with the transmission line circuit model of the ABS stubs connected into the output and input ports

Table 3.1: The physical dimensions of U-shaped BPF

Parameters	Measurements in(mm)
Length (L)	10.05
Taped in length (Lt)	2.62
Space between the resonators (S)	0.5
Gap between open end of U-shaped BPF (G)	2.4
Width (W)	1.25
Width of feed (Wt)	1.15
Taped input (t)	3.75

The parameters $(a1, a2, a3)$, shown in Figure 3.6c, are scaling factors used to optimize the performance of the transmission and absorption. Figures 3.7-3.10 show the parametric studies of the reflection and transmission coefficients and the magnitude of input impedance of the U-shaped quasi-rflectionless bandpass filter. The nominal values

52

of the various parameters are the same value at example given in Section3.3.1.1. As can

be observed, the bandwidth of the quasi-rflectionless filter is mainly determined by the

bandwidth of the absorptive filter that will be discussed in the subsequent part. Typ-

ically, the U-shaped BPF provides larger bandwidth compared to the ABS stubs [29],

where spacing S between the U-shaped resonators governs the bandwidth of the BPF.

Thus, the goal is to make the ABS stub having bandwidth as wide as possible. Fig-

ure 3.7 exhibits the frequency responses of the proposed filter shown in Figure 3.6c for

different values of S. The widest bandwidth can be obtained if $S = 0.2mm$, because

the bandwidth of the U-shaped bandpass filter becomes larger than the reflection band-

width of the ABS stub, so we can leverage from this point to obtain the possible widest

bandwidth. However, for practical issues such as the fabrication tolerances using the

chemical etching method, $S = 0.5mm$ was chosen.

(a)

(b)

(c)

Figure 3.7: Simulated frequency responses of the 3-pole U-shaped quasi-reflectionless BPF with respect to S ($Z_0 = 50\Omega, Z1 = Z0*a1\Omega, Z2 = Z0*a2\Omega, Z3 = Z0*a3\Omega, \theta1 = \theta2 = 90^0, \theta3 = 180^0, a1 = 1, a2 = 1, a3 = 1$)

Moreover, the values of $a1, a2$ and $a3$ can be adjusted to improve the absorption performance (i.e., reducing the reflection in out-of the passband and even inside the passband). In other words, the reflected signals from the main channel of the proposed filter will be largely directed into the absorption branch, the ABS stub. As shown in Figure 3.8 the value of $a1 = 1.128$. When $a1 = 0.9$, the wide band of absorption is noticed, but the filter offers higher reflection compared to the response when $a1 = 1.128$. Also, the filter transmission deteriorates. Here, $a2$ is varied to investigate its
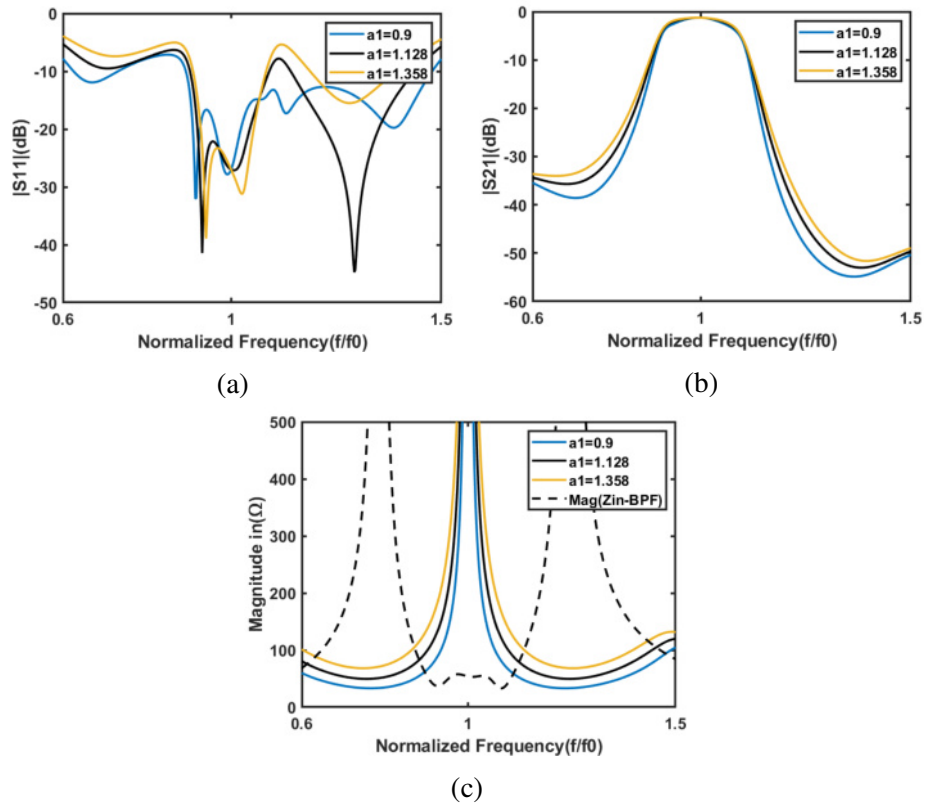
Figure 3.8: Simulated frequency responses of the 3-pole U-shaped quasi-reflectionless BPF with respect to $a1$ ($Z_0 = 50\Omega$, $Z1 = Z0 * a1\Omega$, $Z2 = Z0 * a2\Omega$, $Z3 = Z0 * a3\Omega$, $\theta1 = \theta2 = 90^0$, $\theta3 = 180^0$, $a2 = 1$, $a3 = 1$, $S = 0.5mm$)

influences on the overall performance of the proposed filter. Figure 3.9 demonstrates that the best value of $a2 = 1.43$ in terms of the absorption. The matching between Z_{in-BPF} and Z_{in-ABS} is increased because the value of reflection decreased for the out-of-band of the normalized frequency (f/f_0) ranging from 0.65 to 0.9 (less than is 12 dB), and from 1.12 to 1.145 (less than is 15 dB). In addition, the increase in the

matching inside the band is achieved, although we find that the value of the transmission deteriorated slightly. The value of $a3$ is also chosen to be 1.43, see Fig.3.10.
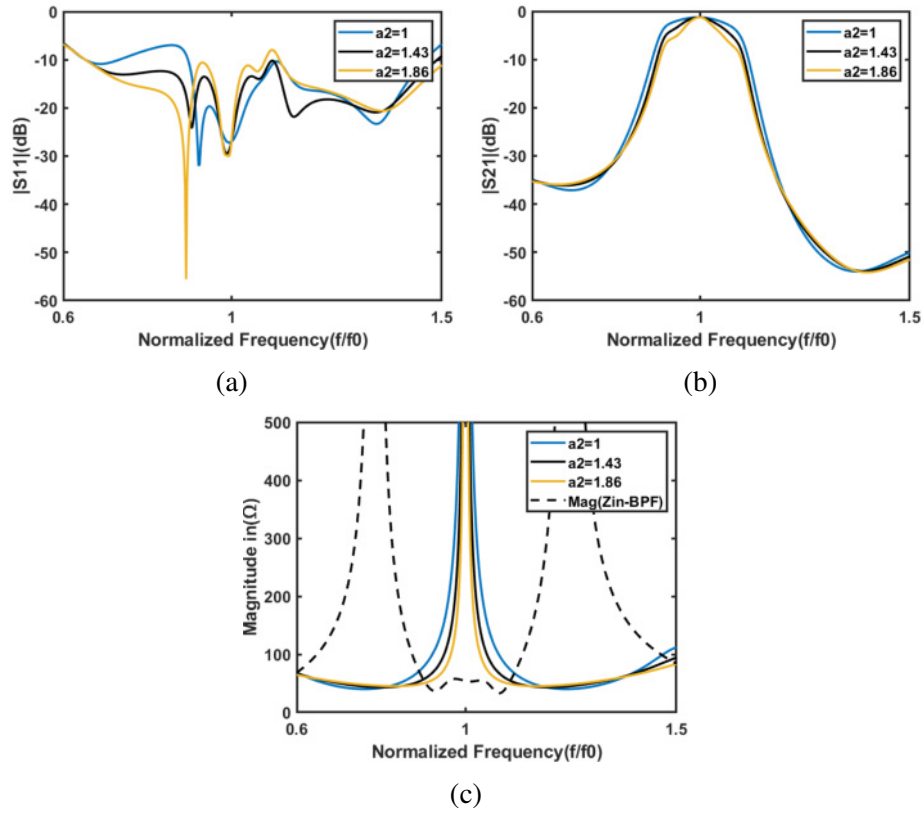
Figure 3.9: Simulated frequency responses of the 3-pole U-shaped quasi-reflectionless BPF with respect to $a2$ ($Z_0 = 50\Omega, Z1 = Z0 * a1\Omega, Z2 = Z0 * a2\Omega, Z3 = Z0 * a3\Omega, \theta1 = \theta2 = 90^0, \theta3 = 180^0, a1 = 1.128, a3 = 1, S = 0.5mm$)

To this end, the most important parameters of the proposed design were optimized. Figure 3.11 shows the transmission and reflection coefficients and the magnitude of input impedance for the optimized 3-pole U-shaped quasi-reflectionless bandpass filter and the conventional 3-pole U-shaped BPF. Obviously, both designs given in Figure 3.6 show the same transmission characteristics with a passband centered at $3.5GHz$ and two cutoff frequencies ($f1 = 3.16GHz$) and ($f2 = 3.83GHz$). The filter in Figure 3.6c has higher selectivity and sharper roll-off compared to the design in Figure 3.6b, thanks to the ABS stub section. The reduction in the reflection coefficient is very apparent. In other word, the quasi-reflection less property is satisfied. The dashed red trace in Figure 3.11 show three reflection zeros in the reflection coefficient response to confirm that the
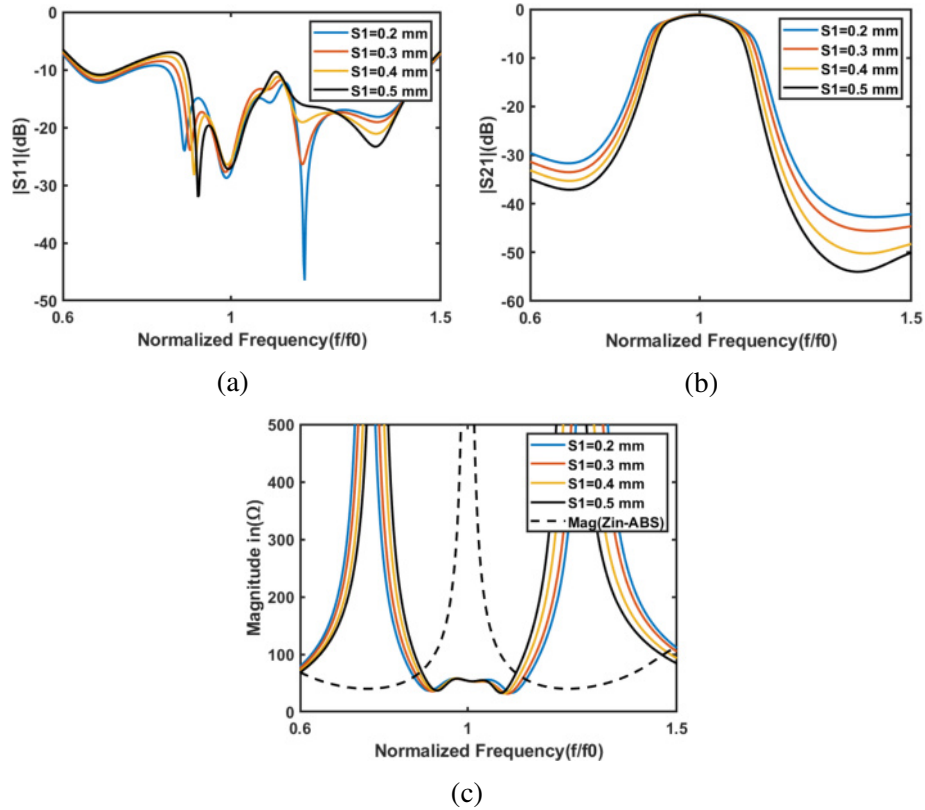
(a)

(b)

(c)
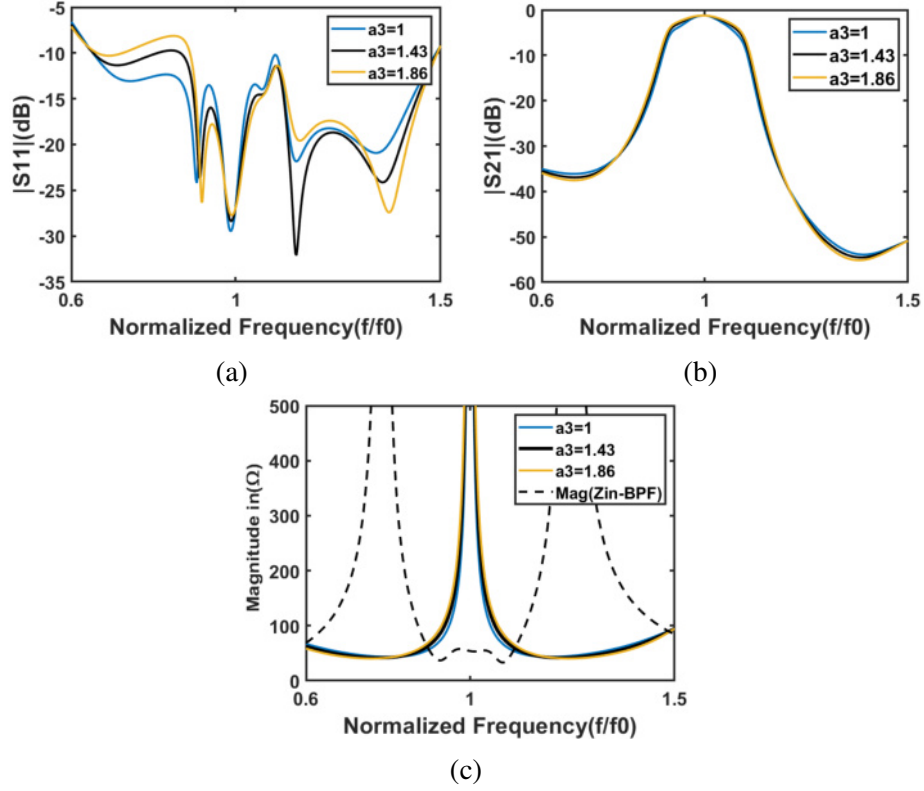
Figure 3.10: Simulated frequency responses of the 3-pole U-shaped quasi-reflectionless BPF with respect to $a3$ ($Z_0 = 50\Omega$, $Z1 = Z0 * a1\Omega$, $Z2 = Z0 * a2\Omega$, $Z3 = Z0 * a3\Omega$, $\theta1 = \theta2 = 90^0$, $\theta3 = 180^0$, $a1 = 1.128$, $a2 = 1.43$, $S = 0.5mm$)

filter consists of three resonators. More reflection zeros are added by the ABS to the full response of the proposed design (i.e., the blue solid trace). The proposed design has almost input impedance equal to 50Ω of $2GHz$ to $5.5GHz$, although there is a ripple in the center frequency owing to the change in the phase of the transmitted signal near the resonance. The input impedance is between $32.3\Omega and 83\Omega$ at the that frequency range. The reflection response of the 3-pole U-shaped quasi-reflectionless filter is below -$20dB$ across the frequency range of $3.96GHz-4.07GHz$ and near -$10dB$ for the range from $2.18GHz-3.012GHz$. Also, full matching inside the passband is carried out, and the ABS filter helps to eliminate out-of-band signals near the passband and significantly improves the close-in rejection.

56

(a)   (b)

(c)
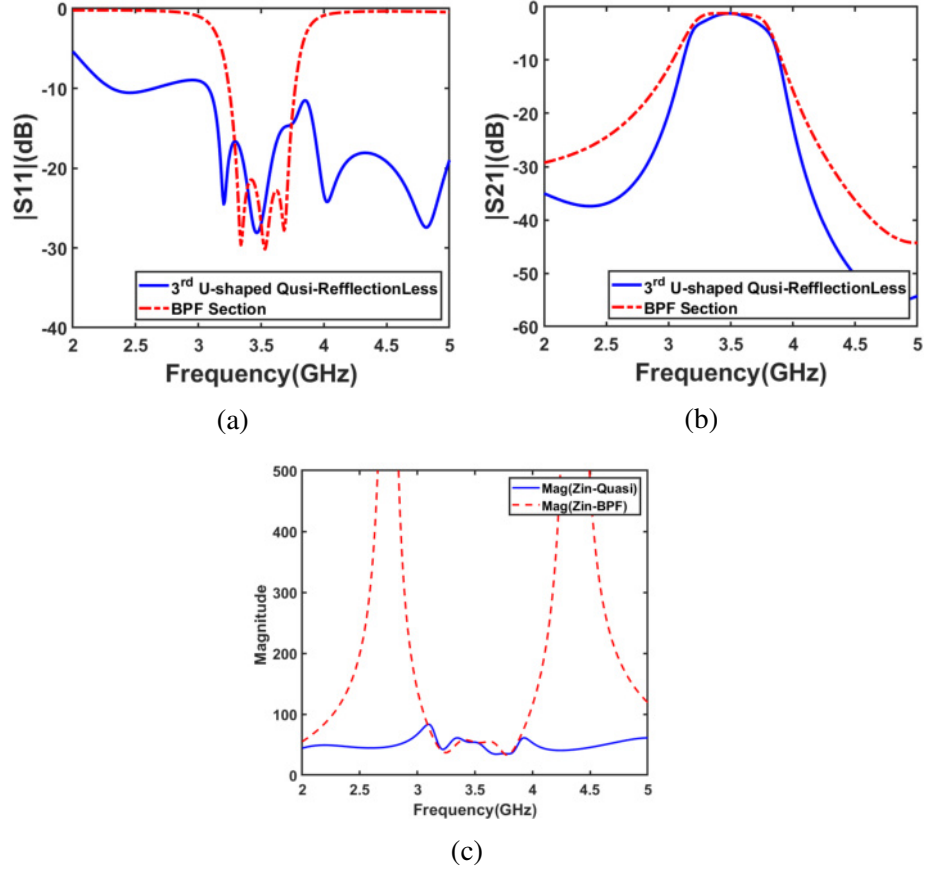
Figure 3.11: Simulated frequency responses of the 3-pole U-shaped quasi-reflectionless BPF and its bandpass section ($Z_1 = 56.4\Omega, Z2 = 71.5\Omega, Z3 = 71.5\Omega, \theta1 = \theta2 = 90^0, \theta3 = 180^0, a1 = 1.128, a2 = 1.43, a3 = 1.43, S = 0.5mm$)

3.3.2.2 Discussion on The filter Bandwidth

Figure 3.12 compares the transmission coefficient of the 3-pole quasi-reflectionless filter $|S_{21-Q}|$, the reflection coefficient of its absorptive filter $|S_{11-ABS}|$ and the transmission coefficient of BPF section . Here, the subscript Q and ABS stand for quasi-reflectionless BPF and absorptive filter, respectively. From 3.12, we can see that S_{21-Q} (blue trace) is almost the same as $|S_{11-ABS}|$ in term of the bandwidth. A qualitative explanation can be offered as follows In a resistor-embedded circuit (i.e., the quasi reflectionless filter) of Figure 3.6, the input signal power is either reflected, transmitted,
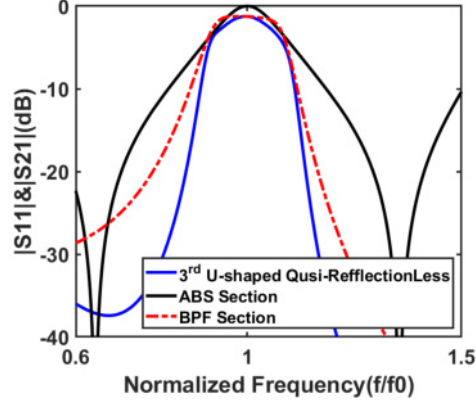
Figure 3.12: Simulated comparison between the transmission of U-shaped quasi-reflectionless BPF (Fig.3.6) and the reflection of absorptive filter in (Fig.3.2c)

or absorbed. Conservation of power requires

$$|S_{11-Q}|^2 + |S_{21-Q}|^2 + |S_{a-Q}|^2 = 1 \tag{3.8}$$

where S_{a-Q} is the absorption coefficient of the quasi-reflectionless BPF. Since $S11_Q \approx 0$ for the quasi-reflectionless filter within the operating bandwidth, Eq.3.8reduces to

$$|S_{21-Q}|^2 + |S_{a-Q}|^2 = 1 \tag{3.9}$$

Comparing 3.5 and 3.9 leads to the conclusion that $S_{21-Q} = S_{11-ABS}$[36]. From this math, the transmission coefficient of the quasi-reflectionless bandpass filter is close to the reflection coefficient of the ABS branch under some restrictions such as slight difference in the impedances. Therefore, the quasi-reflectionless BPF has almost identical BW3dB (passband) as the BW3dB (reflection) for the ABS stub.

To remark the main points, this procedure can be considered as an initial step to design and synthesize the reflectionless filters in terms of the bandwidth requirements.

3.3.2.3 Extension to Higher-Order Designs

Adding more resonators to the BPF branch enhances the filter selectivity but at the cost of design complexity and size. Thus, a filter satisfying the prescribed design requirements with less number of resonators is the aim of most filter designers. As in Figure3.6, extending the filter order is achieved. Higher-order quasi-reflectionless BPFs can be readily realized by cascading more U-shaped resonators. Figure 3.13a and 3.13b show examples of the 4 and 5-pole U-shaped quasi-reflectionless filters, respectively. Note that the added U-shaped resonators have the same parameters as for the resonators in the 3-pole proposed filter.

(a)

(b)
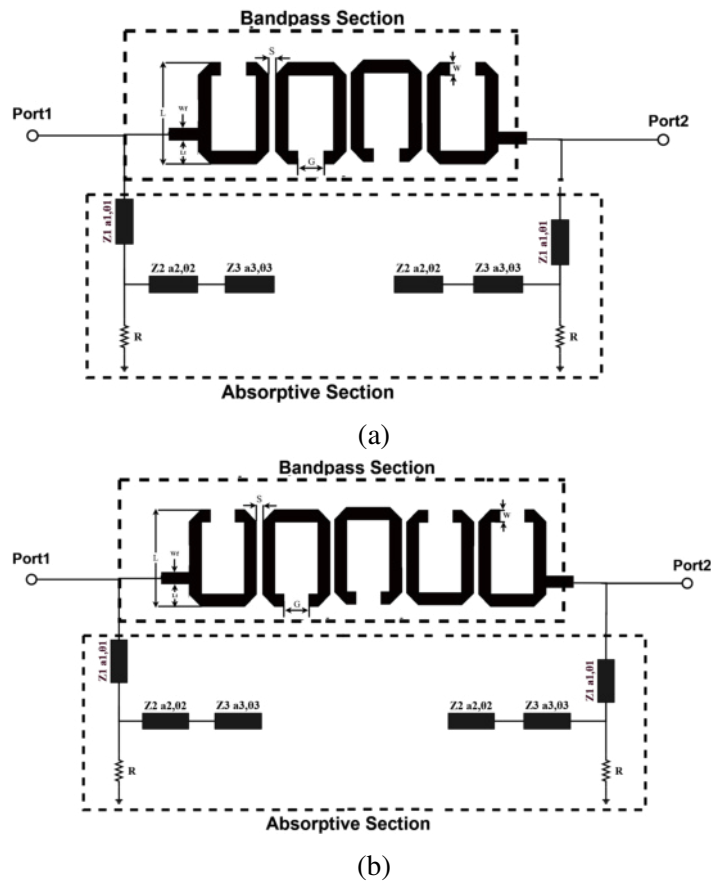
Figure 3.13: The layout of n-pole U-shaped BPF with the transmission line circuit model of the ABS stubs connected into the output and input ports (a) 4th order (b) 5th order

Figure 3.14a and b show the frequency responses (reflection, transmission, and

input impedance) of the 4-pole and 5-pole U-shaped quasi-reflectionless filters with varying S, respectively. $a1, a2,$ and $a3$ are assumed the same as in the optimized 3-pole quasi-reflectionless BPF. As S changes, the frequency responses of the higher order filters do not change noticeably. The reason is that the rejection bandwidth of the ABS stub is larger than the bandwidth of the main channel of the proposed filter .

(a)   (b)
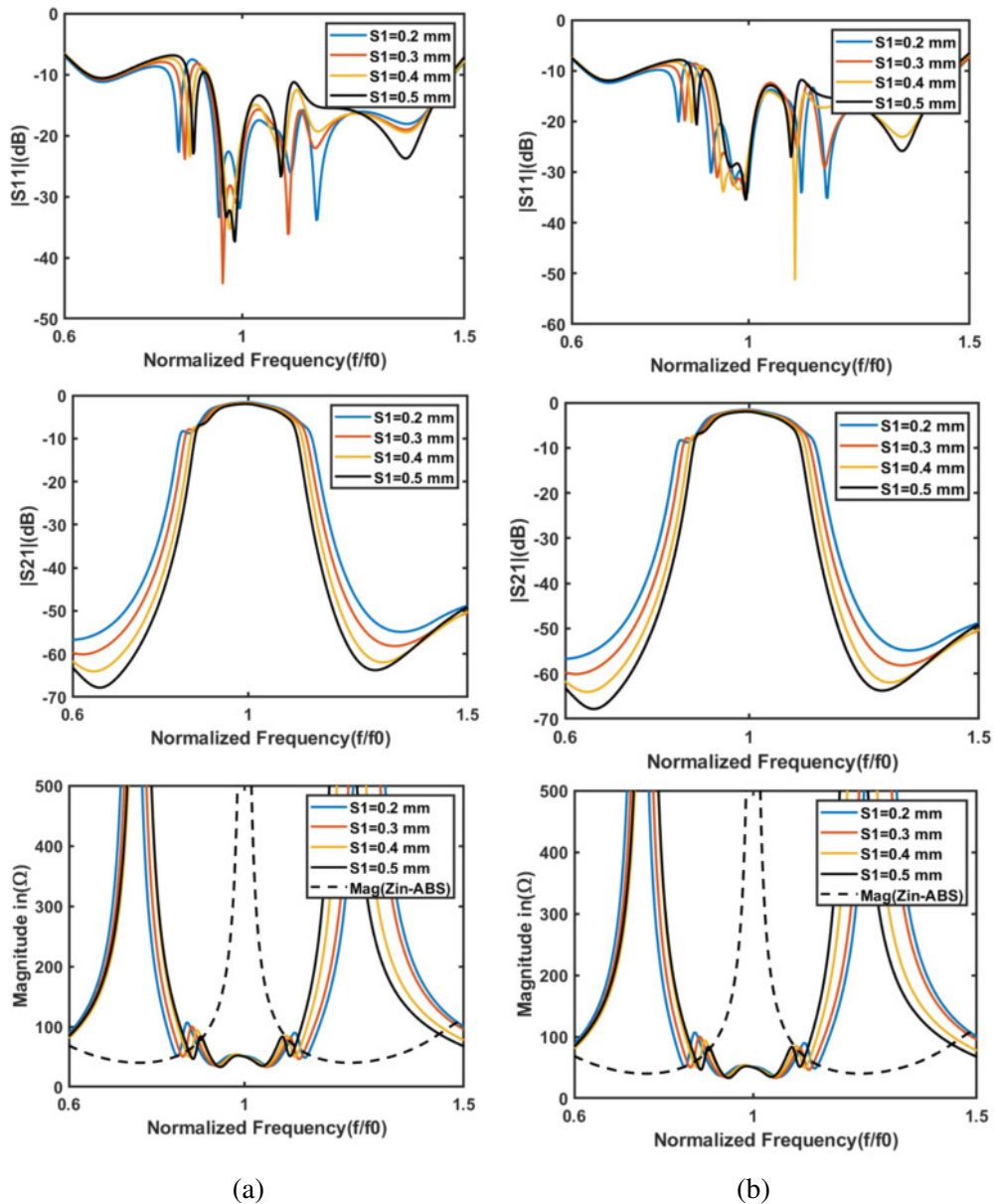
Figure 3.14: All frequency responses of the 4-pole and 5-pole U-shaped quasi-reflectionless filters with varying S a)reflection S11 b) transmission S21 c) magnitude of input impedance mag(Zin)

Figure 3.15 compares the simulated frequency responses (i.e., the transmission

and reflection coefficients, and the magnitude of input impedances) of the $3, 4$, and 5-pole U-shaped quasi-reflectionless filters using the same order ABS stub. The three simulated filters have almost the same passband bandwidth although the increase in the filter order enhances the far-out-of-band rejection. Accordingly, controlling the passband bandwidth and the absorption ratio requirements can be independently satisfied. Also, fluctuations in the input impedance is lowered with the increase in the filter order.
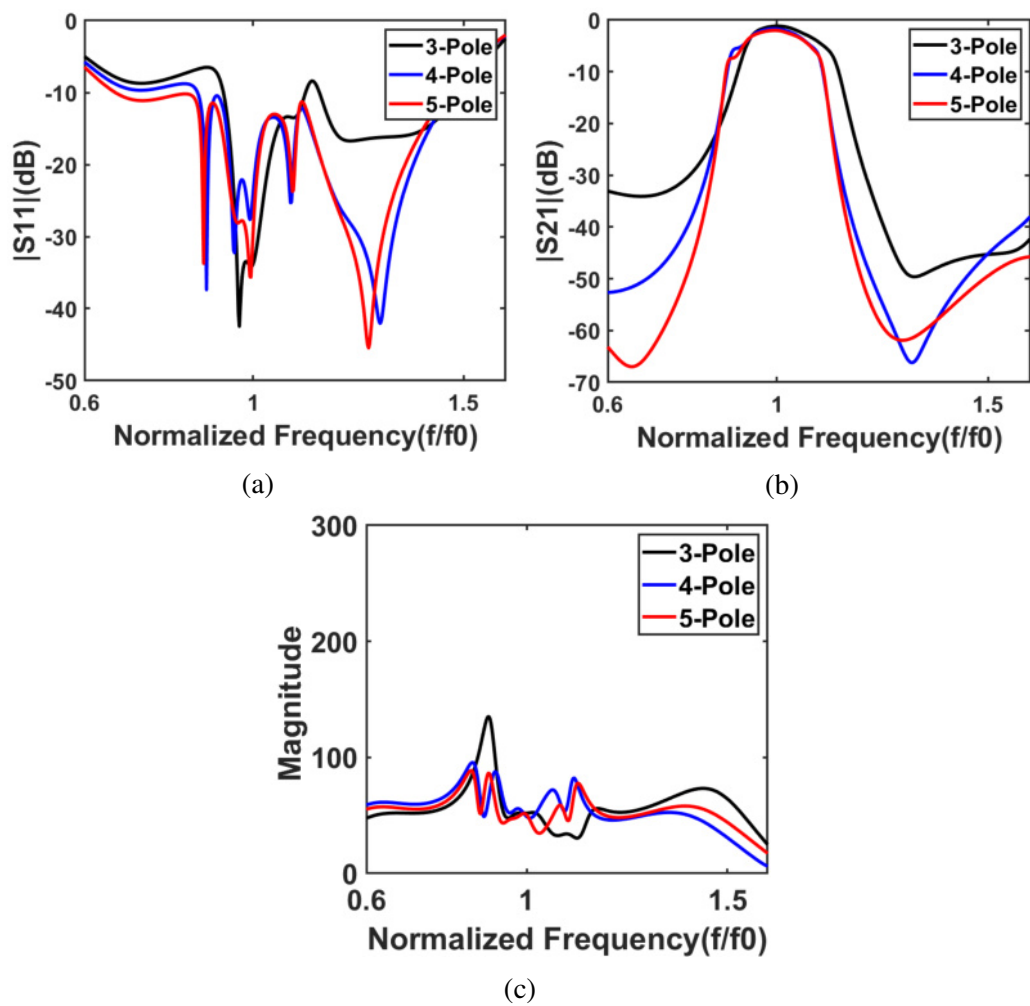
(a)

(b)

(c)

Figure 3.15: Compares the simulated frequency responses (the reflection and transmission coefficients, and the magnitude of input impedances) of the $3, 4$, and 5-pole U-shaped quasi-reflectionless filters

61

3.3.2.4 Cross-Coupling for Improved Out-of-Band Rejection

The proposed filter response may be further enhanced if the cross-coupling technique is utilized. The cross-coupling method is commonly utilized in the design of microwave filters. To do so, the ABS stub are placed close to each other to excite the coupling between them. This method introduces transmission zeros into the filter response because there will be other signal paths between the input and output ports, leading into sharper rejection compared to the same filter without cross-coupling.

Figure 3.16 states where the cross-coupling is introduced. The last stub in each ABS stub are adjacently vertically placed, converted from Figure3.6c to Figure 3.16.This method operates to merge these two stubs to a coupled transmission line.
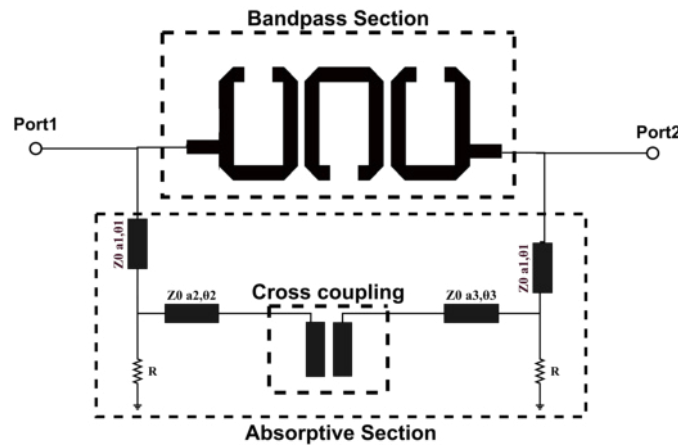
Figure 3.16: The prototype of 3-pole U-shaped quasi-reflectionless with cross coupling

Two transmission zeros are added to the response as shown in Figure3.17. One transmission zero is generated at $(f/f_0 = 1.495)$ that means at $5 GHz$, while the other transmission zero was not shown here for the sake of simplicity. Interestingly, the cross-coupling also aids to enhance the absorption (i.e., reduce the reflection coefficient). This essentially merges the two stubs into one. As seen in Figure 3.17,

(a) (b)
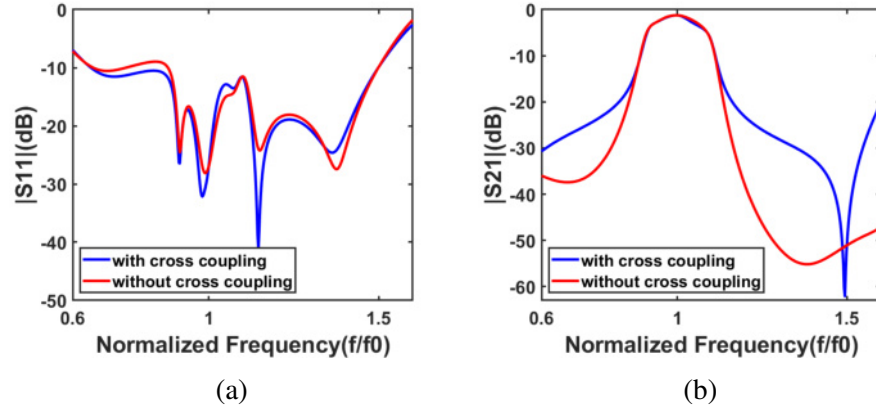
Figure 3.17: Compares the simulated frequency responses the reflection and transmission coefficients of the 3-pole U-shaped quasi-reflectionless filters with and without cross coupling

3.3.3 Design Procedure

To follow an obvious procedure relying on the analyses discussed above, The steps can be summarized as:

1. Design 3-pole U-shaped BPF with center frequency f_0 and fractional bandwidth FBW.

2. Bandstop filter is synthesized from the lowpass filter prototype [Figure 3.2a] with f_0 and FBW. Then, the BSF is converted into its ABS counterpart, see Figure 3.2 for the conversion process. The ABS consists of three transmission lines with initial impedances $(Z_1, Z_2, and Z_3)$ which are equal to reference impedance Z_0 multiplied by an initial scale parameter (a1, a2, and a3). By default, the scale parameters will be assumed as one. Also, the electrical lengths of the absorptive section are $(\theta 1 = \theta 2 = 90^0, \theta 3 = 180^0)$, terminated with absorptive resistor R that can be set to be the same with the termination reference impedance Z_0.

3. Adjust the scale parameters $(a1, a2, a3)$ to obtain the magnitude of input impedance as high as possible for the ABS part at BW3dB of the BPF, see Figures 3.7-3.10. Also, the magnitude of input impedance of the U-shaped quasi-reflectionless BPF

63

equal to Z_0 at all frequencies that means matching will occur at in and out of - band. See Figures 3.8-3.11. Eq.3.4 can be used to calculate the $S11$.

4. To increase the absorptivty and selectivity of the proposed filter, the technique of cross-coupling can be adopted, Figures.3.16-3.17. Also, the increase in the order of U-shaped BPF filter enhances the filter selectivity, Figures.3.14-3.15.

3.3.4 Tunable U-Shaped Quasi-Reflectionless Bandpass Filter

The quasi-reflectionless filter discussed in this chapter operates at a certain resonant frequency. It consists of two parts; the first one, which allows the passage of the desired signals, and the other part is the absorptive stub. The matching between these two parts is important for the signal to pass without distortion or attenuation. In order to make it tunable, this matching must be taken into account. So, two varactor diodes were placed on each end of each part; meaning one of them was placed on the ends of the U-shaped part and the other at absorptive stub ends. Both were connected to the same DC bias circuit. The main idea for using the same DC bias circuit is that the diodes add an extra electrical length. As diodes have larger capacitance, the electrical length will be longer, thereby resonating at lower frequency. Therefore, the use of different DC bias circuits leads to a difference in electrical length between the two parts, which increases the mismatch.

The diode chosen in all simulations is skyworks smv1430 in [48], and a curve of the equivalent capacitance with dc voltage is shown in Figure 3.18.
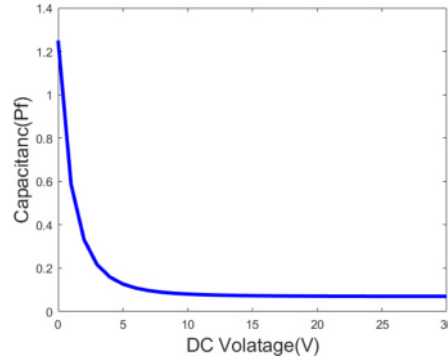
Figure 3.18: RSMV1430 Capacitance vs Dc voltage

3.4 Third Order Magneticless Nonrecirocal U-Shaped Bandpass Filter

This section presents a magneticless nonreciprocal bandpass filter based on spatio-temporally modulation STM technique using distributed open-ended U-shaped resonator with length of $\lambda g/2$. The proposed filter is designed and simulated on FR4 substrate by using Key Sight Advanced Design System software (ADS). The operating frequency of the proposed filter is $f01 = 3.5$GHz and the 3dB fractional bandwidth are ($FBW = 0.2$ or 20%). This section is organized as follows. The first subsection introduces the required mathematical background about nonreciprocity devices based on saptio-temporal modulation(STM) technique. The second subsection presents the design of the 3-pole U-shaped nonreciprocal BPF. Several parameters will be investigated to optimize the overall performance. In the last subsection, the numerical validations of the U-shaped nonreciprocal band pass filter is introduced.

3.4.1 Nonreciprocity Devices based on Saptio-Temporal Modulation(STM) Technique

Having discussed the single U-shaped resonator in chapter 2, subsection 2.4.3, several of them will be placed close to each other to create the filter design. However, here we will discuss the filter using the general resonator term regardless of the resonator type (i.e., distributed or lumped). Conventionally, the reciprocity is an inherent problem in the passive microwave devices because the separation between the transmitted and received signals is difficult especially if the receive- and transmit- channels have the same frequency spectrum. Also, the backward propagation signals harm the circuits especially the nonlinear ones. Therefore, this subsection concerns about how to break the reciprocity.

The spatial-temporal modulation STM technique is utilized to obtain the nonreciprocal. This technique does not need a magnetic field to achieve the non-reciprocity. Typically, the resonators consist of parallel LC tank. To make each lumped element modulated, the L and C should be capable of being modulated. The capacitor is possible if the varactor diode is used, but the inductor is not an easy task. Fortunately, the DC biasing circuit used to inject the modulation signals. However, the modulation signals are very low frequency about several megahertz. Furthermore, the sinusoidal signals with the same frequency are applied to each resonator, but with different phase. The phase should be progressive in one direction depending on where the signal should be propagated. The phase difference between any adjacent two resonators should be kept the same. The proposed filter consists of three STM resonators. As can be seen, each resonator has its own modulating frequency source.

The coupling-routing diagram and conceptual power reflection coefficient (S11), transmission coefficient (S21) and isolation coefficient (S12) responses of the proposed

non-reciprocal BPF are shown in Figure 3.19. The progressive phase starts from the left to right, so the S21 will be obtained, whereas the S12 will be attenuated, see Figure3.19c. However, to obtain the S12 and reduce the S21, the progressive phase starts from the right to left. Furthermore, the DC source is added to alter the resonant frequency of resonators, but the same value should be assigned for all DC sources. Varactor-based variable and modulated capacitors are considered the constituent elements. Figure 3.19b shows the modulating signals where the signals have the same frequency and different phases.

(a)

(b)

(c)
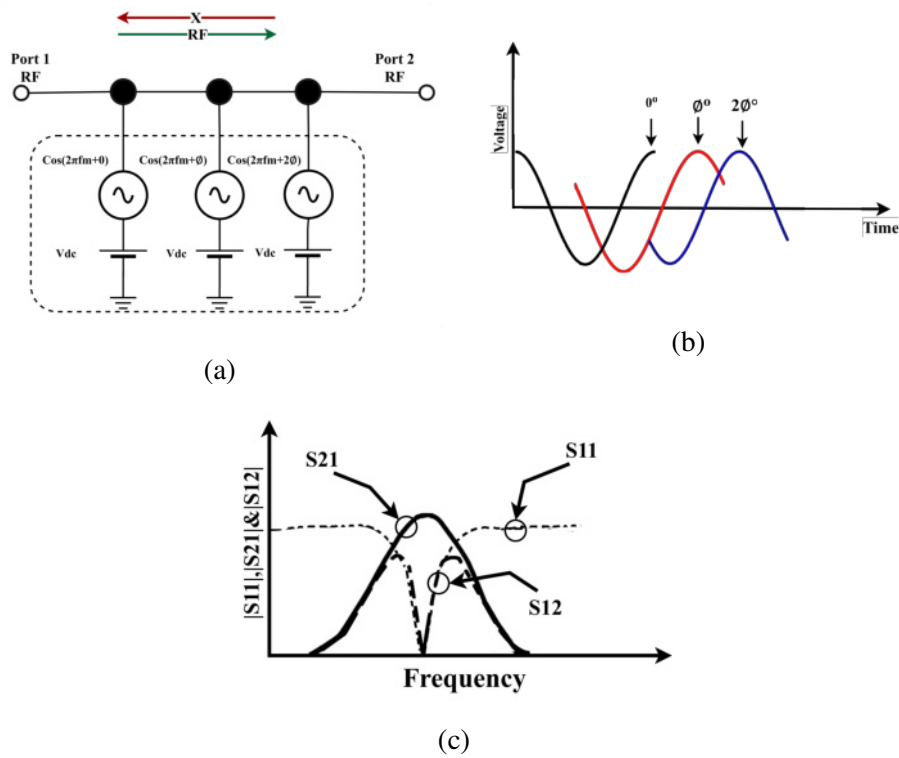
Figure 3.19: Concept of magneticless non-reciprocal BPF based on modulated RF resonators (a) Coupling-routing diagram (b) Conceptual illustration of the AC modulation signals applied on the DC-biased resonator varactors. (c) all response of the nonreciprocal BPF

In Figure 3.19a, white circles: input and output; black circles: frequency resonator , fm-modulated, DC biased resonators with external AC sources. Figure 3.20 shows the conceptual circuit topology of the proposed 3-pole nonreciprocal BPF. Rs and RL are the source and load impedances and are both assumed to be 50Ω. J_{12} and J_{23} are ideal

67

time-invariant J-inverters, which determine the couplings in conventional static filter designs [5].
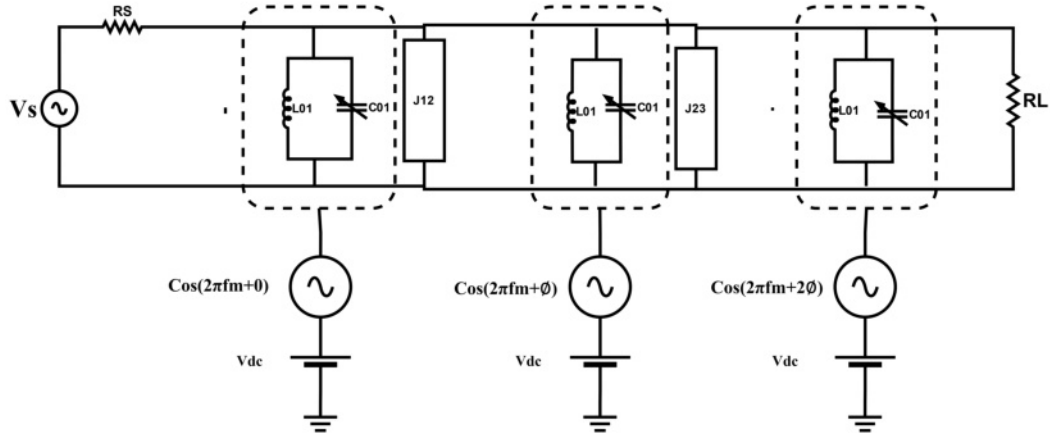
Figure 3.20: 3-pole non-reciprocal band pass filter with ideal time-varying capacitors by using (STM)

The modulated capacitors can be represented as:

$$C_n(t) = C_0 + \Delta C \cos(2\pi f m t + (n-1)\phi); (n = 1, 2) \tag{3.10}$$

where ΔC is the amplitude of the capacitance variation, fm is the modulation frequency, and ϕ is the phase difference between any two adjacent modulation sources. Here, we define

$$K_m = \frac{\Delta C}{C_0} \tag{3.11}$$

where K_m is the capacitance modulation index. The center frequency (f_0) of the non-reciprocal band pass filter are determined by the static inductance $L01$ and static capacitance $C01$. To guarantee modulation occurring in the proposed filter, the Km should not be equal to zero. There will be a series of intermodulation (IM) products at $f_{RF} \pm k f m$ $(k = 1, 2, 3, \dots)$, when the capacitors are modulated. A portion of the transmitted power will be transferred to IM products. Then, to reduce losses in the propagation di-

rection, the power should be returned back to the fundamental RF frequency. However, in the opposite direction, most of the power will convert into the IM products. This can occur only through the phase shift difference and the direction of phase propagation, leading into the nonreciprocal devices.

3.4.2   3-pole U-Shaped Nonreciprocal Bandpass Filter Design

In this subsection, the 3-pole U-shaped nonreciprocal BPF is designed and analyzed. For this design, the fractional bandwidth $FBW = 20\%$ or $FBW = 0.2$ at a resonant frequency $f_0 = 3.5GHz$, $n = 3$ (Butterworth lowpass type).

The lowpass prototype parameters, with respect to a normalized lowpass cutoff frequency $\omega_c = 1$, are $g_0 = 1, g_1 = 1, g_2 = 2$ and $g_3 = 1$ and by using Eqs.2.48-2.50 with analysis curves in Figure 2.16. To obtain physical parameter of U-shaped BPF shown in Figure 3.21a, Table.3.2 illustrates the physical dimensions. In Figure.3.21b,time varying varactor diode are connected into the open ends of U-shaped resonator , converting the conventional bandpass filter into nonreciprocal bandpass filter.

Table 3.2: The physical dimensions of U-shaped BPF

Parameters	Measurements in(mm)
Length (L)	10.05
Taped in length (Lt)	2.62
Space between the resonators (S)	0.5
Gap between open end of U-shaped BPF (G)	2.4
Width (W)	1.25
Width of feed (Wt)	1.15
Taped input (t)	3.75

The nonreciprocity was previously defined and to achieve it, the parametric studies of the circuit responses with various modulation parameters are present in Figure 3.22. As seen in Figure 3.22a, the modulation frequency(fm) increases from (200 MHz

(a)

(b)
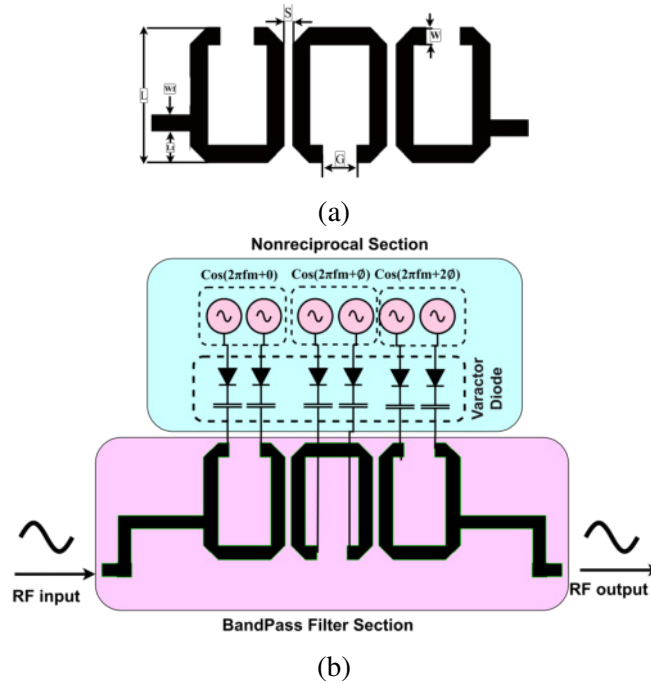
Figure 3.21: a) The layout of 3-pole U-shaped BPF b) the layout of 3-pole U-shaped BPF with time varying varactor diode connected into the open end of U-shaped resonator .

to 260 MHz), the forward transmission (S21) is improved and the port reflections(S11) are relatively stable. An optimal fm of 240 MHz is chosen for large reverse attenuation and relatively small forward insertion loss.

The concept of nonreciprocity was clarified above by applying the STM technique on the conventional DBPF as shown in Figure 3.22. Here, effects of the main parameters on the overall performance (i.e., the circuit responses, (S11, S22, S12 and S21)) will be introduced, see Figure 3.22a, First, the modulation frequency increases from 200 MHz to 260 MHz. The forward transmission (S21) is improved and the backward transmission (S12) is attenuated.

The S12 changes with the fm. The reflection (S11=S22) does not obviously affect as shown in Figure 3.22a. The optimal fm is 240 MHz because it offers the large reverse attenuation and relatively small forward insertion loss. The other parameter is the modulation index K_m, see see Figure 3.22b. When it becomes more than 0.22, the transmission coefficient deteriorates and the isolation coefficient has attenuation larger

than 20 dB. The optimum value of K_m is chosen as 0.23 due to its the small insertion loss and large backward attenuation. The reflection loss is relatively stable. see Figure 3.22c depicts effects of the modulation phase ϕ. When ϕ is equal to 0, the time-varying capacitors shown in Figure 3.21 are only modulated in time,so, the responses that result is reciprocal responses with 11.5 dB passband insertion loss for both forward and backward transmissions. The large loss occurs because of the uncontrolled power conversion to the IM products. When ϕ is nonzero, the three resonators in Figure 3.21 are modulated simultaneously in both space and time (i.e., STM). The ϕ is 57^0, representing the optimal value. Figure 3.22c represents the forward insertion loss and the reverse attenuation of backward transmission S12.

(a)   (b)

(c)
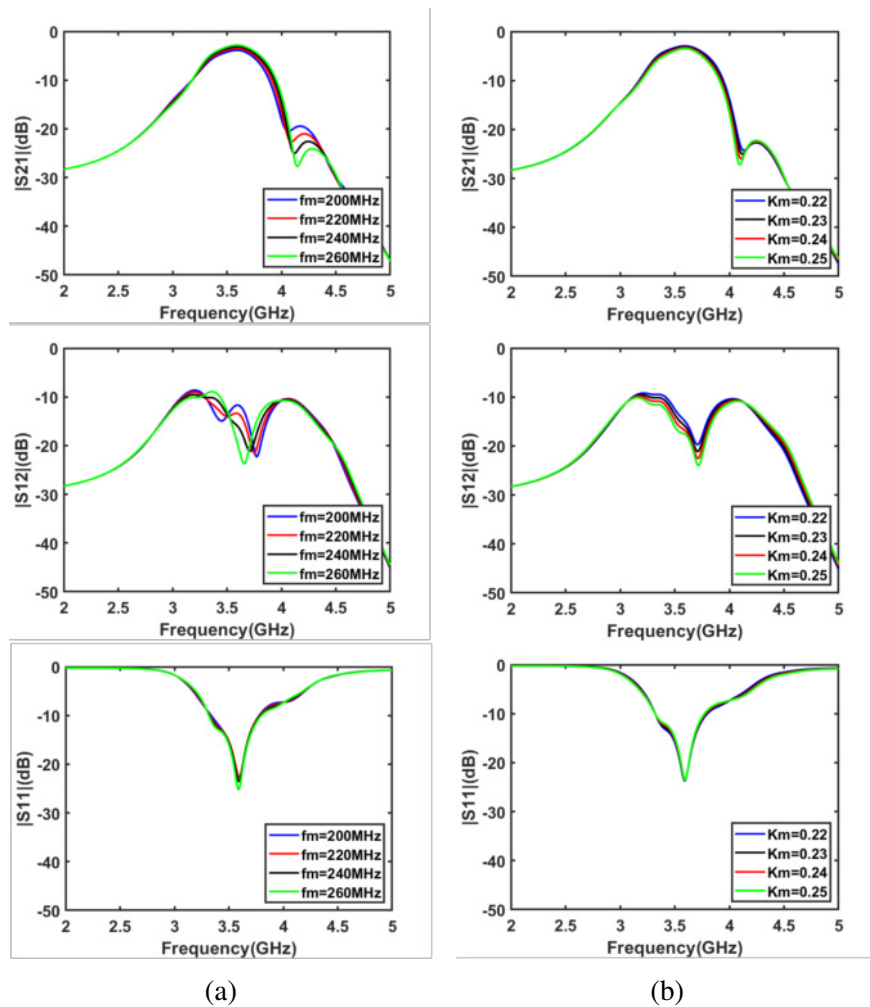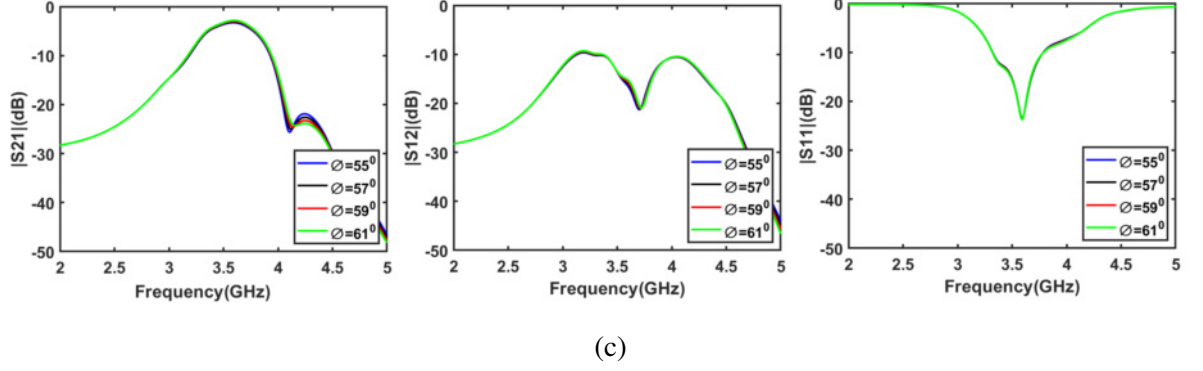
Figure 3.22: Parametric studies of the 3-pole U-shaped non-reciprocal BPF responses with with respect to (a) modulation frequency fm ($K_m = 0.23$; $\phi = 57^0$); (b) modulation index K_m ($fm = 240MHz$, $\phi = 57^0$); (c) phase ϕ ($fm = 240MHz$, $K_m = 0.23$)

3.5 Spatial-Temporal Modulation Technique Based Tunable Nonreciprocal Dual Band Pass Filter

This section presents the 3-pole U-shaped tunable nonreciprocal dual-band pass filter which was proposed, analyzed, designed, and simulated. The first part was to make the resonator operating with dual bands, using a stub loaded into the main resonator. The loaded varactor-based variable capacitors performed two functions, the tunability and the nonreciprocity. The STM technique was exploited to realize the nonreciprocal responses. The proposed filter is mathematically analyzed and numerically simulated to demonstrate its performance. Several parameters have an influence on the overall performance are investigated. As a proof-of-concept, 3-pole U-shaped tunable nonreciprocal dual-band pass filter DBPF is designed and simulated on Rogers-RO3210 substrate by using Keysight Advanced Design System software (ADS). The operating frequencies of conventional dual Bandpass filter are ($f_{01} = 2.24$GHz and $f_{02} = 3.73$GHz), while the 3dB-fractional bandwidths are (FBW1=0.139 and FBW2=0.133).

The section is organized as follows. The first subsection introduces the required mathematical background and investigations for the proposed design. This subsection is divided into three parts, and each part discusses a specific topic. In the second sub-

section, the tunable 3-pole U-shaped nonreciprocal dual-band pass filter design is presented. Several parameters will be investigated to optimize the overall performance. Next, the numerical validations of the tunable nonreciprocal dual-band pass filter are introduced.

3.5.1 Methodology of The proposed Filter

Figure 3.23 shows the flowchart of the methodology of multi-function filter.
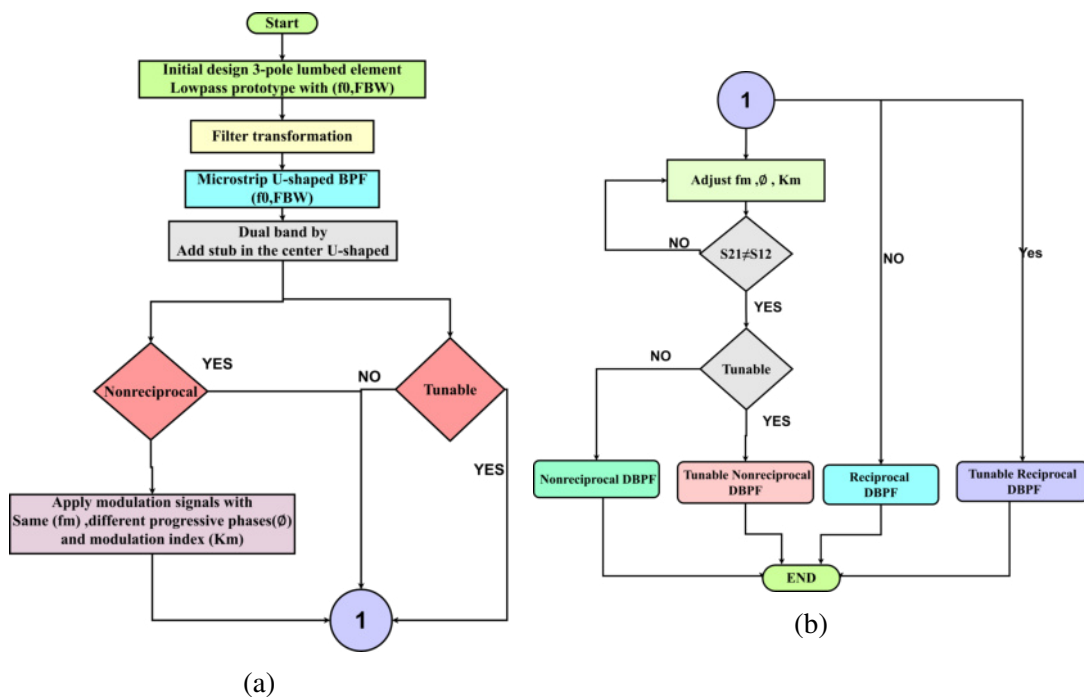
Figure 3.23: Methodology flowchart of multi-function filter a) part 1 b) part 2

3.5.2 Mathematical Background of The Proposed Filter

The main points discussed in this section are the fundamental background of the proposed filter including the required mathematical derivation. It discusses the conventional U-shaped dual band pass filter (DBPF), and explains the Tunability of Dual Frequency Resonances. The last part in this section deals with Nonreciprocal Devices

73

3.5.2.1 U-Shaped Dual-Band Resonator

A dual-band resonator is adopted to design the proposed nonreciprocal dual-band-pass filters based on the coupling scheme as shown in Figure3.24. Each elliptical shape in Figure3.24 represents a single resonator. No real connection exists between any two adjacent resonators, but the electromagnetic coupling operates to transfer the energy from one to another. Thus, the gap separating between them plays a vital role in deter-
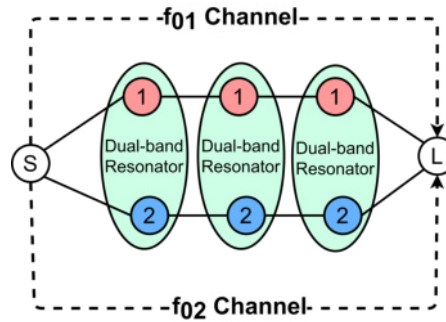
Figure 3.24: The schematic structure of the dual-band filter using dual-band.

mining the amount of coupling which in turn specifies the ultimate bandwidth. Although the two resonance frequencies can be chosen freely relying on the physical dimensions of the U-shaped dual-band resonator, there is some limitations that will be shown later on. Figure 3.25a shows the adopted microstrip U-shaped dual-band resonator, which consists of an open-end resonator in a form of the U-shaped structure with a stub mounted into its center. The distributed resonator without the stub resonates at its fundamental frequency f_{01} when the whole length about half wavelength. The second frequency harmonic f_{02} occurs when the whole resonator length is equal to one wavelength. The second harmonic is harmful in many situations. Here, we will control it when adding the central loading stub to make it useful. The f_{02} can be shifted down toward f_{01} by increasing the stub length Lf2. Figure3.25b also illustrates that when the Lf2 increases, the f_{02} decreases, tending to reach the f_{01}. As can be seen, f_{01} does not affect.
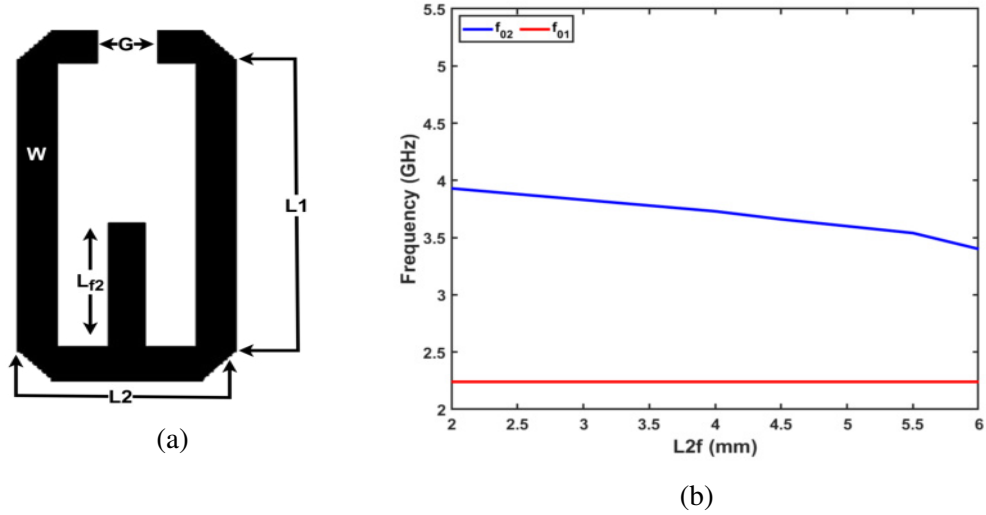
Figure 3.25: (a) The schematic layout of the dual-band U-shaped resonator (b) Its first two resonant frequencies versus the length of central loading stub

To check effects of the gap s between resonators, the s is changed from 0.3mm to 1mm with a step of 0.1mm. As expected the coupling coefficient (Mi,i+1) given by 3.12 is decrease for both resonances, see Figure 3.26.

$$M(i, i+1) = \frac{f_2^2 - f_1^2}{f_2^2 + f_1^2} \tag{3.12}$$

where f_1, f_2 lower and upper cutoff frequency . In other words, it means that the bandwidth decreases as well. Also, the open-end direction change the amount of coupling but the adopted one is the best choice because of exciting both magnetic and electric coupling. The other important design parameter is the external quality factor for both input and output, Qei/o. Because of our design is symmetrical, the output and input external quality factors are identical. The external quality factor is given by 3.13

$$Q_{(}ei/o) = \frac{f_0}{BW_{3dB}} \tag{3.13}$$

where f_0 is resonance frequency and bandwidth ($BW_{3dB} = f_2 - f_1$) is the difference between upper and lower cutoff frequency i.e. [1].
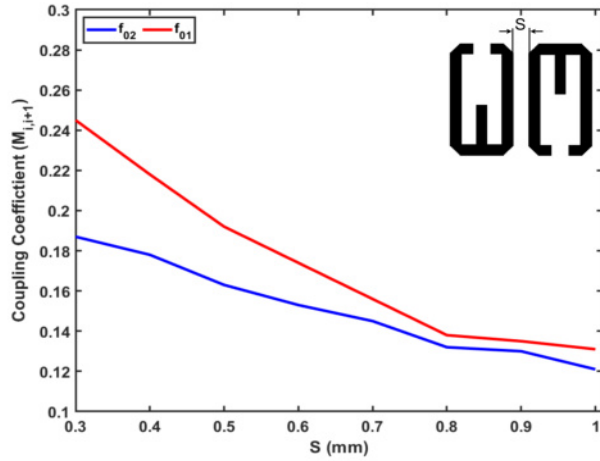
Figure 3.26: The coupling coefficient Mi,i+1versus s for both bands.

The feeding transmission line is attached to a resonator at a distance from the center t. A 50Ω feeding line with a length of (Lf) and a width of (Wf), which is folded to decrease the overall size, excites the resonator. A gap (gf) is created whereas the Lf increases, the coupling between the resonator and the feeding line increases. Also, the t parameter governs the external quality factor. Figure 3.27 shows the external quality factor versus the Lf parameter for one state of t. Both $Q_e1,2$ traces refer to the lowest external factor when the Lf=6.2mm. The lowest external quality factor aids to transfer the higher energy from the port to the resonator.
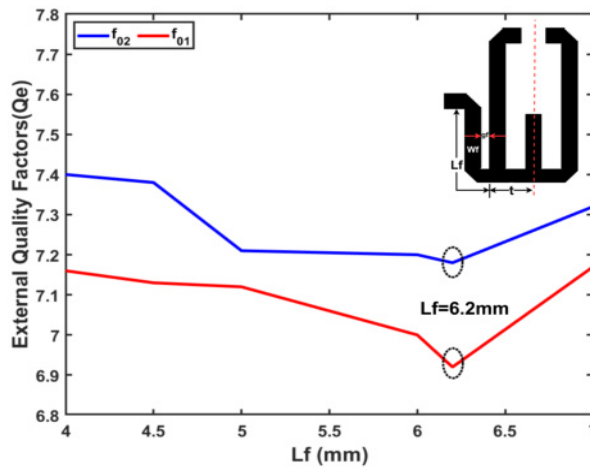
Figure 3.27: The external quality factor Qe1,2 versus Lf for both bands with tapped length (t=2mm).

3.5.2.2 Tunable Dual Frequency Resonators

The resonators investigated above operate at dual fixed resonance frequencies. Sometimes we need to cover several bands with the same design and not at the same time, making the design tunable. This feature improves the whole design performance. To do so, few diodes will be integrated to the open ends of the resonator as depicted in Figure 3.28. However, the DC-biasing circuit is required to make the diodes operating in the appropriate way. The diodes add an extra electrical length.
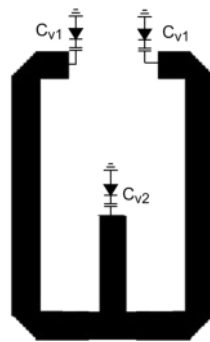
Figure 3.28: Schematic of tunable dual-mode U-shaped resonator.

As diodes have larger capacitance, the electrical length will be longer, thereby resonating at lower frequency. As will be seen in the mathematical analysis, either the second band or both bands will be tuned at once. The even-odd mode approach is utilized to figure out how to control diodes.

The resonator is divided into two halves at its symmetrical plane, see Figure 3.29. The odd-mode (electric wall (short circuit)) half resonator resonates at the higher band f_0^o, while the even-mode (magnetic wall (open circuit)) half resonates at the lower band f0e because it has longer length. As can be seen, the varactor diode (Cv1) control the higher band only, while the (Cv2) control both bands. The Cv1,2 represents the diode capacitance at a certain applied reverse-biasing voltage. When Cv2 varies, the higher band will be moved lower or upper depending on the voltage. Moreover, the Cv1

operates to alter both bands simultaneously. This observation is obvious in Figure 3.29 where the diode Cv1 exists in both modes. When Cv1 varies from $Cv1 - 1$ to $Cv1 - 2$ used to shift the odd mode frequency from f_{01}^o to f_{02}^o and even-mode frequency f01e to f02e proportionally by loading capacitance while Cv2 varies from $Cv2 - 1$ to $Cv2 - 2$, the even-mode frequency shifts from f_{01}^e to f_{01}^e and the odd-mode frequency does not shift . To obtain the odd –and – even frequencies mode , by placing a short or open circuit at the symmetrical plane of the circuit in Figure 3.28 as shown in Figure 3.29.
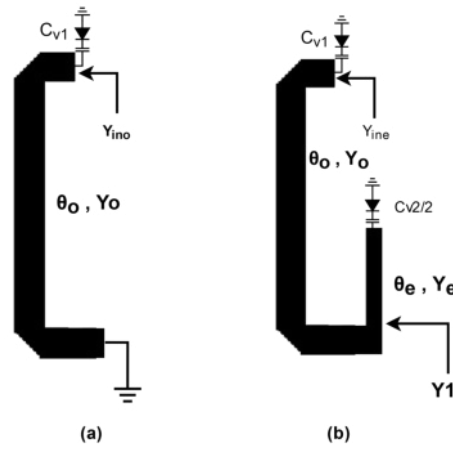
Figure 3.29: Circuit mode(a) odd mode (b) even mode .

The admittance of the odd mode is given by

$$Y_{ino} = j(\omega C v_1 - \frac{Y_o}{\tan(\theta_o)})$$

(3.14)

, and for the even mode is

$$Y_{ine} = j(Y_o \frac{Y1 + Y_o \tan(\theta_o)}{Y_o + Y1 \tan(\theta_o)} + \omega C v_1)$$

(3.15)

With

$$Y1 = j(Y_e \frac{\omega C v_2/2 + Y_e \tan(\theta_e)}{Y_e - \frac{\omega C v_2}{2} + Y_e \tan(\theta_e)})$$

(3.16)

The resonant frequencies of the odd and even modes can be found by solving

78

$$Im(Y_{ino}) = Im(Y_{ine}) = 0 \tag{3.17}$$

The odd frequency (f_0^o) is

$$f_0^0 = \frac{Y_o}{2\pi C v_1 \tan(\theta_o)} \tag{3.18}$$

, and the even frequency (f_0^e) is

$$f_0^e = \frac{Y_e^2 \tan(\theta_e)[Y_o - \tan(\theta_o)\omega C v_1] + Y_e[Y_o^2 \tan(\theta_o + Y_o\omega C v_1)]}{\pi C v_2[Y_o(Y_e + Y_o\tan(\theta_o)^2\omega C v_1) + \omega C v_1 Y_e \tan(\theta_e)]} \tag{3.19}$$

From Eq3.18, it can be seen that the odd-mode resonant frequency depends on the parameters Cv1, Yo, and θ_o. It means that when the Cv1 varies, the resonant frequency of the higher band will be varied. Eq 3.19 reveals that the even resonant frequency depending on both Cv1 and Cv2. Also, it can be observed when changing Cv2, only the resonant frequency of the lower band will be changed. To this end, the conversion from fixed resonant frequency into the tunable structure is carried out. In summary, the conversion process will be exploited to convert the structure from reciprocal to nonreciprocal without going through how to design reciprocal tunable band pass filter for the sake of simplicity.

3.5.2.3   Nonreciprocal Devices

This section concerns about how to break the reciprocity in the dual band resonator. The principle of the nonreciprocity is the same that in Section 3.4. The STM technique is utilized to obtain the nonreciprocal of DBPF. The sinusoidal signals with the same frequency and different phase are applied to each resonator. The proposed filter

consists of three STM resonators. As can be seen, each resonator has its own modulating frequency source. The coupling between the resonators diagram and all responses, reflection coefficient (S11), transmission coefficient (S21) and isolation coefficient (S12) in Figure 3.30.

(a)

(b)

(c)
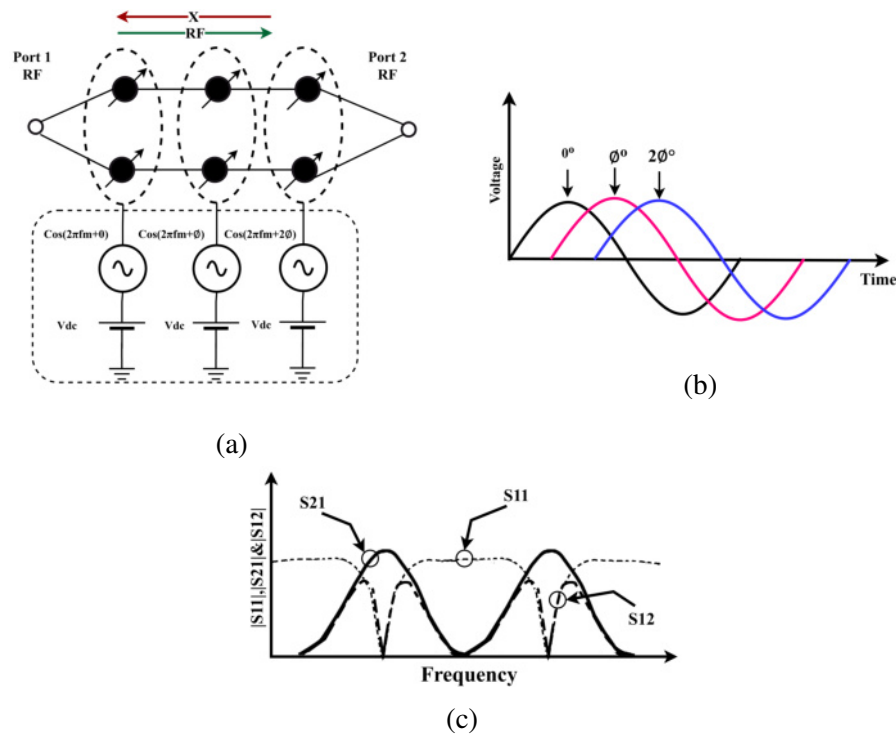
Figure 3.30: The scenario of nonreciprocal dual-band BPF based on STM modulated RF resonators (a) the coupling between the resonators diagram (b) conceptual illustration of the AC modulation signals (c) conceptual power transmission (S21), reflection (S11), and isolation (S12) responses of the nonreciprocal dual-band BPF.

In Figure 3.30a, white circles represent input ,while the black circles is represent a tunable resonators. The progressive phase starts from the left to right, so the S21 will be obtained, whereas the S12 will be attenuated, see Figure 3.30c. However, to obtain the S12 and reduce the S21, the progressive phase starts from the right to left. Furthermore, the DC source is added to alter the resonant frequency of resonators, but the same value should be assigned for all DC sources. Varactor-based variable and modulated capacitors consider the constituent elements. Figure 3.30b shows modulating signals where the signals have the same frequency and different phases.

The same manner of the topology is used in nonreciprocal BPF ,but each reso-
nant circuit consists of a capacitor and a inductor in parallel form,these component is
convert into resonant circuit separately, Where the capacitive transform into a resonant
circuit consisting of a inductor L01 and an capacitor C01 in parallel ,while the inductive
transform into a capacitor C02 and a inductor L02 in series as shown in Figure 3.31.
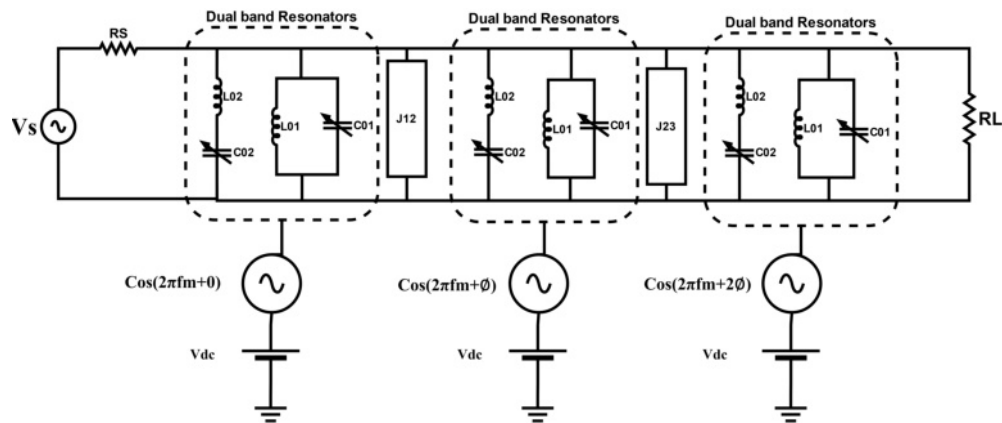
Figure 3.31: 3-pole nonreciprocal dual-band pass filter with ideal time-varying capaci-
tors using (STM)

The center frequencies ($f0_1$ and $f0_2$) of the nonreciprocal dual-band pass filter
are determined by the static inductance L01, L02, and static capacitance C01, C02. The
modulated capacitors and capacitance modulation index, It's the same as previously
3.10 - 3.11 defined in nonreciprocal BPF.

3.5.3 Tunable 3-Pole U-Shaped Nonreciprocal Dual-Band Pass Filter Design

This section is divided into three parts. The first part deals with the design of a
conventional 3-pole U-shaped Dual Band Pass Filter (DBPF). Then, in the second part,
discussing Tunable 3-pole U-shaped DBPF is carried out. The last part discusses the
3-pole U-shaped nonreciprocal dual-band pass filter.

3.5.3.1 3-Pole U-Shaped Dual-Band Pass Filter (DBPF)

In this subsubsection, the 3-pole U-shaped dual-band pass filter is designed where its type is Chebyshev prototype with $g0 = g4 = 1.0, g1 = g3 = 0.8516$, and $g2 = 1.1032$ for a passband ripple of 0.04321 dB . The first band is to have a fractional bandwidth $FBW = 0.139$centered at 2.23 GHz. The second band has a center frequency of 3.74 GHz with FBW = 0.133 by using Eqs.3.20-3.21 with analysis curves in Figure 3.25. Figure 3.32 displays the filter layout, while Table.3.3 presents the physical dimensions.

$$Q_{e1} = \frac{g_0 g_1}{FBW}, Q_{en} = \frac{g_n g_{n+1}}{FBW} \tag{3.20}$$

$$M_{i,i+1} = \frac{FBW}{\sqrt{g_i g_{i+1}}} \tag{3.21}$$

Figure 3.32 displays the filter layout, while Table.3.3 presents the physical dimensions.
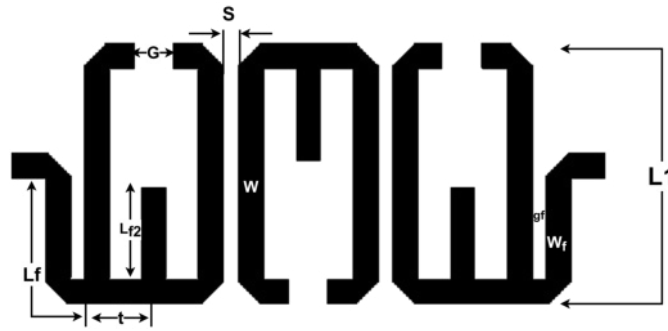
Figure 3.32: The layout of 3-pole U-shaped DBPF

Table 3.3: The physical dimensions of U-shaped DBPF

parameters	Measurements in(mm)
L1	11.08
W	0.92
S	0.8
G	1.84
Lf2	3.95
Wf	0.92
Lf	6.184
Gf	0.752
t	2

3.5.3.2 Tunable 3-Pole U-shaped DBPF

In this subsubsection, the tunable 3-pole U-shaped DBPF is designed. The filter presented above operates at certain two resonance frequencies. To make it tunable, the varactor diodes with DC biasing circuit as shown in Figure 3.33 are connected to the ends and middle of each U-shaped resonator.
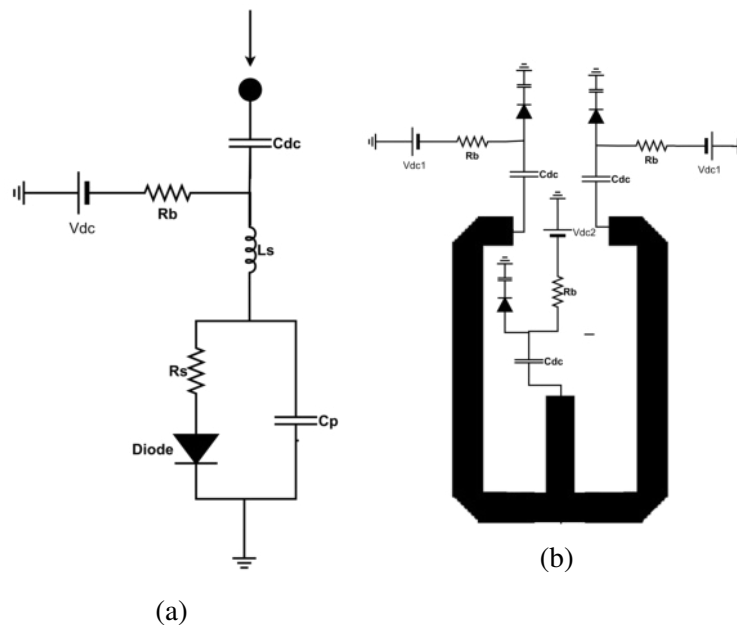
Figure 3.33: a) Spice mode of Varactor diode with DC biasing circuit b) The layout of 3-pole U-shaped tunable DBPF with varactors diode are basied by two dc voltage (Vdc1 and Vdc2)

The DC biasing circuit consists of a DC block capacitor Cdc and a resistor Rb. The

Cdc prevents the DC biasing signals to flow into resonators, while the Rb inhibits the RF signals affecting on the DC biasing circuit. Cp and Ls denote the parasitic effects of the diode packaging, and Rs is the series resistance of the varactor diode. The smallest value of Cp and Rs and a large value of Ls are chosen [49].

The diode chosen in all simulations is skyworks smv2019 in [48], and a curve of the equivalent capacitance with dc voltage is shown in Figure 3.34.
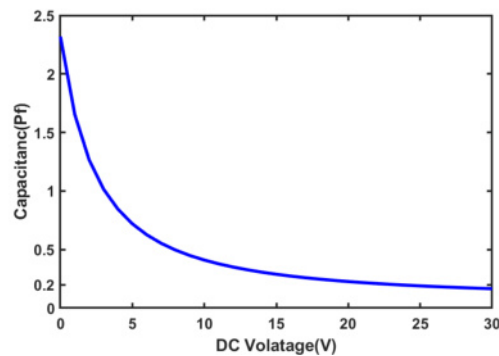
Figure 3.34: SMV2019 Capacitance vs Dc voltage

Figures 3.35 -3.37 show the parametric studies of the reflection and transmission coefficients of the tunable U-shaped dual bandpass filter in three cases.

Case 1, when the dc voltage (Vdc1) changes and Vdc2 is not found, the dual bands can be tuned simultaneously as shown in Figure 3.35.

(a)   (b)
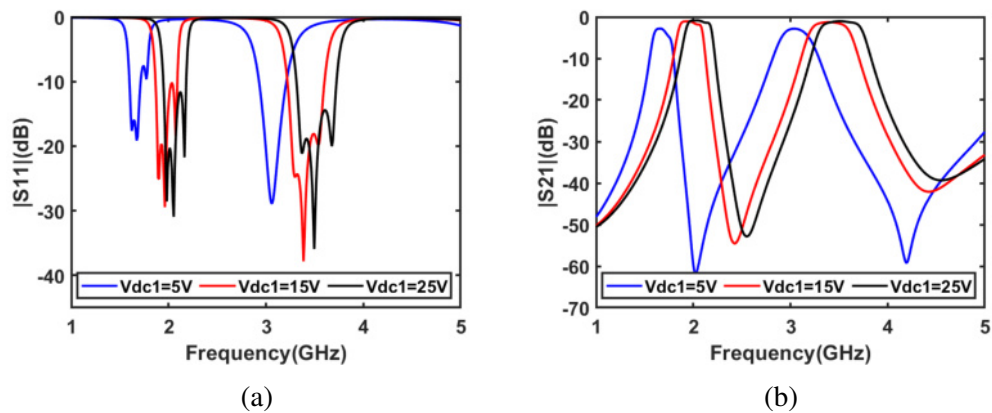
Figure 3.35: Simulated frequency responses of the 3-pole U-shaped dual-band pass filter with respect to Vdc1 (5, 15, and 25V).

Case 2, when the dc voltage (Vdc2) changes and Vdc1 is not found, the second band is tuning while the first band is fixed as shown in Figure 3.36.

(a)

(b)
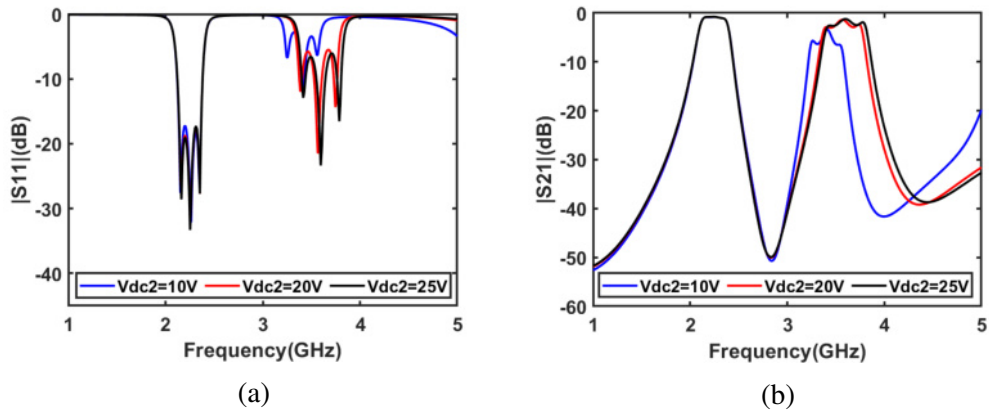
Figure 3.36: Simulated frequency responses of the 3-pole U-shaped dual-band pass filter with respect to Vdc2 (10, 20, and 25V).

Case 3, when both dc voltages (Vdc1) and (Vdc2) change, the range of tunable of the second band increases compared to case 1 as shown in Figure 3.37.

(a)

(b)

(c)
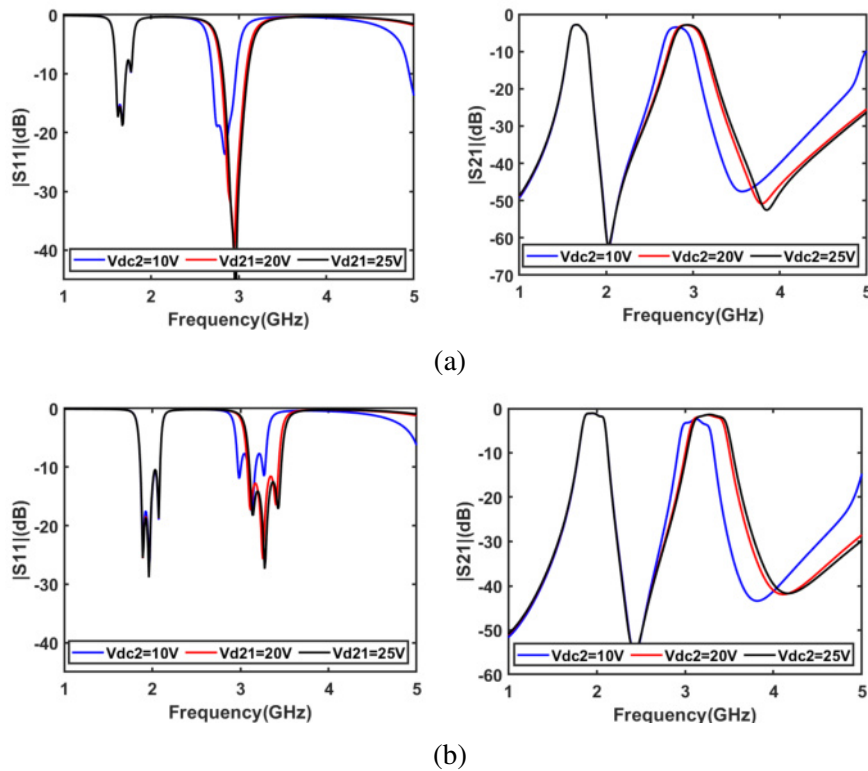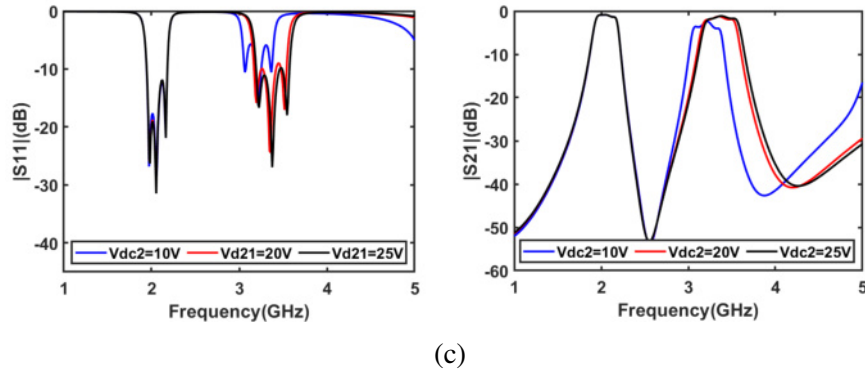
Figure 3.37: Simulated frequency responses of the 3-pole U-shaped dual-band pass filter with respect to a) Vdc1 =5V and Vdc2 (10, 20, and 25V) b) Vdc1 =15V and Vdc2 (10, 20, and 25V) c) Vdc1 =25V and Vdc2 (10, 20, and 25V)

3.5.3.3   3-Pole U-Shaped Nonreciprocal Dual-Band Pass Filter

The concept of nonreciprocity was clarified above by applying the STM technique on the conventional DBPF as shown in Figure3.38. Here, effects of the main parameters on the overall performance (i.e., the circuit responses, (S11, S22, S12 and S21) will be introduced, see Figure 3.39. First, the modulation frequency increases from 100 MHz to 160 MHz. The forward transmission (S21) is improved and the backward transmission (S12) is attenuated.
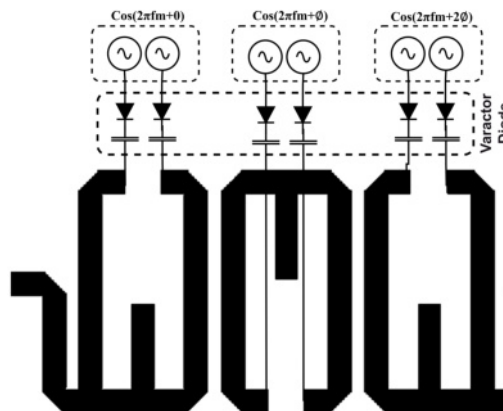
Figure 3.38: 3-pole U-shaped nonreciprocal dual-band pass filter base on STM technique

The S12 changes with the fm. The reflection (S11=S22) does not obviously affect as shown in Figure 3.38. The optimal fm is 120 MHz because it offers the large re-

86

verse attenuation and relatively small forward insertion loss. The other parameter is the modulation index K_m, see Figure 3.38. When it becomes more than 0.42, the forward transmission deteriorates and the backward transmission has attenuation larger than 20 dB. The optimum value of K_m is chosen as 0.44 due to its the small insertion loss and large backward attenuation. The reflection loss is relatively stable.

Figure 3.39c depicts effects of the modulation phase ϕ. When ϕ is equal to 0, the time-varying capacitors shown in Figure 3.31 are only time-modulated, resulting in reciprocal responses with 9.3 dB passband insertion loss for both transmission coefficient S21 and isolation coefficient S12.

(a)   (b)

(c)
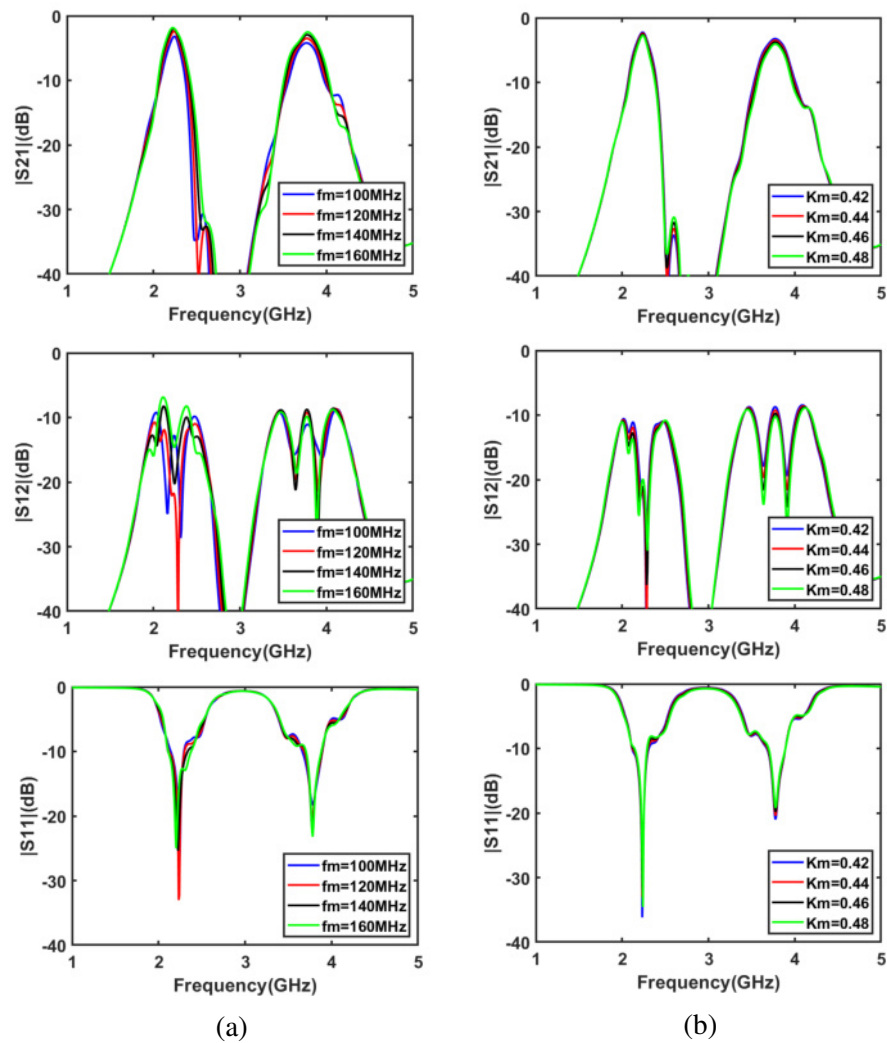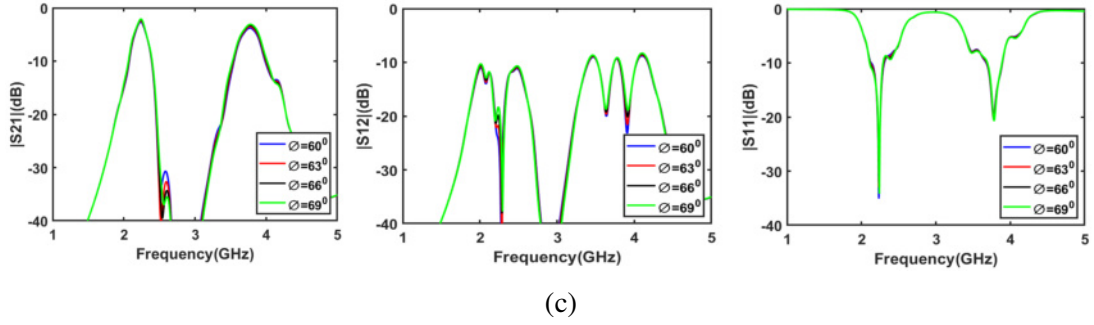
Figure 3.39: Parametric studies of the 3-pole U-shaped nonreciprocal filter dual-band pass filter responses with respect to (a) modulation frequency fm ($K_m = 0.44$; $\phi = 63^0$); (b) modulation index $K_m = 0.44$ (fm = 120 MHz,$\phi = 63^0$); (c) phase ϕ (fm = 120 MHz, $K_m = 0.44$)

The large loss occurs because of the uncontrolled power conversion to the IM products. When ϕ is nonzero, the three resonators in Figure 3.31 are modulated simultaneously in both time and space (i.e., STM). The ϕ is 63^0, representing the optimal value.

3.6   Nonreciprocal Quasi- Reflectionless Band Pass Filter

Having designed, simulated, optimized, fabricated, and tested RF structures solving problems of the power reflections and reciprocity in Section 3.3 and 3.4, respectively, both structures will be combined in one design. Fortunately, both designs employ the U-shaped resonators as the main blocks of the proposed filter. This has eased the procedure to combine both functionalities only in one design. Figure 3.40 depicts the entire design of the proposed quasi-reflectionless nonreciprocal bandpass filter. Also, the figure displays all functions separately when exciting some control voltages. Thus, the proposed filter can carry out the prescribed function depending only on the voltage applied to terminals of the proposed filter.

Any programmable device such as the FPGA, or Arduino can be utilized to do the task. Four DC voltage sources, and three AC voltage sources (i.e., modulation sources)

88
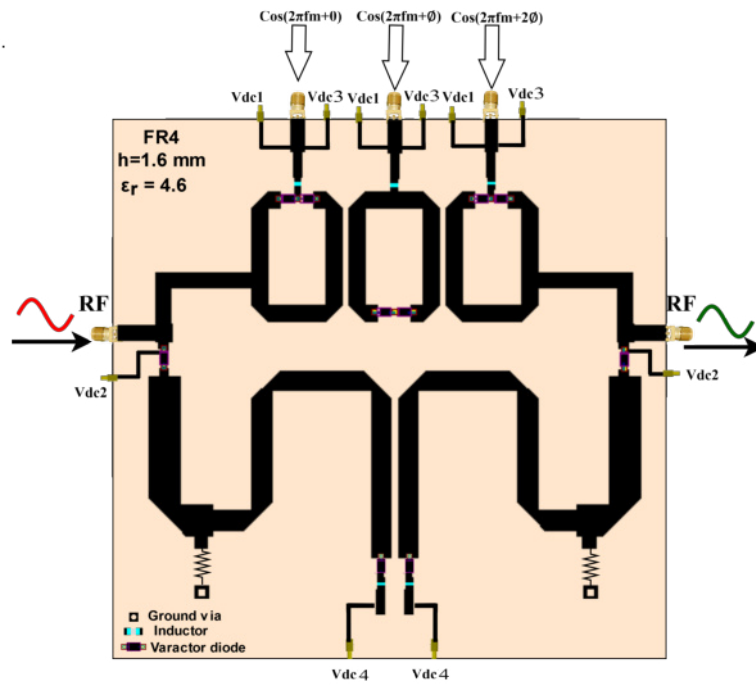
Figure 3.40: The layout of the 3-pole U-shaped nonreciprocal quasi[reflectionless BPF

are required to fully control the proposed device. Moreover, the AC sources have the same frequency, but different phase shifts which is the key to construct or destruct the propagation RF signal. This design is reported for the first time according to the best of knowledge of the researcher. The design solves the problems of the thesis stated in Chapter 1.

CHAPTER 4

RESULTS AND DISCUSSIONS

4.1 Introduction

This chapter introduces the results for all designs explained in the previous chapter. staring with the results of the nonreflectless and reflectionless BPFs. The comparison between the simulated and measured results is also introduced. Then, the chapter discusses the results of the nonreciprocal BPFs. Tunable and dual-band non-reciprocal BPFs will be presented in this chapter. Finally, the chapter will present all results regarding designs with nonreciprocal and reflectionless properties in the same design.

4.2 Results Discussions of 3-pole quasi-reflectionless bandpass filter

In this section, the 3-pole U-shaped quasi-reflectionless bandpass filter is designed, simulated, fabricated, and measured. Figure 4.1a and 4.2a show the simulated and fabricated prototypes of the proposed designs. $FR4$ substrate with relative a dielectric constant $\varepsilon r = 4.6$, dielectric thickness $h = 1.6mm$, and dielectric loss tangent $tan(\delta D) = 0.02$ is used. The operating frequency is $3.5GHz$ and the 3dB fractional bandwidth is 20%. The Keysight Advanced Design System software (ADS) is utilized to analyze and carry out the schematic and EM designs. Following the design procedure, all physical dimensions of the proposed filters are mentioned in Figure 4.1a and 4.2a.
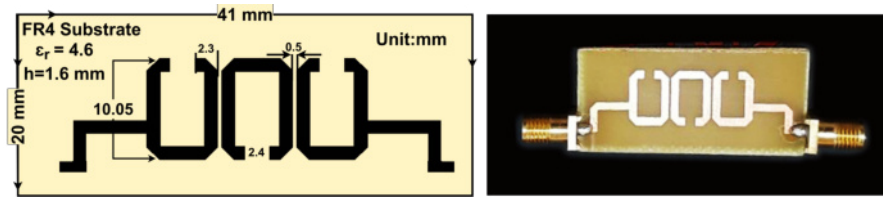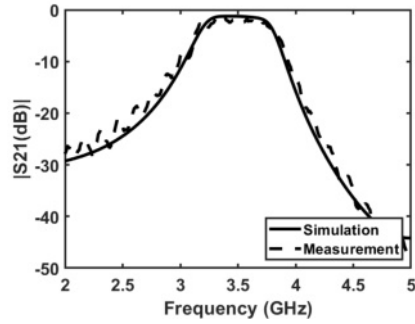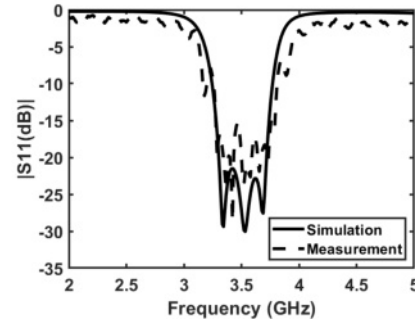
Figure 4.1: Experimental validations of 3-pole U-shaped BPF a) The layout and photograph of the 3-pole BPF b) simulated and measured transmission coefficients S21 c)simulated and measured reflection coefficients S11
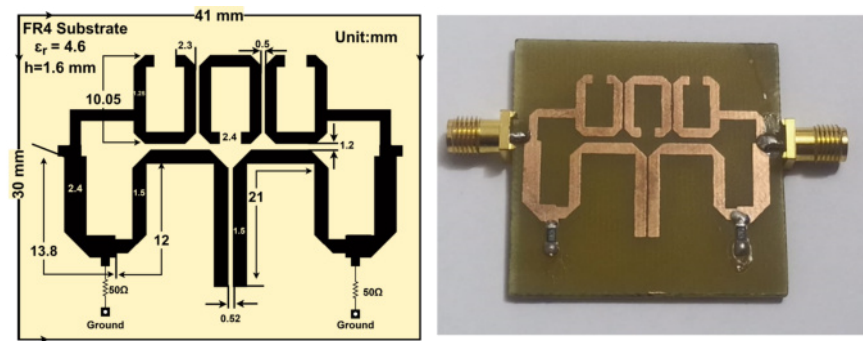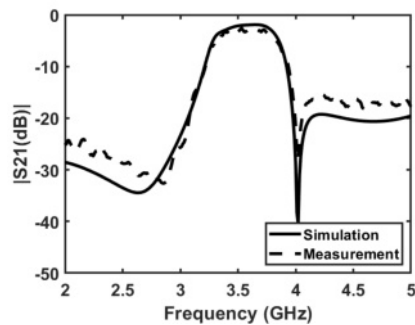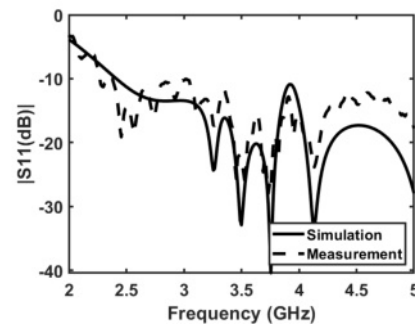
Figure 4.2: Experimental validations of 3-pole U-shaped quasi-reflectionless BPF a) The layout and photograph of the 3-pole quasi-reflectionless BPF b) simulated and measured transmission coefficients S21 c)simulated and measured reflection coefficients S11

As expected, the measured results agree very well with the simulated ones. This confirms that the analyses provided above are valid. Figures 4.2a and b compare between the measured and simulated results for the transmission and reflection coefficients, respectively. The measured reflection coefficient $S11$ is less than 10dB from $2.25GHz$ to beyond the $5GHz$, not shown here for the sake of simplicity. The discrepancy between the simulated and measured results belongs for many reasons. the proposed work was fabricated using the chemical etching process, so there will be some differences in dimensions. Also, the measurements were done with the use of simple VNA, KC901V

4.3 Results Discussions of 3-pole tunable U-shaped quasi-reflectionless bandpass filter

The 3-pole tunable U-shaped quasi-reflectionless bandpass filter is designed, simulated in this section. Figure 4.3 shows the simulated prototype of the proposed design. FR4 substrate with relative dielectric constant $\varepsilon r = 4.6$, dielectric thickness h = 1.6mm, and dielectric loss tangent $tan(\delta D) = 0.02$ is used. The operating frequency is 3.5GHz and the 3dB fractional bandwidth is 20%. The tunable frequency range (3.28-3.5 GHz). All details can be found in Figure Figure 4.3b- 4.3c and Table 4.1.

Table 4.1: All details of simulated responses

Tunable range of frequencies	Transmission coefficient S21 in dB	Reflection coefficient S11 in dB
3.28-3.5 GHz	- Near to -3.5dB at 3.5 GHz - Near to -5dB at (3.2-3.48)	- less - 23 at 3.5GHz - Less -10 at$(3 - 3.6)$GHz - Less -5 at $(3.61 - 3.9)$GHz

(a)

(b)

(c)
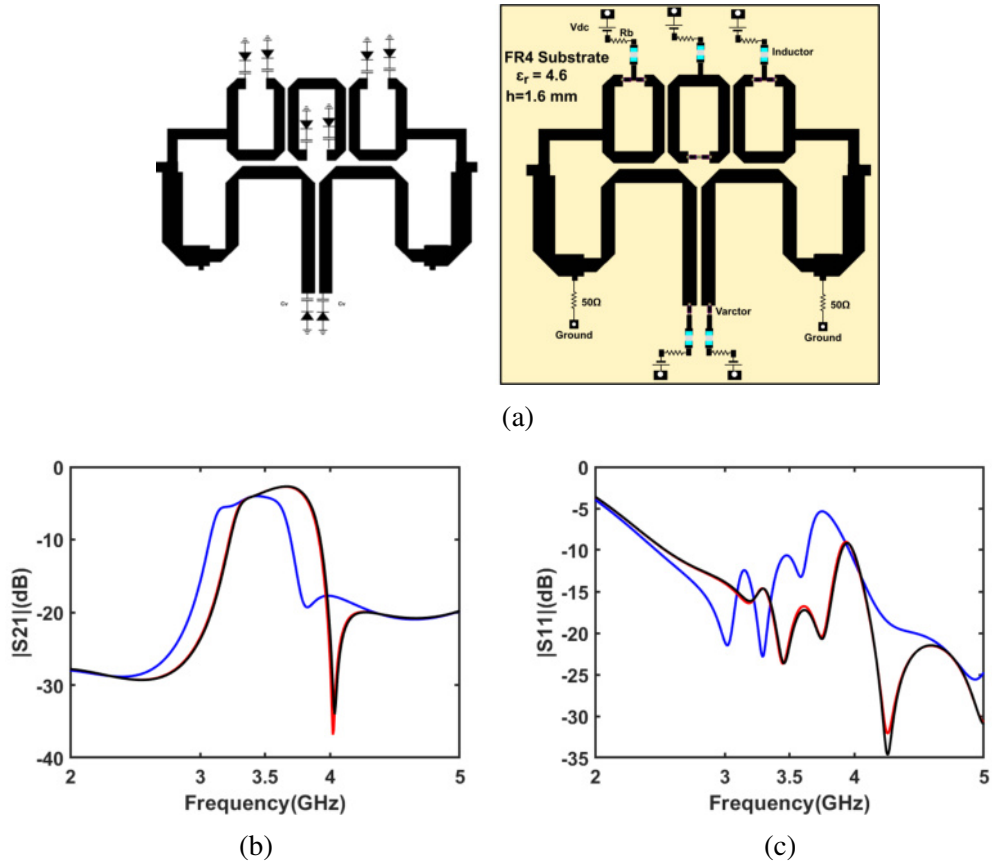
Figure 4.3: Simulation of 3-pole tunable U-shaped quasi-reflectionless BPF a) The layout and photograph of the 3-pole quasi-reflectionless BPF b) simulated transmission coefficients S21 c)simulated reflection coefficients S11

4.4 Numerical Validations of The magneticless Nonreciprocal BPF

This section describes the magneticless nonreciprocal BPF. The presented filter is three poles using the U-shaped resonators. Figure 4.4 shows the simulated prototypes of the proposed design using the advanced design system, ADS, and Table.3.2 summarizes the filter dimensions.

The substrate utilized in the design is FR4 with a relative dielectric constant εr of 4.6, dielectric thickness h of 1.6mm, and dielectric loss tangent $\tan(\delta D)$ of 0.02. The operating frequency is ($f_0 = 3.5GHz$), the 3dB fractional bandwidth is $FBW = 0.2$. Also, the figure shows that the proposed filter attenuates the backward propagation (response) S12 by less than 10dB.

93

(a)

(b)

(c)

(d)
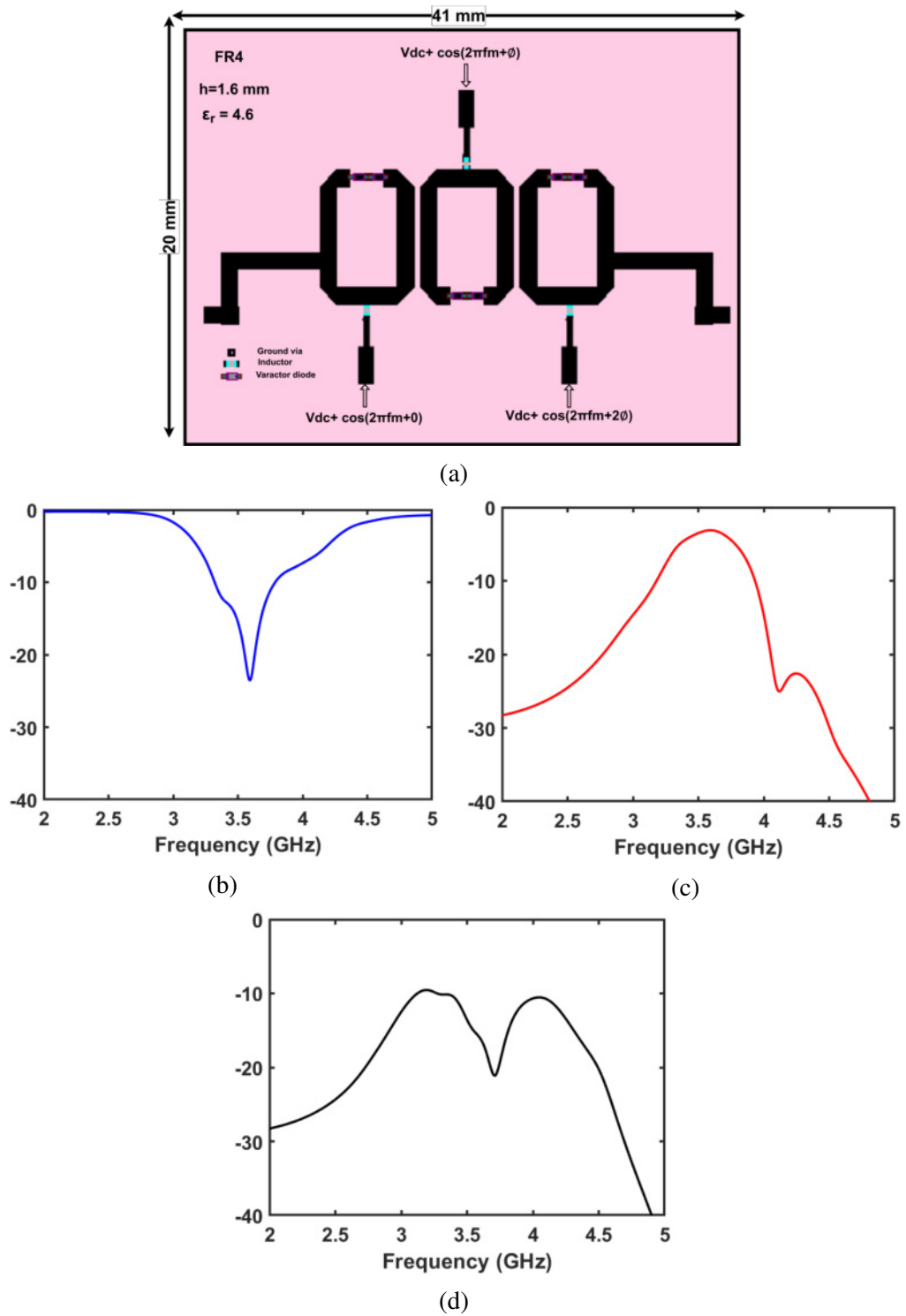
Figure 4.4: Simulation of 3-pole U-shaped nonreciprocal BPF (a) the layout and photograph of the 3-pole nonreciprocal BPF (b) simulated reflection coefficients S11 (c) simulated transmission coefficients S21 (d) simulated isolation coefficients S12

4.5 Numerical Validations of The tunable Nonreciprocal Dual-Band Pass Filter

This section describes the tunable nonreciprocal dual-band pass filter. The presented filter is three poles using the U-shaped resonators. Figure 4.5 shows the simulated prototypes of the proposed design and Table 3.3 summarizes the filter dimensions. The substrate utilized in the design is Rogers-RO3210 with a relative dielectric constant εr of 10.2, dielectric thickness h of 1.27mm, and dielectric loss tangent $tan(\delta D)$ of 0.003. The operating frequencies are ($f_{01} = 2.24GHz$ and $f_{02} = 3.73GHz$), the 3dB fractional bandwidths are FBW1=0.139 and $FBW2 = 0.133$ for the first and second band, respectively. The tunable frequency range of the first band is 1.6-2.05GHz and the second band is 2.8-3.6GHz. All details can be found in Figure 4.7. Also, the figure shows that the proposed filter attenuates the backward propagation (response) S12 by less than 10dB for both bands.
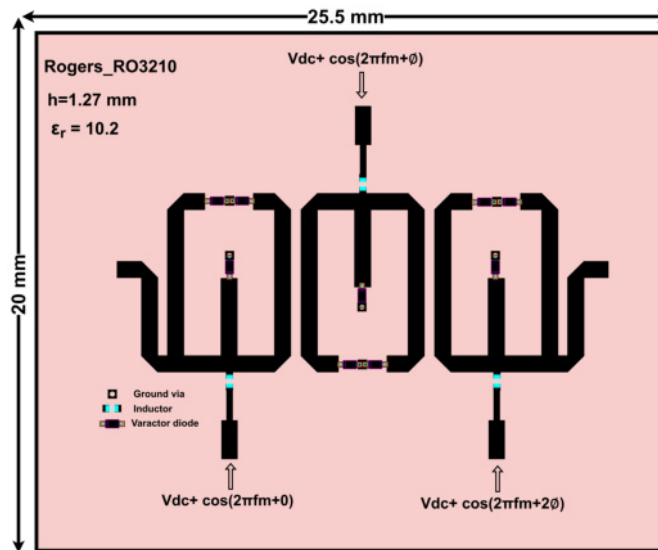
Figure 4.5: The layout of the 3-pole Tunable U-shaped nonreciprocal dual-band pass filter

Four cases are shown in Figure 4.7 to present the filter non-tunable DBPF, tunable DBPF, nonreciprocal DBPF, and nonreciprocal tunable DBPF.

(a)   (b)
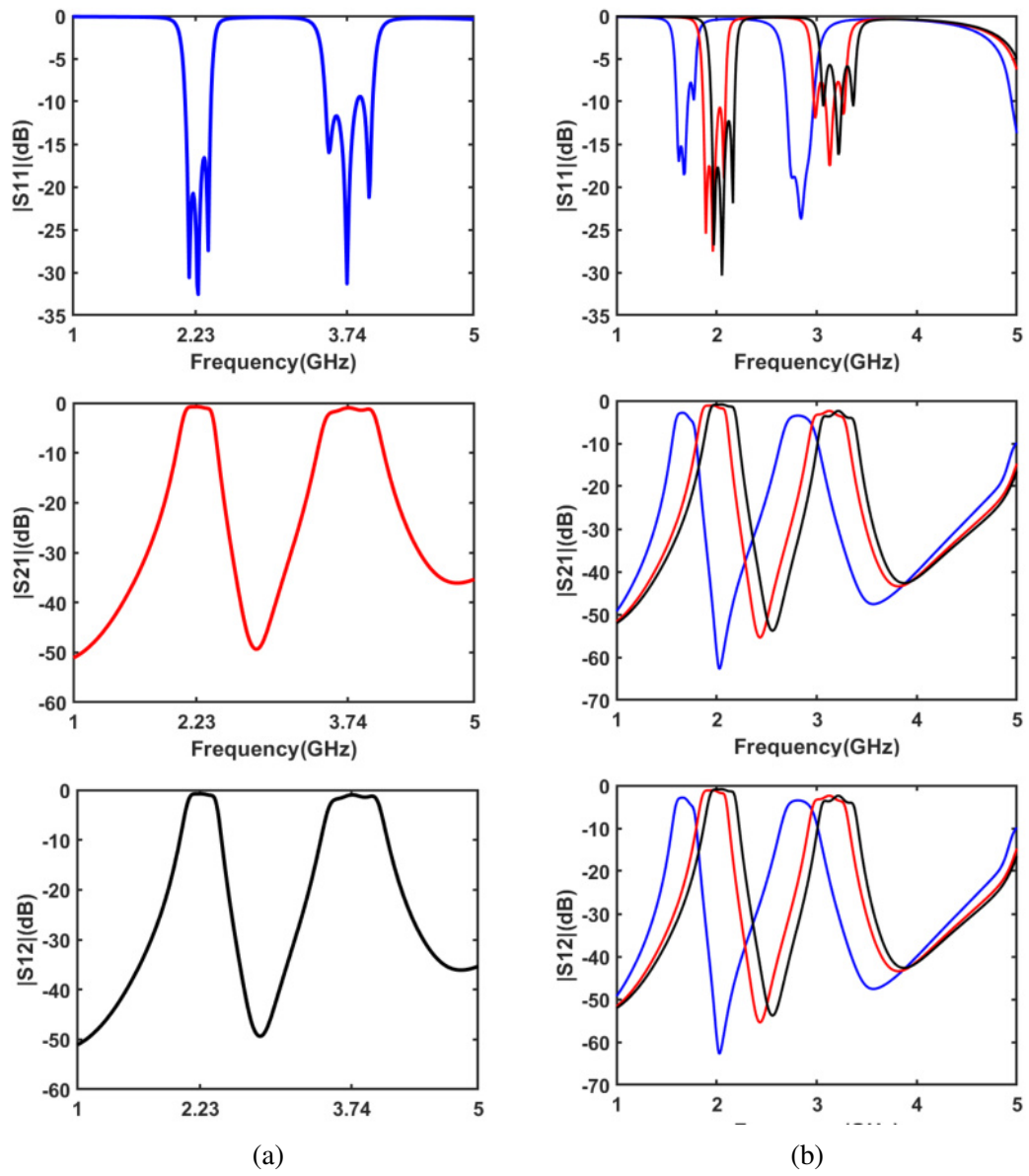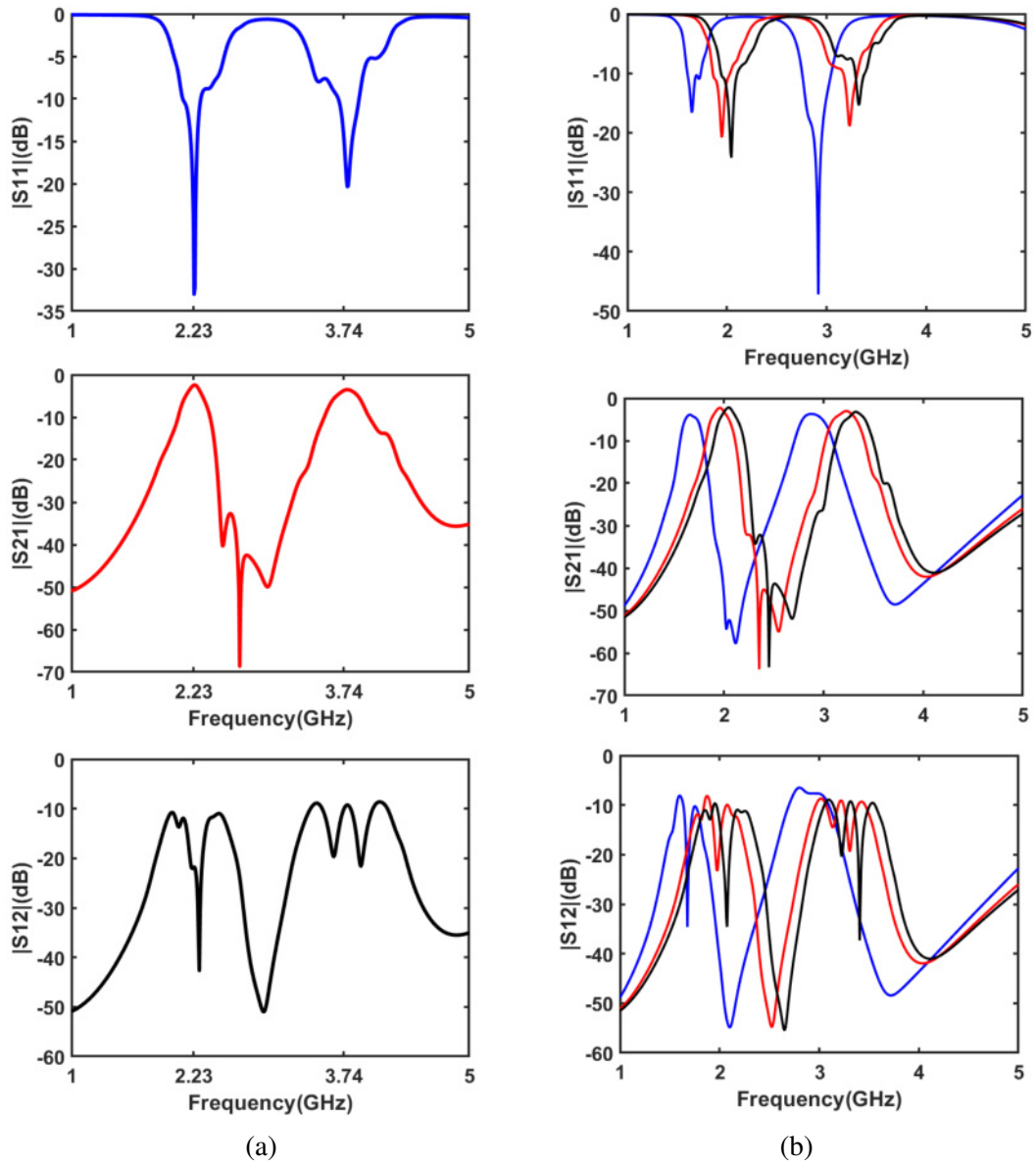
Figure 4.7: Four cases output response of the proposed filter a)Non-tunable DBPF b)Tunable DBPF response c)Nonreciprocal DBPF response d)Nonreciprocal tunable DBPF response

4.6 Results and Discussions of Nonreciprocal Reflectionless Filter

In this section, the 3-pole U-shaped nonreciprocal quasi-reflectionless bandpass filter is designed and simulated.Figure 4.8 and Table 4.2 show all states that filter can support. When all DC and AC sources are turned off, the filter behaves like conventional filters. It means that the filter is reflective-type and nonreciprocal, see Figure 4.8a. As can be seen, the S21 and S12 are both supported by the device with the interesting frequency band. Also, the S11 is fully reflected at out of the band of interest. Once Vdc2 is turned on, the filter will be changed into the quasi-reflection bandpass filter, see Figure 4.8b. The S11 is less than -10dB for the entire range displayed in the figure. To make the BPF is only nonreciprocal, only the Vdc3 and Aac sources are turned on. The optimal phase shift difference between any two adjacent resonators is 57°, the fm is 240MHz, and the Vdc is 1v. The resonator is on the far left considers as the reference element, where the S21 is supported as shown in Figure 4.25.c. On contrast, when the far right resonator considers as the reference element, the S12 is supported as shown in Figure 4.8d.

Figure 4.8e shows the filter response for the quasi-reflectionless nonreciprocal bandpass filter state. In this state, the Vdc2, Vdc3, and Vac sources are turned on while others are turned off. The S11 and s12 are less than -10dB. To make the design more functional, the tunability is also demonstrated. When Vdc1 and Vdc4 sources are turned off, Vac is off Vdc2 is on, and Vdc3 is varied from 5v to 25v, the tunable quasi-reflectionless filter is obtained as shown in Figure 4.8f. Moreover, When Vdc3 and Vdc4 sources are varied from 5v to 25 v, Vac is on Vdc2 is off, and Vdc1 is off, the tunable nonreciprocal filter is obtained as shown in Figure 4.8g. More detail can be found in Table 4.2, and will not be mentioned here for the sake of simplicity.

(a)

(b)

(c)

(d)

(e)

(f)

(g)
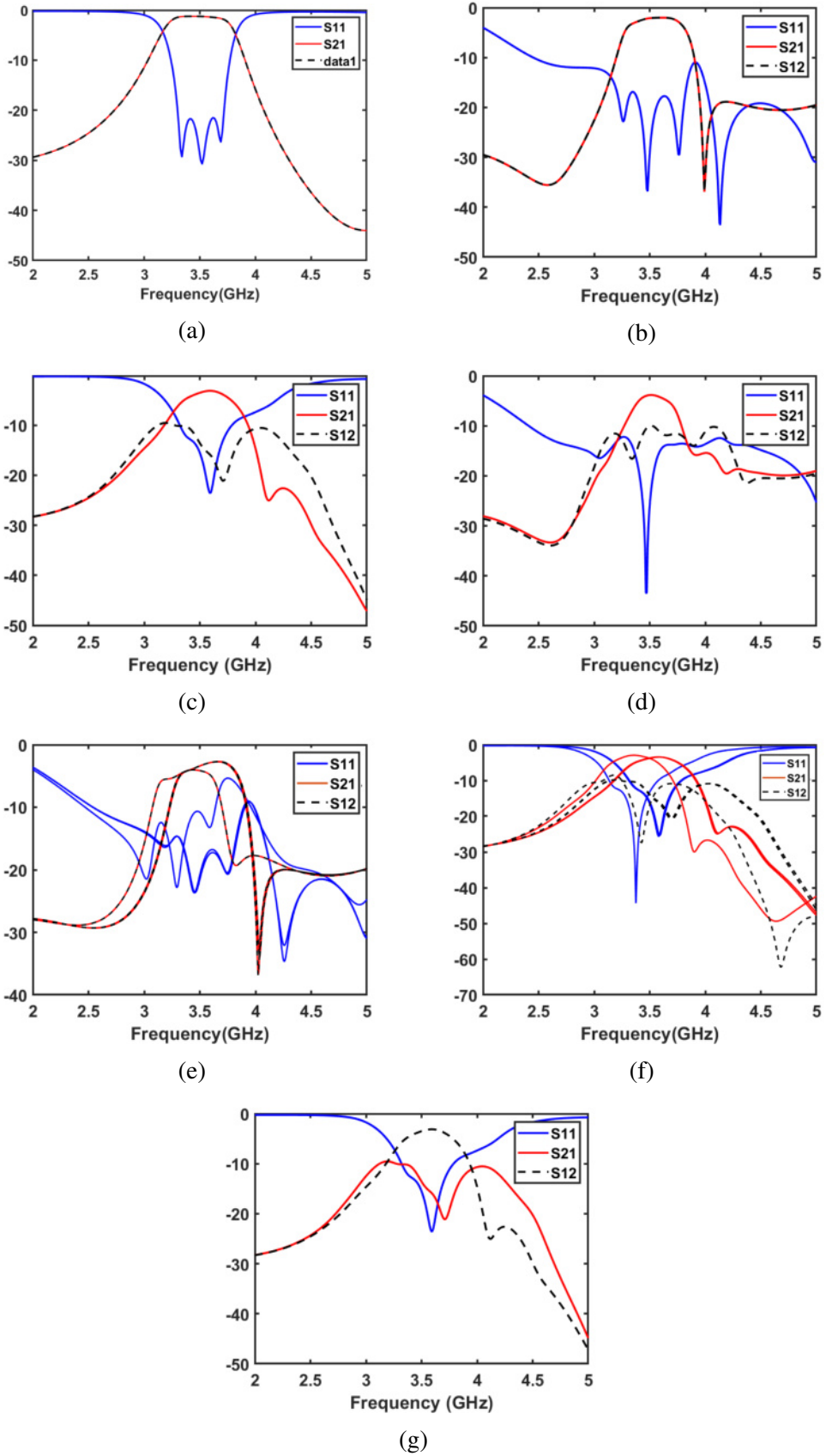
Figure 4.8: Programable BPF Responses a) Bandpass Filter b) quasi-Reflectionless BPF c) nonreciprocal BPF in direction from port 1 to port 2 d) quasi-Reflectionless Nonreciprocal BPF e) tunable Reflectionless Filter f)tunable Nonreciprocal Filter g)) nonreciprocal BPF in direction from port 2 to port 1

Table 4.2: Seven cases of programmable BPF

Case of DC voltage (Vdc1, Vdc2, Vdc3, Vdc3)	Case of AC Signale (fm,ϕ,Km)	BPF Response	Reflection coefficient S11 in dB	transmission coefficient S21 in dB	Isolation coefficient S12
Vdc1=OFF Vdc1=OFF Vdc3=OFF Vdc4=OFF	AC=OFF	Reciprocal BPF	-30	-1.257	-1.257dB
Vdc1=OFF Vdc2=ON Vdc3=OFF Vdc4=OFF	AC=OFF	Quasi-Reflectionless BPF	-43 at 3.5GHz Less -10 at (2.5 − 3)GHz Less -15 at (3.8 − 5)GHz	-1.77	1.77dB
Vdc1=ON Vdc2=OFF Vdc3=OFF Vdc4=OFF	AC=ON fm=240MHz $\phi1=0^0,\phi2=57^0,\phi3=114^0$ Km=0.23	Nonreciprocal BPF form port1 to port2	-23.8	-3.17	-21.2dB at f=3.7 GHz Less -10 dB at (3.1 − 3.97)GHz
Vdc1=ON Vdc2=ON Vdc3=OFF Vdc4=OFF	AC=ON fm=240MHz $\phi1=0^0,\phi2=57^0,\phi3=114^0$ Km=0.23	Nonreciprocal quasi-reflection$_{Less}$ BPF	-25.38 at 3.5GHz Less -10 at(2.34 − 3)GHz Less -12 at (3.75 − 5)GHz	-3.36	-16.98 at f=3.28 GHz Less -10 dB at(3.16 − 3.71)GHz
Vdc1=OFF Vdc2=ON Vdc3=5-25V Vdc4=5-25	AC=OFF	Tunable quasi-eflectionless BPF with tunable range (3.28-3.5)GHz	Less -23 at 3.5 Less -10 at (3-3.6)GHz Less -5 at(3.62 -3.9)GHz	-3.5 at 3.5GHz Near to -5 at (3.2-3.48) GHz	-3.5 at 3.5GHz Near to -5 at (3.2-3.48) GHz
Vdc1=ON Vdc2=OFF Vdc3=5-25V Vdc4=OFF	AC=ON fm=240MHz $\phi1=0^0,\phi2=57^0,\phi3=114^0$ Km=0.23	Tunable nonreciprocal BPF with tunable range (3.37-3.6)GHz	Less 25 at (3.37-3.6GHz)	-2.9 at (3.37-3.6)GHz	Less -25 at 3.4-3.5GHz Less -10dB at (3.- 4GHz)
Vdc1=ON Vdc2=OFF Vdc3=OFF Vdc4=OFF	AC=ON fm=240MHz $\phi1=114^0,\phi2=57^0,\phi3=0^0$ Km=0.23	Nonreciprocal BPF form port2 to port1	-23.8 at 3.5GHz	-21.2 at f=3.7 GHz Less -10 dB at (3.1 − 3.97)GHz	-3.17

CHAPTER 5

CONCLUSION AND SUGGESTIONS FUTURE WORKS

5.1 Conclusion

In this thesis, the power reflection and reciprocity had been solved and the results showed that the proposed designs were able to deal with these two issues. First, the research solved the power reflection by adding an absorptive stubs into the main filter which is the U-shaped BPF. Most power in signals out of the band-of-interest was routed into the load to absorb it. The mathematical model was derived to support the proposed design. Also, the practical prototype was fabricated and tested to obtain a comparison between the simulated and measured results. The FR4 substrate was used to print the design and the measured results were in a good agreement with the simulated ones. Also, the results showed that the reflection coefficient was less than -10dB for a wide range of frequencies. Then, the reciprocity was broken using the STM technique. The same U-shaped PBF was utilized, but with integrating varactor diodes to their open-ends and applying modulating signals to terminals of the varactor diodes. As demonstrated in the results, the design allowed signals to propagate only in one direction either the transmit or receive side. When the S21 was supported, the S12 was attenuated into low than -10dB. The direction of the progressive phase shift was playing a vital role in determining which S21 or S12 is supported. Furthermore, the design frequency was tuned to be altered from (3.37 to 3.6)GHz. This property enabled our proposed designs to operate at different wireless systems. Not only the tunable property was presented, but also, the dual-band nonreciprocal PPF was introduced in the research. These different

functionalities gave the author the ability to provide a variety of designs to work within.

Finally, both solutions mentioned above had been introduced in one prototype called the programmable reflectionless nonreciprocal PBF which was able to change its response relying on the voltage applied to its terminals

5.2 Suggestions Future Works

This section provides the readers what are the possible future works as follows:

1. Use the optimization and machine learning techniques to reduce time of the design (i.e., accelerating design procedures)

2. Design a nonreciprocal duplexers or circulators by using a combination of structures presented in Chapter 4.

3. Fabricate and measure the nonreciprocal filter.

4. Integrate an antenna to the receiving and transmitting nonreciprocal filters.

5. Use lumped elements to design new nonreciprocal filters in order to miniaturize the filter designs.

BIBLIOGRAPHY

[1] J.-S. G. Hong and M. J. Lancaster, *Microstrip filters for RF/microwave applications*. John Wiley & Sons, 2004.

[2] K. E. Kolodziej, B. T. Perry, and J. S. Herd, "In-band full-duplex technology: Techniques and systems survey," *IEEE Transactions on Microwave Theory and Techniques*, vol. 67, no. 7, pp. 3025–3041, 2019.

[3] A. Sabharwal, P. Schniter, D. Guo, D. W. Bliss, S. Rangarajan, and R. Wichman, "In-band full-duplex wireless: Challenges and opportunities," *IEEE Journal on selected areas in communications*, vol. 32, no. 9, pp. 1637–1652, 2014.

[4] Y. X. Tu, "Design, modelling and implementation of several multi-standard high performance single-wideband and multi-wideband microwave planar filters," Ph.D. dissertation, University of Bradford, 2016.

[5] D. M. Pozar, *Microwave engineering*. John wiley & sons, 2011.

[6] F. Bashore, "Rf circuit design: Theory and applications," *Microwave Journal*, vol. 43, no. 3, pp. 200–200, 2000.

[7] A. Grebennikov, *RF and microwave transmitter design*. John Wiley & Sons, 2011.

[8] M. A. Morgan, "Think outside the band: Design and miniaturization of absorptive filters," *IEEE Microwave Magazine*, vol. 19, no. 7, pp. 54–62, 2018.

[9] B. Mini-Circuits *et al.*, "Reflectionless filters improve linearity and dynamic range," *Microw. J.*, vol. 58, no. 8, pp. 42–50, 2015.

[10] M. A. Morgan, *Reflectionless filters*. Artech House, 2017.

[11] D. Psychogiou and R. Gómez-García, "Reflectionless adaptive rf filters: Bandpass, bandstop, and cascade designs," *IEEE Transactions on Microwave Theory and Techniques*, vol. 65, no. 11, pp. 4593–4605, 2017.

[12] M. Khalaj-Amirhosseini and M.-M. Taskhiri, "Twofold reflectionless filters of inverse-chebyshev response with arbitrary attenuation," *IEEE Transactions on Microwave Theory and Techniques*, vol. 65, no. 11, pp. 4616–4620, 2017.

[13] R. Gómez-García, J.-M. Mu, D. Psychogiou *et al.*, "Split-type input-reflectionless multiband filters," *IEEE Microwave and Wireless Components Letters*, vol. 28, no. 11, pp. 981–983, 2018.

[14] M.-F. Gomez-Garcia, J.-M. Roberto, and D. Psychogiou, "Symmetrical quasi-absorptive rf bandpass filters," *IEEE Transactions on Microwave Theory and Techniques*, vol. 67, no. 4, pp. 1472–1482, 2019.

[15] R. Gomez-Garcia, J.-M. Munoz-Ferreras, and D. Psychogiou, "High-order input-reflectionless bandpass/bandstop filters and multiplexers," *IEEE Transactions on Microwave Theory and Techniques*, vol. 67, no. 9, pp. 3683–3695, 2019.

[16] D. M. Cannell, *George Green: Mathematician and Physicist 1793–1841: The Background to his Life and Work*. SIAM, 2001.

[17] J. W. Strutt, "V. on the constant of magnetic rotation of light in bisulphide of carbon," *Philosophical Transactions of the Royal Society of London*, no. 176, pp. 343–366, 1885.

[18] H. Helmholtz, "On the physical significance of the principle of least action," *J. Reine Angewandte Mathatik*, vol. 100, pp. 217–222, 1886.

[19] J. R. Carson, "Reciprocal theorems in radio communication," *Proceedings of the Institute of Radio Engineers*, vol. 17, no. 6, pp. 952–956, 1929.

[20] S. Ballantine, "Reciprocity in electromagnetic, mechanical, acoustical, and interconnected systems," *Proceedings of the Institute of Radio Engineers*, vol. 17, no. 6, pp. 927–951, 1929.

[21] L. Onsager, "Reciprocal relations in irreversible processes. i." *Physical review*, vol. 37, no. 4, p. 405, 1931.

[22] H. B. G. Casimir, "On onsager's principle of microscopic reversibility," *Reviews of Modern Physics*, vol. 17, no. 2-3, p. 343, 1945.

[23] J. D. Adam, L. E. Davis, G. F. Dionne, E. F. Schloemann, and S. N. Stitzer, "Ferrite devices and materials," *IEEE transactions on microwave theory and techniques*, vol. 50, no. 3, pp. 721–737, 2002.

[24] N. Reiskarimian, A. Nagulu, T. Dinc, and H. Krishnaswamy, "Nonreciprocal electronic devices: A hypothesis turned into reality," *IEEE Microwave Magazine*, vol. 20, no. 4, pp. 94–111, 2019.

[25] A. Nagulu and H. Krishnaswamy, "Non-magnetic non-reciprocal microwave components—state of the art and future directions," *IEEE Journal of Microwaves*, vol. 1, no. 1, pp. 447–456, 2021.

[26] A. Kord *et al.*, "Magnetless circulators based on linear time-varying circuits," Ph.D. dissertation, 2019.

[27] M. A. Morgan and T. A. Boyd, "Theoretical and experimental study of a new class of reflectionless filter," *IEEE Transactions on Microwave Theory and Techniques*, vol. 59, no. 5, pp. 1214–1221, 2011.

[28] M. A. Morgan, W. M. Groves, and T. A. Boyd, "Reflectionless filter topologies supporting arbitrary low-pass ladder prototypes," *IEEE Transactions on Circuits and Systems I: Regular Papers*, vol. 66, no. 2, pp. 594–604, 2018.

[29] J. Hong, *Advances in Planar Filters Design*. Institution of Engineering and Technology, 2019.

[30] J. Lee, B. Lee, S. Nam, and J. Lee, "Rigorous design method for symmetric reflectionless filters with arbitrary prescribed transmission response," *IEEE Transactions on Microwave Theory and Techniques*, vol. 68, no. 6, pp. 2300–2307, 2020.

[31] C. Jackson, "Transmission line replacements for a lumped element reflectionless filter," in *2014 IEEE Radio and Wireless Symposium (RWS)*. IEEE, 2014, pp. 166–168.

[32] R. Gomez-Garcia, J.-M. Munoz-Ferreras, and D. Psychogiou, "High-order input-reflectionless bandpass/bandstop filters and multiplexers," *IEEE Transactions on Microwave Theory and Techniques*, vol. 67, no. 9, pp. 3683–3695, 2019.

[33] J.-Y. Shao and Y.-S. Lin, "Narrowband coupled-line bandstop filter with absorptive stopband," *IEEE Transactions on Microwave Theory and Techniques*, vol. 63, no. 10, pp. 3469–3478, 2015.

[34] S.-W. Jeong, T.-H. Lee, and J. Lee, "Absorptive filter prototype and distributed-element absorptive bandpass filter," in *2018 IEEE MTT-S International Conference on Numerical Electromagnetic and Multiphysics Modeling and Optimization (NEMO)*. IEEE, 2018, pp. 1–4.

[35] X. Wu, Y. Li, and X. Liu, "High-order dual-port quasi-absorptive microstrip coupled-line bandpass filters," *IEEE Transactions on Microwave Theory and Techniques*, vol. 68, no. 4, pp. 1462–1475, 2019.

[36] X. Wu, Y. Li', and X. Liu, "Quasi-reflectionless microstrip bandpass filters with improved passband flatness and out-of-band rejection," *IEEE Access*, vol. 8, no. 4, pp. 160 500–160 514, 2020.

[37] J. P. Kim, "Improved design of single-section and cascaded planar directional filters," *IEEE transactions on microwave theory and techniques*, vol. 59, no. 9, pp. 2206–2213, 2011.

[38] C. K. Seewald and J. R. Bray, "Ferrite-filled antisymmetrically biased rectangular waveguide isolator using magnetostatic surface wave modes," *IEEE Transactions on Microwave Theory and Techniques*, vol. 58, no. 6, pp. 1493–1501, 2010.

[39] A. Morse and L. Huelsman, "A gyrator realization using operational amplifiers," *IEEE Transactions on Circuit Theory*, vol. 11, no. 2, pp. 277–278, 1964.

[40] S. Tanaka, N. Shimomura, and K. Ohtake, "Active circulators—the realization of circulators using transistors," *Proceedings of the IEEE*, vol. 53, no. 3, pp. 260–267, 1965.

[41] G. Carchon and B. Nanwelaers, "Power and noise limitations of active circulators," *IEEE Transactions on Microwave Theory and Techniques*, vol. 48, no. 2, pp. 316–319, 2000.

[42] M. M. Biedka, R. Zhu, Q. M. Xu, and Y. E. Wang, "Ultra-wide band non-reciprocity through sequentially-switched delay lines," *Scientific reports*, vol. 7, no. 1, pp. 1–16, 2017.

[43] D. L. Sounas, C. Caloz, and A. Alu, "Giant non-reciprocity at the subwavelength scale using angular momentum-biased metamaterials," *Nature communications*, vol. 4, no. 1, pp. 1–7, 2013.

[44] M. Nafe, X. Wu, and X. Liu, "Wideband non-reciprocal magnetic-free devices based on high-order spatio-temporal modulation," University of California Davis Davis United States, Tech. Rep., 2019.

[45] A. Kord, D. L. Sounas, and A. Alu, "Pseudo-linear time-invariant magnetless circulators based on differential spatiotemporal modulation of resonant junctions," *IEEE Transactions on Microwave Theory and Techniques*, vol. 66, no. 6, pp. 2731–2745, 2018.

[46] X. Wu, X. Liu, M. D. Hickle, D. Peroulis, J. S. Gómez-Díaz, and A. Á. Melcón, "Isolating bandpass filters using time-modulated resonators," *IEEE Transactions on Microwave Theory and Techniques*, vol. 67, no. 6, pp. 2331–2345, 2019.

[47] X. Wu, M. Nafe, A. Á. Melcón, J. S. Gomez-Diaz, and X. Liu, "Frequency tunable non-reciprocal bandpass filter using time-modulated microstrip λ g/2 resonators," *IEEE Transactions on Circuits and Systems II: Express Briefs*, vol. 68, no. 2, pp. 667–671, 2020.

[48] V. E. C. Model, "Varactor spice models for rf vco applications," 2010.

[49] M. A. Latip, M. M. Salleh, and I. Pasya, "Tuning circuit using varactor diode for tunable bandstop resonator," in *2011 IEEE Symposium on Wireless Technology and Applications (ISWTA)*. IEEE, 2011, pp. 17–20.

LIST OF PUBLICATIONS

1. Alkhuwaildi, Bahaa Hamzah, and Nasr Alkhafaji. "Third Order U-Shaped Quasi-Reflectionless Bandpass Filter." Progress In Electromagnetics Research C 123 (2022): 27-43.

2. The research paper "Spatial-Temporal Modulation Technique based Tunable Nonreciprocal Dual Band Pass Filter" has been submitted to a journal TELKOMNIKA Telecommunication, Computing, Electronics and Control.

3. The research paper "Third Order Magneticless Nonrecirocal U-Shaped Bandpass Filter " has been submitted to a journal Al-Furat Journal of Innovation in Electronic and Computer Engineering.

4. The paper"programmable nonreciprocal quasi-reflectionles BPF" is under working.

5. The paper"Tunable quasi-reflectionles nonreciprocal BPF" is under working.

الخلاصة

تعد القدرة المنعكسة والتبادلية من التحديات الرئيسية التي تواجه مصممي دوائر الترددات الراديوية لأسباب عديدة. عندما تنعكس القدرة بشكل كامل في خارج نطاق الترددات المرغوب فيها، فان هذه القدرة تتلف او تأثر بشكل سلبي على عمل الاجهزة المجاورة لهذه الدوائر. اما بخصوص التبادلية والتي تعني انتقال الاشارات بكلا الاتجاهين يسبب توهين داخل هذه الاجهزة لذا فان العزل بين إشارات الإرسال والاستقبال مهم. هاتين المشكلتين سيتم التحقيق فيهما لتقليلهما إلى حد جيد فقط في تصميم واحد تم اقتراحه لأول مرة في الأدبيات.

في هذه الرسالة ، تم اقتراح مرشح غير متبادل غير عاكس للقدرة وقابل للبرمجة. يمكن للمرشح المقترح تغير حالته بالاعتماد على فولتيات تحكم تربط الى اطراف التحكم الخاصة بها. حيث يمكن للمرشح تغير حالته من مرشح غير عاكس للقدرة الى مرشح عاكس او من مرشح ارسال الى مرشح استلام او العكس. قد يتم ذلك تلقائيا اذا تم استخدام تقنيات الذكاء الاصطناعي مع اجهزة اف بي جي اي او الادوينو. لذا فان الرسالة تكون كالاتي:

اولا ستناقش وتقترح الرسالة حلا للقدرة المنعكسة . وكما متعارف عليه في معظم تصاميم دوائر الترددات الراديوية ان ممانعة هذه الاجهزة تتوافق عند الترددات المطلوبة او المرغوب بها و انعكاسها في باقي الترددات. لذا يغير المرشح المقترح مسار هذه القدرة الى احمال امتصاصية. ولإثبات صحة هذا المفهوم تم تصنيع مرشح غير عاكس من المرتبة الثالث.

اما الجزء الثاني من الرسالة يتناول حل مشكلة التبادلية. تقليدي ، يتم كسر هذه الخصيصة من خلال استخدام المواد المغناطيسية كما هو الحال في السركوليتر، لكن العديد من العيوب المصاحبة لهذا النوع من التكنولوجيا مثل ضخمة وغير متوافقة مع الدوائر المطبوعة ومكلفة. لذا تم الاعتماد على تقنية اخرى تعتمد على التضمين المكاني الزماني . نظرًا لأن دوائر الرنين في المرشحات ثابتة ولا يمكن تغيير خصائصها ، لذا تم دمج الثنائيات المتغيرة (الفاركتر دايود) في دوائر الرنين الرئيسية. حيث يمكن أن يغير الفاركتر دايود قيم

السعة إذا تغير الجهد المطبق. وبالتالي ، يتم التحكم في التيار المستمر والتردد والطور للاشارات المضمنة بعناية للتحكم في اتجاه انتشار الإشارات. العامل الرئيسي الذي يحدد اتجاه الانتشار هو الاتجاه التدريجي لانزياح الطور. في وقت ما ، يتم دعم الانتشار بالاتجاه الامامي وعدم دعم الانتشار العكسي ، والعكس صحيح. ايضا ، تم تقديم مرشح ثنائي النطاق وقابل للتوليف غير التبادلي.

تصميم وتنفيذ نظام ترددات راديوية غير عاكسة غير تبادلية

الرسالة
مقدمه الى قسم هندسة تقنيات الاتصالات كجزء من متطلبات نيل درجه الماجستير في
هندسة الاتصالات

تقدم بها

بهاء حمزة جاسم

أشراف

المدرس الدكتور

نصر نوماس

2022

جمهورية العراق

وزارة التعليم العالي والبحث العلمي

جامعة الفرات الاوسط التقنية

الكلية التقنية الهندسية نجف

تصميم وتنفيذ نظام ترددات راديوية غير عاكسة غير تبادلية

بهاء حمزة جاسم

ماجستير في هندسة تقنيات الاتصالات

2022